INTERPRETATION OF THE NEUTRAL HELIUM TRIPLET SPECTRUM IN PLANETARY NEBULAE

Thesis by

Sven Eric Persson

In Partial Fulfillment of the Requirements

For the Degree of

Doctor of Philosophy

California Institute of Technology

Pasadena, California

1972

(Submitted July 28, 1971)

ACKNOWLEDGEMENTS

I wish to thank Professor Guido Münch for suggesting the problem, and for his encouragement, advice, and accessibility. I have also benefited from discussions with Professors Sargent, Oke, Neugebauer and Greenstein, and Dr. E. Becklin.

I thank the Director of the Hale Observatories for my allotment of observing time. Night Assistants E. Hancock, H. Schaefer, M. Jacquez, J. Dittmar and G. Tuton were most helpful.

I owe special thanks for encouragement to Drs. D. Peterson, R. Schild, and I. Danziger.

I have enjoyed valuable discussions and friendships with G. Shields, J. and R. Lindal, and Drs. M. B. Wilson, and R. W. O'Connell.

Financial support from Graduate Research Assistantships, an Earle C. Anthony Fellowship, a Virginia Scott Steele Fellowship, and my parents is gratefully acknowledged.

My thanks are due to Bill and Mary Bauer, who typed the thesis.

Finally, I wish to acknowledge the unwavering support and love my parents have given me all my life.

ABSTRACT

The theory of the He I triplet spectrum is modified to include the effects of solid particles within the ionized regions of planetary nebulae. New observations of the emission lines λλ5876, 7065, and 10830 are presented for over twenty nebulae, extending the list of objects studied previously by O'Dell. The empirical ratios $R_1 \equiv I(\lambda 10830)/I(\lambda 5876)$ and $R_2 \equiv I(\lambda 7065)/I(\lambda 5876)$ are combined with the theory to study the discrepancies between the He I 2^3S depopulation rates D_1(derived from R_1), D_2 (from R_2), and D_t (theoretical). If the presence of dust is neglected, the discrepancies are such that $D_1 > D_t > D_2$, in most cases. This is essentially the result found earlier by Capriotti for a smaller sample of objects. Estimates of $\tau_d(\lambda 10830)$, the λ10830 dust optical depths which force $D_1 = D_t$, are derived by accounting for the resonance trapping and dust absorption of the λ10830 radiation. These estimates are consistent, on an order-of-magnitude basis, with values implied by observed infrared excesses in planetary nebulae, and by simple models of reradiating dust shells.

The important effects of nebular structural features upon the He I triplet spectrum are studied theoretically and observationally. Overall correlations between the apparent 2^3S depopulation rate discrepancies and nebular parameters are shown to have a connection with a wide range of nebular problems.

TABLE OF CONTENTS

TABLE OF CONTENTS

TABLE OF CONTENTS

TABLE OF CONTENTS

LIST OF TABLES

LIST OF FIGURES

NOMENCLATURE

A	Angstroms; Argon.
A( )	Einstein A-values, transition in parentheses.
$\alpha(\ )$, $\alpha(\lambda)$	Effective recombination rate to a state ( ), or for a spectral line λ.
a	Radius of a dust grain.
$\underline{a}$	Damping parameter $A/4\pi\Delta\nu_d$.
$B_\nu(T)$	Planck function.
b_n	Population of level n relative to LTE case.
C	$\Delta\log[I(H\beta)]$, interstellar. In Chapter II, C is Penning Ionization parameter.
Γ_x	Grain heating rate by species x.
D, $D_{1,2}$, t, x	He I (2^3S) depopulation rate, determined from R_1, R_2, theoretically; due to process x.
$\Delta\lambda_d$, $\Delta\nu_d$	Doppler width.
$E(\lambda)$	Energy generation rate of spectral feature λ.
$E_\nu(a,\lambda)$	Flux from a grain.
ε, η	Resonance photon escape (or destruction) probability per scattering.
$F(\lambda)$; F_ν	Fluxes in spectral line λ, or in continuum at ν.
f(1), f(2)	He I emission line enhancement factors due to conversion of $n^3P - 2^3S$ photons.

$q(\ )$	Maxwell-Boltzmann - averaged collisional rate for transition ( ).
R	Spherical model nebular radius.
R_1	Observed (corrected for reddening) ratio $I(\lambda 10830)/I(\lambda 5876)$.
R_2	Same as R_1 for $I(\lambda 7065/I(\lambda 5876)$.
R_S	Radius of nebular central star.
r	Physical separation between central star and a point in nebula.
$S(X)$	Nebular surface brightness of a nebular in spectral feature X.
s	Distance to an object. (Not App. 2)
σ	Reaction cross section; standard error.
T_j	Electron temperature $T_e \div 10^j$.
T, T_s	Temperature; (stellar).
$T_c(\lambda_1,\lambda_2)$	Color temperature.
$\tau_0(\ )$	Line center optical depth in transistion ( ). Through slab or along radius of static sphere.
τ_c	Lyman continuum ($\lambda 912$) optical depth.
$\tau_d(\lambda)$	Dust optical depth at λ along radius of sphere.
ϕ	Angular radius (arc sec) of an object.
$V(R)$, $V(TH)$	Surface expansion velocity; Ionic thermal velocity.
υ, v	Relative velocity of two species.

f_x	Pathlength traversed by resonance photon x, in units of nebular radius.
$f(\lambda)$	Seaton's (1960) reddening function.
θ	Angular radius (radians) of an object.
$I(\lambda)$	Intensity in spectral line λ.
$I_c(\lambda)$, $I_\nu(\lambda)$	Continuum intensity (Hz^{-1}) at λ.
$\kappa_0(\lambda)$	Line center absorption coefficient for spectral line λ. Static models.
k_ν, k_x	He I 2^3S photoionization cross section at frequency ν, or for spectral feature x.
L_ν	Stellar luminosity.
$L_\odot$	Solar luminosity.
ℓ	Photon mean-free-path.
$N(n^{2s+1}L_j)$	Number density of ions (standard notation).
N_x, $N(X)$	Number density of species x, X.
ξ	V(R)/V(TH) expansion parameter. Surface outward velocity relative to thermal velocity.
P, p, Ξ, T, B	Dummy variables.
Q	Number of resonance scatterings of a resonance photon before destruction or escape.
$Q(a,\lambda)$	Absorption efficiency of a grain of radius a at wavelength λ.

X	An Atomic Species.
Z	Dust particle step size distribution.

I. INTRODUCTION

This thesis is an investigation of several neutral Helium triplet lines in the emission spectra of planetary nebulae - a problem suggested to me by Professor Guido Münch. It arises as much from his observations of anomalously weak λ3889 absorption features in the spectra of stars embedded in H II regions (Münch and Wilson 1962, Münch 1964, 1970) as from the photoelectric observations of several planetaries by O'Dell (1963b), and the subsequent attempts to reconcile theory and observation. In essence, the problem may be understood with reference to Figure 1, a schematic energy-level diagram of the lowest-lying singlet and triplet levels of He I. In those regions of a planetary nebula where He is mostly singly ionized, recombination of He^+ results in cascade through the neutral levels ending with population of the lowest triplet or singlet levels in the ratio 3:1. One-photon electric dipole or multipole radiative decay of He I 2^3S, is forbidden ($\Delta S \neq 0$), and deactivation of this level may occur for $N_e = 0$ by two-photon decay and magnetic dipole one-photon spontaneous decay to 1^1S_0 at a rate $1.2\times10^{-4}\,sec^{-1}$. The result is a large overpopulation of 2^3S ($b_n \sim 10^{11}$). This fact has several consequences for the emission lines which arise from levels close to 2^3S. First, since the mean electron kinetic energy is a few eV under typical

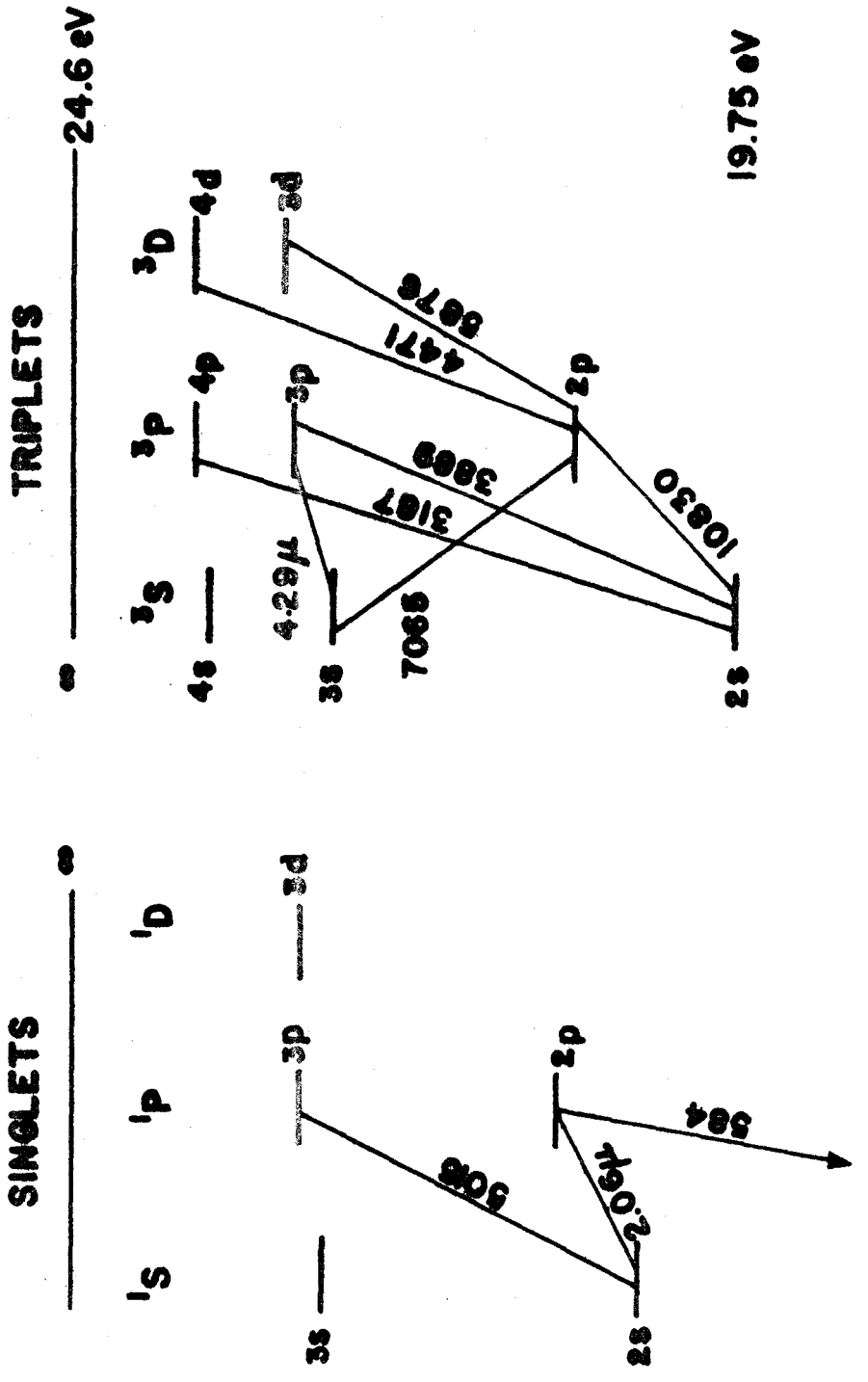

Fig. 1. - Partial Grotrian Diagram for He I.

nebular conditions, the 2^3S level provides a source for collisional excitation of 2^3P, giving rise to $\lambda 10830$ radiation, since $A(2^3P \rightarrow 2^3S) \sim 10^7$ sec^{-1}. Second, the large population $N(2^3S)$ provides a substantial optical depth through the nebula (e.g., $\tau_0[\lambda 3889] \sim 10$) in the lower triplet transitions. The creation and escape of these resonance-like photons are thus described by the solution of a transfer problem. Given the excitation rate $q(2^3S \rightarrow 2^3P)$, one can deduce the population $N(2^3S)$ by measuring the intrinsic intensity $I(\lambda 10830)$ relative to a triplet recombination line if it is assumed that all $\lambda 10830$ photons created eventually escape the nebula. In an isothermal, homogeneous nebula, statistical equilibrium between the lower levels determines $N(2^3S)$:

$$N(2^3S)D = \alpha(2^3S)N_e N(He^+), \qquad \text{(I-1)}$$

$$E(\lambda 10830) = h\nu_{10830}[\alpha(2^3P)N_e N(He^+)$$

$$+ N(2^3S)N_e q(2^3S \rightarrow 2^3P)], \qquad \text{(I-2)}$$

$$E(\lambda 5876) = h\nu_{5876}[\alpha(\lambda 5876)N_e N(He^+)], \qquad \text{(I-3)}$$

and thus

$$R_1 \equiv \frac{I(\lambda 10830)}{I(\lambda 5876)} = \frac{5876}{10830}\left[\frac{\alpha(2^3P)}{\alpha(\lambda 5876)} + \frac{\alpha(2^3S)}{\alpha(\lambda 5876)} N_e \frac{q(2^3S \rightarrow 2^3P)}{D}\right] \qquad \text{(I-4)}$$

In the above equations, D is the depopulation rate of 2^3S, and $E(\lambda)$ is the emission coefficient cm^{-3}. Equation (I-1) is the steady state condition for 2^3S, equation (I-2) is the λ10830 emission rate due to recombinations and collisional excitation of 2^3P by electrons, equation (I-3) is the λ5876 emission rate, and equation (I-4) is the resulting equation for D. It is assumed here that optical depths $\tau_0(2^3S\text{-}n^3P)$ for $n > 3$ do not affect $E(\lambda5876)$ or $E(\lambda10830)$. A measurement of R_1, corrected for interstellar reddening, should thus determine D, if N_e and T_e are known. The problem has been that in summing the possible theoretical components of D, viz., photoionization, collisional deactivation, and radiative decay, one always finds that R_1 is <u>too small</u>; in other words, the theoretical rates are insufficient to account for the lowering of $N(2^3S)$ and the resulting lowering of λ10830 production (equation [I-2]).

Another approach to the determination of D is the following: since $\tau_0(\lambda3889)$ may be large, a λ3889 photon created by recombination or collisional excitation will be scattered by He^0 atoms in the state 2^3S. A He^0 atom excited to 3^3P by absorption of λ3889 may decay to either 3^3S or back to 2^3S; the branching ratio being $\sim$ 1/10. Thus in 10 scatterings, a λ3889 photon is effectively destroyed, i.e., converted to the set 4.2μ, λ7065, λ10830.

In a particular volume element in the nebula, the population $N(2^3S)$ and the intensity $I_\nu(\lambda 3889)$ thus determine the emission rate of $\lambda 7065$ radiation:

$$E(\lambda 7065) = h\nu_{7065}[\alpha(3^3S)N_e N(He^+)$$

$$+ PN(2^3S) \times \int_{-\infty}^{+\infty} d\nu \int_{4\pi} d\Omega \; I_\nu(\lambda 3889) B\phi(\nu)$$

$$+ P\,N(2^3S)N_e q(2^3S \rightarrow 3^3P)] \,, \qquad \text{(I-5)}$$

where P is the branching ratio $A(3^3P \rightarrow 3^3S)/[A(3^3P \rightarrow 2^3S) + A(3^3P \rightarrow 3^3S)]$, B is the Einstein transition probability for $2^3S \rightarrow 3^3P$, and $\phi(\nu)$ is the normalized absorption profile. Expansion of the nebula allows the easier escape of $\lambda 3889$ radiation, and a resulting drop in $E(\lambda 7065)$ occurs. In order to predict $R_2 \equiv I(\lambda 7065)/I(\lambda 5876)$, an equation of transfer must be solved for the 2^3S-n^3P radiation fields, and in principle, one can then find $N(2^3S)$ or D, by measuring R_2.

The characteristics of the He I triplet spectra in dilute radiation fields have been studied by several authors. The two-photon decay rate of 2^3S was calculated by Mathis (1957), and later, Pottasch (1961) studied the effect of optical depths on the triplet spectra. His work did not include expansion of the nebula, or detailed line shapes, and has been shown by subsequent work to seriously underestimate $N(2^3S)$. O'Dell (1963b) reported photo-

electric measures of the important line ratios for several nebulae and later (O'Dell 1965) studied the various depopulation mechanisms in an attempt to explain the anomalously low measured values of R_1. At the suggestion of Münch (1964) he included in the calculation of D_t the large H I Lyα radiation field. Since H I Lyα is severely trapped within the nebula, each resonance photon travels many ($>10^5$) mean-free paths before destruction or escape, thus increasing the Lyα energy density f times, say, with respect to the optically thin case. This trapped radiation can ionize He I (2^3S), and O'Dell (1965) tried to predict f assuming that Lyα was the governing 2^3S depopulation mechanism. The values of f deduced in this way were larger than could be accounted for theoretically, so the values of R_1 were unexplained. Capriotti (1967c), using the transfer solutions of Robbins (1968a,b) and the values of f estimated (Capriotti 1967b) from Lyman continuum optical depths (Capriotti 1967a) showed that the theoretical rates D_t were too small to be compatible with the values of D_1, the depopulation rates deduced from R_1, but obtained better agreement for D_2, the depopulation rates deduced from R_2. Robbins (1968c) added autoionization to the list of possible deactivation mechanisms, and finally Persson (1970) showed that for some nebulae, the interaction of solid particles with the trapped λ10830 radiation may influence the deduced values D_1. Vaughan (1968) has also discussed

the triplet spectra, and has given λ10830 emission profile observations of several nebulae. The general conclusion to date has been that despite inclusion of Lyα, the discrepancy between D_1 and D_t remains.

In the following chapters, a detailed reconsideration of the problem is made. Several effects not previously included are studied; in particular (a) the infrared excesses of several nebulae are related to the destruction of the resonance(-like) trapped photons of Lyα and λ10830; (b) the $2^3P \rightarrow 1^1S$ radiative decay as a mechanism for depopulation is discussed insofar as it affects D_t for large $\tau_0(\lambda 3889)$; (c) new values for the collisional rates which differ substantially from the older ones are shown to have a significant effect if (d) density and temperature fluctuations are included in the nebular models; and (e) we consider the emission of [O I] radiation as it pertains to the maintenance of condensations and infrared excesses.

In Chapter II the theory is redeveloped in detail, in order to show the importance of each parameter or condition which enters into the determination of D_1, D_2 or D_t. In Chapter III are presented new observations of the fluxes I(λ5876), I(λ7065) and I(λ10830) from several nebulae, bringing the total number observed to twenty-seven. Recent infrared (IR) observations of nebulae are discussed in Chapter IV. These observations are compared with simple

models of radiating dust shells. In Chapter V we compile the observations and theory to illustrate the results of comparing the depopulation rates as Capriotti (1967c) did, and then proceed to discuss the effects of including a small amount of dust (τ_d[visual] $\sim$ 0.2) upon the spectra. It is shown that values of τ_d deduced from the measured values of R_1 may be compared with the values of τ_d derived from recent infrared measurements of planetary nebulae. In Chapter VI a quantitative analysis is made, wherein the transfer models of Robbins (1967c) are utilized to reproduce in a general way the effects of fluctuations. We also discuss the observations of Vaughan (1968) in terms of these inhomogeneous models. Chapter VII concludes the thesis with a summary of the investigation insofar as it provides new input to the problem. The expected and derived correlations between various parameters of the nebulae are discussed, and some comments upon the relationship between planetary nebulae, variable stars and interesting infrared objects such as IRC +10216 are made.

II. BASIC THEORY

In this chapter we refine the theory of the emission spectra of the He I triplet lines affected by the metastability of 2^3S by reconsidering the parameters which enter the calculation of the depopulation rates, and by analyzing the effects which may operate to alter the expected values of R_1 and R_2. Each section of this chapter deals with a specific aspect of the problem, and we begin with a brief summary of the interactions of the singlet and triplet states.

(a) The Effect of the 2^1S and 2^1P Levels of He I

The values of D_t depend strongly upon exchange collisions between the 2^3S and 2^1S, 2^1P states. It is shown in Appendix 1 that the two-photon decay rate of He I 2^1S limits the number of collisional transitions $2^1S \rightarrow 2^3S$ or 2^3P, and $2^1P \rightarrow 2^3S$ or 2^3P, despite the large number of scatterings of He I Lyα photons which populates He I 2^1P, $Q(\sim 10^3)$ times before destruction. The recombination rate $\alpha^*(2^3S)$ due to singlet recombination plus singlet-to-triplet transitions is $\sim 10\ ^3\alpha(2^3S)$, and may be ignored.

(b) The Use of Robbins' Models

Robbins (1968a,b) has computed theoretical He triplet spectra for a series of nebular models. Since his results are useful for predicting D_1 and D_2 from the observations,

a brief description is given here. He begins (Robbins 1968a) by solving the cascade-matrix equations for the effective recombination coefficients to the lower triplet states. These coefficients are needed in the transfer problem (Robbins 1968b) which he sets up and solves. His models are homogeneous, isothermal spheres, expanding with constant velocity gradients. The number of absorptions at each location in the model nebula is used to give the emission line strengths in the optically thick transitions. For a given expansion velocity V(R) at the surface, the relevant parameter is $\xi = V(R)/V(TH)$, where V(TH) is the thermal Doppler velocity. The other parameter which governs the escape of the resonance photons, and hence $I(\lambda 7065)$, is the line center optical depth $\tau_0(\lambda 3889)$ given by

$$\tau_0(\lambda 3889) = \kappa_0(\lambda 3889) N(2^3S) R, \qquad \text{(II-1)}$$

where the absorption coefficient $\kappa_0(\lambda 3889) = 5.71\times10^{-14}/\sqrt{T_4}\ cm^2$ ($T_4 \equiv T_e\times10^{-4}$). Robbins tabulates $I(\lambda)/I(\lambda 4471)$ for values of T_4 = 1 and 2, values of $\tau_0(\lambda 3889)$ = 0, 10, 20, 50 and 75, and ξ = 0, 3, and 5. The values of $I(\lambda)/I(\lambda 4471)$ may then be used to find the run of R_1 and R_2 when allowance is made for collisional excitation of 2^3P and 3^3P. Given a value of R_1 or R_2, and T_e, one may then interpolate in the tables to find $\tau_0(\lambda 3889)$. Degradation of higher ($2^3S \rightarrow n^3P$) photons enhances both R_1 and R_2, so that

$$R_1 = \frac{5876}{10830}\left[\frac{\alpha(\lambda 10830)f(1) + \alpha(2^3S)N_e q(2^3S \rightarrow 2^3P)/D}{\alpha(\lambda 5876)f(2)}\right], \qquad \text{(II-2)}$$

where f(1) and f(2) are the enhancement factors of the respective line intensities over their pure recombination values for particular combinations of ξ, T_e and $\tau_0(\lambda 3889)$.

The parameters needed in the calculations of D_1 are the following. The measured flux F (corrected for interstellar absorption) in the $\lambda 5876$ line is related to the surface brightness S by the relation

$$S(\lambda 5876) = F(\lambda 5876)/\theta^2, \qquad \text{(II-3)}$$

where θ is the optical angular radius. S is also the volume integrated energy flux through the nebular surface, so that

$$S(\lambda 5876) = \frac{4}{3}\frac{\pi R^3 \alpha(\lambda 5876) N_e N(He^+) h\nu_{5876} f(2)}{4\pi R^2}, \qquad \text{(II-4)}$$

where we have assumed a homogeneous spherical model. Using equation (I-1) to eliminate $N_e N(He^+)$, and equation (II-1) for $\tau_0(\lambda 3889)$ we have

$$D_1 = \frac{\kappa_0(\lambda 3889)}{\tau_0(\lambda 3889)}\frac{\alpha(2^3S)}{\alpha(\lambda 5876)f(2)}\frac{3S(\lambda 5876)}{h\nu_{5876}}. \qquad \text{(II-5)}$$

The measured value of $S(\lambda 5876)$ is used with T_e in equation (II-5) to find D_1 for each value of $\tau_0(\lambda 3889) > 0$ used by

Robbins. The values of f(1) and f(2) are found by interpolation at the given value of V(R) at each $\tau_0(\lambda 3889)$ and T_4. Power law dependences on T_e of f(1) and f(2) and also the ratios of the α's are assumed since the effective recombination rates vary approximately as power laws in T_e. Given N_e and T_e, $N_e q(2^3S \rightarrow 2^3P)$ is found, and the second term in equation (II-2) is computed for each $\tau_0(\lambda 3889)$. The predicted value of R_1 for each $\tau_0(\lambda 3889)$ is thus obtained, and a final interpolation for R_1 (observed) yields $\tau_0(\lambda 3889)$ (inferred) and D_1 from equation (II-5). It is noted that f(1) and f(2) are typically 1.10 and 1.05 respectively, and vary slowly. The ratios of the α's change little with T_e; the only sensitive term is thus the 2^3P collisional excitation rate.

The procedure for finding D_2 from R_2 is similar to the above. We have chosen to interpolate, using power laws in T_e, to find the values of the ratios R_2 directly, for each $\tau_0(\lambda 3889)$. The important feature to note is the rather rapid variation in $\alpha(\lambda 5876)/\alpha(\lambda 7065)$ with T_e. The percentage increase in $I(\lambda 7065)$ depends only upon ξ and $\tau_0(\lambda 3889)$ and not upon T_e (a fact well reproduced in the tables), and thus the assumed temperature variation of $I(\lambda)$ for any V(R), T_e, $\tau_0(\lambda 3889)$ combination will be the same as that assumed for the pure recombination case. We use these power laws to extend the tabular results to lower, as well as intermediate temperatures. The collisional

excitation contribution to R_2 should be small for typical nebulae, but may be important for high density or high temperature objects. For a given $\tau_0(\lambda 3889)$, the energy lost by $\lambda 3889$ in the branching decay $3^3P \rightarrow 3^3S$ will be the same regardless of where the $\lambda 3889$ photons originate, and of this energy loss, 55% becomes $\lambda 7065$ radiation. The percentage increase of $I(\lambda 10830)$ by this process is negligible compared to the increase due to $2^3S \rightarrow 2^3P$ excitations. The energy added to the $\lambda 3889$ radiation field is $q(2^3S \rightarrow 3^3P)N_eN(2^3S)h\nu_{3889}$, so the energy gained by $\lambda 7065$ compared to $I(\lambda 4471)$ is

$$\frac{0.55Pq(2^3S \rightarrow 3^3P)N_e\alpha(2^3S)N_eN(He^+)}{D \qquad \alpha(\lambda 4471)N_eN(He^+)} \frac{h\nu_{3889}}{h\nu_{4471}},$$

where P is the fraction of $I(\lambda 3889)$ that is lost by branching (compared to the recombination value) for a particular $\tau_0(\lambda 3889)$ and ξ. The values of $I(\lambda 7065)/I(\lambda 4471)$ are computed for each $\tau_0(\lambda 3889)$ at the required values of V(R) and T_e, with this additional energy, and an interpolation for R_2(observed) yields $\tau_0(\lambda 3889)$ and D_2.

The sensitivity of these methods to various effects will be treated later. It is noted that uncertainties in N_e, T_e, V(R), R_1, R_2 and $S(\lambda 5876)$ reduce the strength of conclusions based upon detailed correlations. The models can, however, distinguish discrepancies of a factor of 2

in the depopulation rates.

The collisional rate $q(2^3S \rightarrow 2^3P)$ has been computed as a function of T_e, assuming a Maxwell-Boltzmann distribution of electron velocities, from the cross sections reported by Burke et al (1967). For $T_4 = 1$ the value is noticeably smaller than that given by Osterbrock (1964), the relative values being 2.0 and 3.4. For $q(2^3S \rightarrow 3^3P)$ we must use Osterbrock's (1964) formula, and judging by the difference for 2^3P excitation, we expect to overestimate the 3^3P collisional excitation contribution to $I(\lambda 7065)$. Since it is generally quite small anyway, it should not affect the values of D_2 appreciably.

(c) A Reëvaluation of the Depopulation Rate Factors Entering D_t

(i) Collisional Deactivation Rates

The new close-coupling cross section calculations for collisional transitions between the He I (n = 2) states by Burke et al (1967) have been used (as in II-[b]) to compute the rates $q(2^3S \rightarrow 2^1S)$, $q(2^3S \rightarrow 2^1P)$ as functions of T_e. The resulting rates (some of which are given by Seaton [1968]) are distinctly higher than those used by Capriotti (1967c) in his comparison of the depopulation rates, e.g., $q(2^3S \rightarrow 2^1P) = 3.1\times10^{-8}\,cm^3\,sec^{-1}$, rather than $5.7\times10^{-9}\,cm^3\,sec^{-1}$ at $T_4 = 1$. We adopt the values shown in Figure 2,

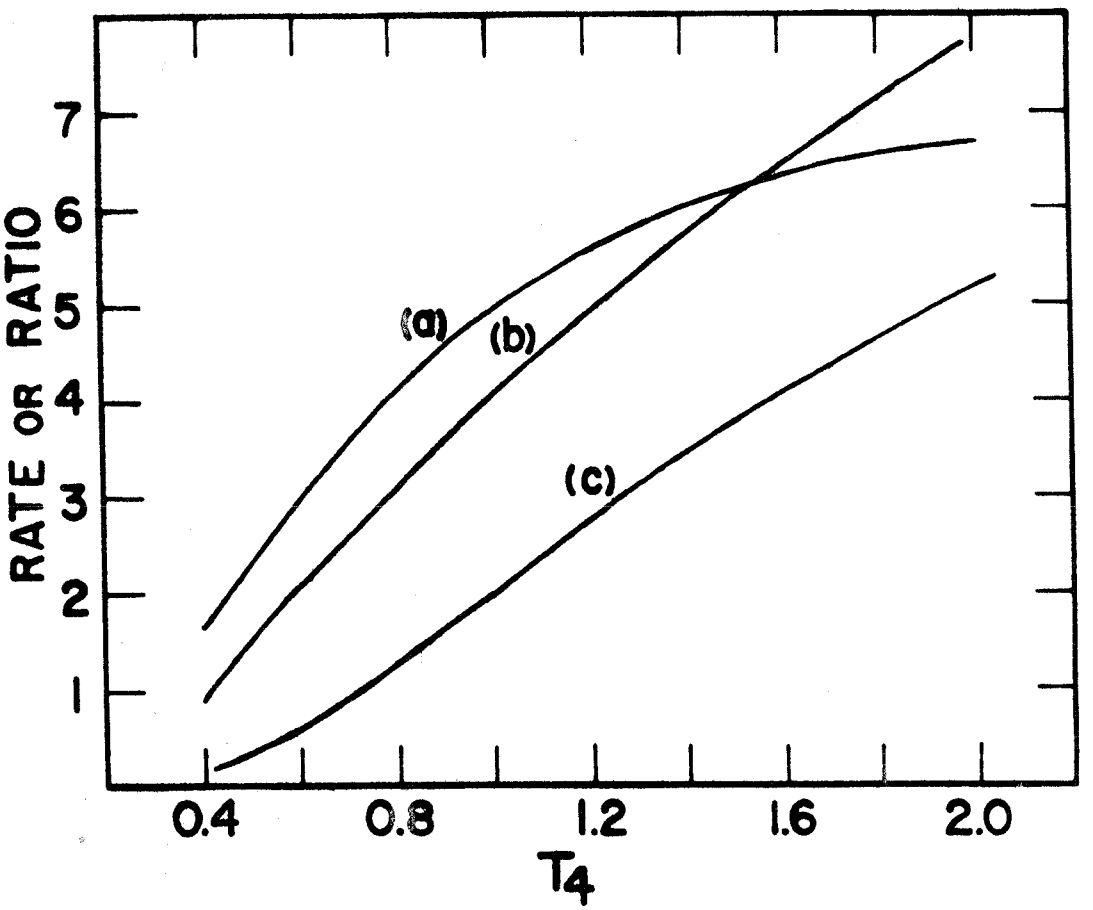

Fig. 2. - Collision rates and ratio as functions of $T_4 \equiv T_e \times 10^{-4}$. (a) $q(2^3S \rightarrow 2^1S + 2^1P + 1^1S) \times 10^8$, (b) $q(2^3S \rightarrow 2^3P)/q(2^3S \rightarrow \text{singlets})$, (c) $q(2^3S \rightarrow 2^3P) \times 10^7$. Rates are in units of $cm^3 sec^{-1}$.

computed for a Maxwellian distribution of electron velocities.

(ii) Radiative Decay

Recently Drake and Dalgarno (1968), and Dalgarno et al (1969) have found the two-photon decay rate $A(2^3S \rightarrow 1^1S) = 4\times10^{-9}sec^{-1}$, compared to the value of $2.2\times10^{-5}sec^{-1}$ found by Mathis (1957). Two-photon decay of He I 2^3S is thus negligible compared to spontaneous one-photon magnetic dipole decay. Griem (1969, 1970) reports $A(1\gamma) \sim 4\times10^{-5}$ sec^{-1}, but we adopt the more recent result of Feinberg and Sucher (1971): $A(2^3S \rightarrow 1^1S) = 1.2\times10^{-4}sec^{-1}$.

(iii) Stellar Ionization Rate

The ionization of 2^3S atoms by the nebular central star radiation was included in D_t by Capriotti (1967c) and was shown to make a small contribution for most, but not all, of the nebulae studied by him. The photoionization cross section $k_\nu(2^3S \rightarrow \text{continuum})$ given by Huang (1948) is used; the dependence of k_ν on frequency is such that for a given luminosity, cooler stars will depopulate 2^3S more rapidly. Approximating the central star as a black-body radiating at temperature T, the luminosity L_ν(erg sec^{-1} Hz^{-1}) is

$$L_\nu = 4\pi^2 R_S^2 B_\nu(T) \qquad \text{(II-6)}$$

where R_S is the stellar radius and

$$B_\nu(T) = \frac{2h\nu^3}{c^2} \frac{1}{[\exp(h\nu/kT)-1]} . \qquad \text{(II-7)}$$

For a nebula optically thin in the Lyman continuum (Lyc), the number of 2^3S ionizations in a spherical, homogeneous nebula of radius R is

$$\int_{4\pi} d\Omega \int_0^R r^2 \, dr \, \frac{N(2^3S)}{4\pi r^2} \int_{\nu_I}^{\nu(He)} \frac{L_\nu}{h\nu} k_\nu \, d\nu \quad , \qquad \text{(II-8)}$$

where ν_I corresponds to the 2^3S ionization energy of 4.76 eV(2600.7 A). This gives for the volume-averaged stellar depopulation rate

$$D_* = \frac{6\pi}{c^2}\left(\frac{R_S}{R}\right)^2 \times \int_{\nu_I}^{\nu(He)} \frac{k_\nu \, \nu^2}{[\exp(h\nu/kT)-1]} d\nu, \qquad \text{(II-9)}$$

where $\nu(He)$ is the Lyman limit for He^+, $\lambda 228$. For a nebula optically thick in the Lyman continuum, a factor $\exp[-\tau_\nu(r)]$ must be included under the integral sign for $\nu > \nu_c$(Ly limit) in equation (II-9), where $\tau_\nu(r)$ is the optical depth at frequency ν at a distance r from the central star. As shown in Chapter V the stellar depopulation rates are small ($\sim$ 5% of total) for most nebulae, the notable exception being BD+30°3639. For the other objects, the assumptions of stellar black-body spectra, homogeneity, and small Lyc optical depth are justified. The depopula-

ting effect of the diffuse Lyc radiation may be neglected in comparison to the Lyα radiation trapped inside the H II region, since every Lyc photon eventually becomes a Lyα photon plus other photons, and the mean Lyα photon spends a time $f_\alpha R/c$, $f_\alpha >> 1$, in the H II region.

We use the values of T, R_S and R given by Seaton (1966). The new value of F(Hβ) for BD+30°3639 reported by O'Dell and Terzian (1970) has been used to recalculate the necessary parameters; since F(Hβ) enters the computation weakly, only small differences are introduced by the upwards revision of F(Hβ) by a factor of 30. Harman and Seaton's (1966) method of finding the parameters has been used for a few objects for which values of I(λ4686) were not available in 1966.

The effect of a homogeneous distribution of ν-independent opacity (e.g., dust grains) inside the nebula will be to multiply D_* by $(1 - e^{-\tau})/\tau$, where τ is the radial (dust) optical depth.

(iv) H I Lyα Ionization Rate

The role of H I Lyα in the depopulation rate D_t and its effect upon nebular dynamics has generated much interest recently. Münch (1964) suggested that the increase in the Lyα energy density due to the trapping of the radiation might be enough to explain the low values of $N(2^3S)$

generally believed to exist in gaseous nebulae. As shown by O'Dell (1965), the essential features of the mechanism are the following. Recombination of H^+ to H I (2^1P) produces a Lyα photon which has a short mean-free-path ℓ in the nebula. If all the Lyα eventually escapes by diffusion in frequency away from line center, and this process requires Q resonance scatterings, then the mean distance travelled by a Lyα photon in units of the nebular radius R is

$$f_\alpha = \frac{Q\ell}{R} . \qquad \text{(II-10)}$$

The number of Lyα photons produced per cm^3 per sec is $\alpha(Ly\alpha)N_eN(H^+)$ so that He I (2^3S) is ionized at the rate

$$D_\alpha = \alpha(Ly\alpha)N_eN(H^+)f_\alpha k_\alpha R , \qquad \text{(II-11)}$$

where $k_\alpha = 1.5\times10^{-18} cm^2$ is the 2^3S photoionization cross section at λ1216. Rather than use deduced values of N_e and R, we may use the Hβ surface brightness, modifying equations (II-3), (II-4), and (II-5) to obtain

$$D_\alpha = \frac{\alpha(Ly\alpha)}{\alpha(H\beta)} \frac{3S(H\beta)}{h\nu_\beta} k_\alpha f_\alpha . \qquad \text{(II-12)}$$

This equation is approximately correct for non-homogeneous nebulae also, since the ratio $\alpha(Ly\alpha)/\alpha(H\beta)$ does not change rapidly with N_e or T_e. For high density objects, there is

a contribution to the population of 2^1P from collisional excitation $2^1S \rightarrow 2^1P$. The probability p that an H^+ recombination to H I 2^1S leads to a collisional excitation of 2^1P and the subsequent emission of Lyα is

$$p = \frac{N_e q(2^1S \rightarrow 2^1P)}{A(2^1S \rightarrow 1^1S)+N_e q(2^1S \rightarrow 2^1P)} \times \frac{A(2^1P \rightarrow 1^1S)}{A(2^1P \rightarrow 1^1S)+N_e q(2^1P \rightarrow 1^1S)} .$$

Using the numerical values for the rates listed by Seaton (1958): $q(2^1S \rightarrow 2^1P) = 5.3\times10^{-4} cm^3 sec^{-1}$, we can find p for any N_e. The number of scatterings Q of a Lyα photon is bounded above by the reverse process, i.e., $Q(max) = 1/\eta$ where η is the probability per population of 2^1P by recombination or resonance absorption that two-photon decay will occur following collisional deexcitation $2^1P \rightarrow 2^1S$. Since $\eta \sim 10^{-8}$ (Capriotti 1967b) and Q will actually be $<< 10^8$, this loss process for Lyα is unimportant, and we add the term $p\alpha(2^1S)$ to the recombination coefficient α(Lyα) in equation (II-12).

The main problem now is to estimate f_α. We are not assuming that the inferred depopulation rates specify f_α as O'Dell (1965) did; rather, we attempt to predict reasonable values of f_α for the nebulae. In order to keep the importance of these estimates in perspective, we emphasize post facto that the values of D_α are important ($> 0.2D_t$) only for objects of very high Hβ surface bright-

ness, and furthermore, if a nebula contains solid matter, the effect of Lyα on D_t is determined by the grains and not by f_α (see below). Several attempts have been made to estimate f_α for different model nebulae. Osterbrock (1962) considered a homogeneous, static, source-at-center sphere, of radial optical thickness τ_0 in the center of the Lyα line. Assuming complete redistribution over a pure Doppler profile, and by considering the probability per scattering that the photon is emitted at a frequency where the nebula is optically thin, one finds (Osterbrock 1962, O'Dell 1965)

$$Q = 1/\eta \simeq \tau_0(\pi \ln\tau_0)^{1/2} , \qquad \text{(II-13)}$$

$$\ell/R = 2(\ln\tau_0)^{1/2} / \tau_0 \pi^{1/2} , \qquad \text{(II-14)}$$

and

$$f_\alpha = 2\ln\tau_0 . \qquad \text{(II-15)}$$

At optical depths $\tau_0 > 1.8\times10^4$ photons may diffuse in the damping wings, and Capriotti (1965, 1967b) has refined the scheme to include the damping wings for several plane-parallel slab models of emitting gas. He also considers ionization-bounded slabs in order to derive f_α for the hypothetical case envisaged by O'Dell (1965), viz., a sizable increase in f_α may occur if a neutral hydrogen layer surrounding the ionized region scatters most of the Lyα back into the emitting volume. The possibility that the values of f_α needed to explain the difference between D_t and D_1 are actually attained in some nebulae is rejected by

Capriotti on the grounds that the resulting Lyα radiation pressure in the H II region would blow away the surrounding H I region on a time scale of 100 years. For this reason we shall consider only the pure H II region results of Capriotti.

The application of Monte Carlo techniques to the calculation of emergent line profiles, values of f_α and Q has been reported by Auer (1968). His models are static, homogeneous, isothermal slabs, with line center (total) optical depths $\tau_0 \leq 10^5$, and variable damping parameter. There being moderately good agreement for intermediate values of τ_0 (corresponding to reasonable Lyc optical depths in real nebulae), we have chosen to adopt Capriotti's methods and results for calculating f_α where needed, identifying his τ_0's with the radial τ_0's for spherical nebulae.

None of the models investigated in detail includes the effect of expansion. Capriotti (1965) has computed mean escape probabilities $\varepsilon (\equiv 1/Q)$ for such a case, and finds the general result that ε increases considerably with increasing expansion parameter V(R)/V(TH). Due to the insensitivity of f_α to V(R)/V(TH), and of D_t to D_α, however, we do not include these effects but use the values of f_α derived from Capriotti's (1967b) work. The Lyc optical depths τ_c, to which the required values of τ_0 are proportional ($\tau_0 = \tau_c \times 9350/\sqrt{T_4}$; Seaton 1960) are taken

from Capriotti (1967a). The values of τ_c for those nebulae not studied by Harman and Seaton (1966) have been derived using their method, and τ_c for BD+30°3639 has been recalculated. Harman and Seaton's (1966) values of τ_c fall in the range (τ_c[min], τ_c[max]) derived by Capriotti (1967a), and since f_α varies slowly with τ_0, the use of either τ_c or τ_c(max) is reasonable.

Consider now the effect of Lyα upon $N(2^3S)$ when a finite number of grains exist within the H II region. If the number density of grains N_d is uniform, the radial optical depth for absorption by dust at λ1216 is

$$\tau_d = N_d \kappa_d R \ . \qquad \text{(II-16)}$$

Suppose that the average Lyα photon would undergo Q scatterings before escape in the absence of any absorbers. It would thus travel a physical distance $f_\alpha R$ before escape. In the presence of dust, the average Lyα energy density is found by integrating the instantaneous energy density over the path $f_\alpha R$. This assumes that escape from the nebula would be the eventual fate of every Lyα photon were it not for the dust; i.e., the "quenching" (two-photon conversion) time scale is long compared to $f_\alpha R/c$. The mean energy density is then proportional to a factor Ξ:

$$\Xi = \frac{1}{f_\alpha R} \int_0^{f_\alpha R} \exp(-\tau_d r/R)\, dr$$

$$= (1 - \exp[-f_\alpha \tau_d])/f_\alpha \tau_d \ , \qquad \text{(II-17)}$$

so that the mean Lyα depopulation rate given by equation (II-12) is ΞD , and redefining D_α gives

$$D_\alpha = \frac{\alpha(Ly\alpha)}{\alpha(H\beta)} \frac{3S(H\beta)}{h\nu_\beta} k_\alpha \frac{(1-\exp[-f_\alpha \tau_d])}{\tau_d}, \qquad \text{(II-18)}$$

an equation valid for all τ_d. The process of Lyα scattering by the dust grains is assumed not to influence the character of the Lyα radiation field in any way. Equation (II-18) shows that the dependence of D_α on f_α is essentially removed if $f_\alpha \tau_d > 2$. For some nebulae this may occur, in which case a sizable fraction of the energy input to the grains may come from Lyα. The energy balance of the grains is discussed in Chapter IV.

(v) Excitation Transfer Reactions

Consider the depopulation of He I (2^3S) by the process

$$He(2^3S) + \chi \rightarrow He(1^1S) + \chi^* \ ,$$

$$\chi^* \rightarrow \chi + h\nu \ ,$$

where χ is some ground state atom or ion which possesses an excited state (*) as far above ground as He I (2^3S) lies above He I (1^1S). The wave number difference ω = 159850.318 cm^{-1}(Moore 1949) and the finite width of the 2^3S level,

assumed to be $\Delta\omega \sim 10^{-4}\omega$, serve to place limits on the range of ω for χ^*. Cl^+, the only possible candidate, has an energy level 159840.3 cm^{-1} above ground in the $4s\,^3P_0$ state. The depopulation rate will be $D(Cl) \simeq N(Cl^+)\sigma\upsilon$, where σ is the (unknown) reaction cross section, and υ is the average relative velocity. Assuming a solar abundance of Cl (Allen 1964), and that all Cl is Cl^+, and taking $\upsilon \sim 10^6$cm/sec, $N_e \sim 10^4 cm^{-3}$, we find that in order to compete with one-photon radiative decay, σ must be > $6\times10^{-9}cm^2$. Cross sections of this sort are not likely to be $>10^{-12}cm^2$ however, so this mode of deactivation is completely negligible.

(vi) Penning Ionization

The Penning ionization process

$$He(2^3S) + \chi \rightarrow He + \chi^+ + e^- ,$$

where χ is any atomic system with IP < 19 eV has been studied by Bell, Dalgarno and Kingston (1968), who give the cross section σ for the reaction:

$$\sigma = 1.15\times10^{-14}(C/T)^{1/3}\ cm^2,$$

where C is an experimentally determined constant for each species χ. For H°, C = 87 and the lifetime against this process is $\sim 5\times10^8/N(H^\circ)$ sec (T_4 = 1), which is >> radiative lifetime in a typical H II region. For neutral oxygen,

Bell et al (1968) give the 2^3S Penning ionization rate coefficient K_p. At $T_4 = 0.3$, $K_p(0) \sim 6\times10^{-10}\,cm^3\,sec^{-1}$, so the neglect of these processes is justified for planetary nebulae.

(vii) Autoionization

Robbins (1968c) has suggested that excitation of doubly excited autoionizing states of He by central star line emission may contribute to the 2^3S depopulation rate. His order-of-magnitude calculations show that it is very difficult to estimate reasonable rates for these processes, and that there exist no positive observational tests. Robbins concludes that for most objects the autoionizing rate should compete with two-photon emission, i.e., $2\times10^{-5}sec^{-1}$(old value) and should be larger for compact objects. Since this depopulation rate is so uncertain, it has been omitted in favor of looking for the suggested correlations.

It should be pointed out that Robbins' view that good agreement obtains for the rates D_1 and D_2 is not shared by Capriotti (1967c).

(d) Effects Which Act Upon λ10830 Radiation

Previous work on the interpretation of the ratio R_1 in the nebulae has largely ignored effects which may

(selectively) alter the flux of λ10830 radiation received at the earth. These mechanisms are collected here for the sake of completeness; some may be important, others are completely negligible.

(i) He(2^3S) in the Upper Atmosphere

Calculations by Ferguson and Schluter (1962) give for the column density of He(2^3S) $5\times10^6\,cm^{-2}$. The λ10830 absorption coefficient at line center is $\sim 10^{-12}\,cm^2$, so that τ(absorption) $< 10^{-6}$.

(ii) Interstellar He(2^3S)

The density N(2^3S) in interstellar space is determined by the lifetimes against single-photon decay and Penning ionization by hydrogen, and the He^+ density which in turn depends upon the cosmic ray flux at the relevant energies. Even in a H° cloud of density N(H) = $10^3\,cm^{-3}$, $\upsilon = 10^6$ cm/sec, and the Penning process ionization rate of $10^{-5}\,sec^{-1}$ does not compete with one-photon decay of 2^3S. Rees, Sciama, and Stobbs (1968) use a minimum cosmic ray ionization rate for He° of $R_{min} \sim 1.5\times10^{-17}\,sec^{-1}$. They estimate that the true rate yR_{min} may be $\sim 170\ R_{min}$ so that statistical equilibrium gives

$$N(He^\circ)yR_{min} = (4/3)\ N(2^3S)A(2^3S \rightarrow 1^1S)\ ,$$

or

$$\frac{N(2^3S)}{N(He^o)} \sim 10^{-13}y.$$

Assuming $N(He^o) = 0.1 \times N(H) = 0.1\ cm^{-3}$, the λ10830 line center optical depth for an object 1 kpc away would be $\tau_0 \sim 0.4 \times 10^{-3}y$ for $T = 100^oK$. The absorption profile is smeared out by galactic rotation and random cloud motions however, and for a line width of 0.6 km/sec in a particular cloud, a velocity dispersion of 10 km/sec reduces τ_0 by a factor of 15, so that the effective $\tau_0 \sim 3 \times 10^{-5}y$ and interstellar attenuation of λ10830 is likely to be unimportant. For very distant objects, however, we shall keep this effect in mind when looking for correlations of R_1 with nebular parameters.

(iii) He I 2^3P Leakage Loss

A large optical depth $\tau_0(\lambda 10830) > 100$ will lead to repeated resonance scatterings of λ10830 photons as they diffuse in space and frequency until they escape the H II region. Since the λ10830 upper state 2^3P may decay via a single photon spin-forbidden transition (through the spin-orbit interaction) at a rate $A(2^3P \rightarrow 1^1S) = 199\ sec^{-1}$ (Dalgarno and Drake 1968), a sufficiently large number of λ10830 scatterings will provide a means of quenching the radiation in a manner somewhat analagous to the Lyα two-photon conversion process. The probability per photon

scattering of loss by this decay mode is the branching ratio $T = A(2^3P \rightarrow 1^1S)/A(2^3P \rightarrow 2^3S) = 1.945\times10^{-5}$, so that the probability of being scattered Q times without loss is $P = (1-T)^Q \sim \exp(-TQ)$. Since T is so small, $\tau_0(\lambda 10830)$ and Q must be large in order for this loss mechanism to be non-negligible. The evaluation of Q is discussed in Appendix 2; the resulting loss rate may then be added to the dust absorption loss rate discussed below.

(iv) Dust Absorption Loss

The basic mechanism of resonance radiation trapping and loss on dust grains has been discussed by Robbins (1970a) and Persson (1970), and by Münch and Persson (1971) with reference to the Orion Nebula. The mean λ10830 photon will traverse a distance $f_1 R(cm)$ before escaping the nebula; the parameter f_1 depends upon the line-center radial optical depth $\tau_0(\lambda 10830)$, the velocity field, and the geometry. The emergent intensity will be attenuated by a factor $\exp(-f_1\tau_d)$ where τ_d is the radial dust optical depth at λ10830. Equation (II-15) becomes $f_1 = 2\ln\tau_0(\lambda 10830)$ for zero damping parameter. A comparison of Auer's (1968) and Capriotti's (1967b) values of $f(\tau)$ shows that Auer's values are somewhat larger than Capriotti's for $10 \leq \tau_0 \leq 10^4$; for $\tau_0 = 10$ (through the slab) they differ by more than a factor of 2. Derived values of f_1 for more realistic models are thus bound to be uncertain.

In Appendix 2 are given the results of calculations of f_1 for homogeneous expanding spheres. This modification of Osterbrock's (1962) method includes the fine structure of the λ10830 emission line.

Assuming that the values of f_1 can be predicted to 50% accuracy, we can relate the expected attenuation of λ10830 radiation to the infrared emission of the nebulae, given some model for the grain characteristics and spatial distribution. Infrared excesses over the expected free-free continuum and line emission fluxes have been reported for several nebulae by numerous authors (further details and references will be found in Chapter IV). If the particles are assumed to radiate like inefficient black-bodies, flux measurements at two wavelengths determine a color temperature T_c. The absorption efficiency $Q(a,\lambda)$ for a spherical grain is given by (Wickramasinghe 1967)

$$Q_{abs}(a,\lambda) \equiv Q(a,\lambda) = -4\,\frac{2\pi a}{\lambda}\,\mathcal{I}_m\left[\frac{m^2-1}{m^2+2}\right] + \ldots \qquad \text{(II-19)}$$

for $2\pi a/\lambda \ll 1$. The grains are assumed homogeneous with complex refractive index m, and if $a \lesssim 10^{-5}$cm, equation (II-19) is valid for $\lambda \gtrsim 3\mu$. In any case $Q_{abs}(a,\lambda)$ may be evaluated for any a and λ, using the expansion formulae of Wickramasinghe. At the wavelengths of interest,

$$Q(a,\lambda) = 2\pi a_\mu p/\lambda_\mu^2 \qquad \text{(II-20)}$$

where p is a factor near unity which depends upon the detailed electromagnetic properties of the grain material. Since the grains radiate with the efficiency $Q(a,\lambda)$, the flux per unit frequency interval from a single grain at temperature T_d is

$$E_\nu(a,\lambda) = \frac{2\pi a_\mu}{\lambda_\mu^2} p\, B_\nu(T_d)\, 4\pi^2 a^2, \qquad \text{(II-21)}$$

and the color temperature determined by the observed fluxes F_{ν_1} and F_{ν_2} at λ_1 and λ_2 is given by

$$\frac{F_{\nu_1}}{F_{\nu_2}} = \left(\frac{\nu_1}{\nu_2}\right)^5 \frac{[\exp(h\nu_2/kT_c)-1]}{[\exp(h\nu_1/kT_c)-1]} . \qquad \text{(II-22)}$$

We expect temperatures of 300°K or less judging by the published spectra, and since we use observations at $\lambda \leq 12.5\mu$, equation (II-22) becomes

$$T_c(\lambda_1,\lambda_2) \doteq 6.25\times10^3 \left(\frac{1}{\lambda_2} - \frac{1}{\lambda_1}\right)[5 \log(\lambda_1/\lambda_2) + \log(F_{\nu_1}/F_{\nu_2})]. \qquad \text{(II-23)}$$

[1]

The simplest case is that of a uniform temperature dust sphere coincident with the H II region, so that, identifying $\langle T_c\rangle$ ($T_c[\lambda_1,\lambda_2]$ averaged over all pairs λ_1,λ_2) with T_d, we obtain, for the flux at the earth,

$$F_\nu(a,\lambda) = 4\pi^2 a^2 Q(a,\lambda)\, B_\nu(\langle T_c\rangle) N_d \frac{(4/3)\pi R^3}{4\pi s^2}, \qquad \text{(II-24)}$$

where s is the distance. The optical depth in the dust at λ10830 is

$$\tau_d(\lambda 10830) = N_d \pi a^2 Q(a, 1.083\mu) R, \qquad \text{(II-25)}$$

and may be determined by combining equations (II-24) and (II-25):

$$F_\nu(a,\lambda) = \frac{4\pi}{3} \tau_d(\lambda 10830) \frac{Q(a,\lambda)}{Q(a,1.083\mu)} B_\nu(\langle T_c \rangle) \theta^2, \qquad \text{(II-26)}$$

where θ is the angular radius (in radians) of the object, assumed equal to the optical radius (e.g., in λ5876). The values of τ_d found in this way for objects observed at the infrared wavelengths of interest are given in Chapter IV. For those objects which have not been observed, we take an exploratory point of view in assigning them theoretical values of T_c, determining the values of $\tau_d(\lambda 10830)$ required to fit the depopulation rates D_t and D_l, and predicting the infrared fluxes.

The ratio of the absorption efficiencies $Q(a,\lambda)/Q(a,1.083\mu)$ is a parameter which varies as $(10830/\lambda)^2$ for small particles ($a \lesssim 0.1\mu$) in the Mie theory (equation [II-10]). For larger particles the expansion formulae of Wickramasinghe (1967) must be used, but this procedure is not followed. Due to uncertainties in θ, the spatial dust distribution, the particles' shape, composition and size

distribution, any further refinements are unwarranted at this time.

(e) The Effect of Dust Upon I(λ7065)

The dust optical depths we consider produce attenuation of the nebular light at optical wavelengths, but are not likely to produce a direct observational effect. The asymmetrically split [N II] line profiles reported by Osterbrock et al (1966) and Osterbrock (1970) are attributed by him to density inhomogeneities.

More important is the resonance dust absorption of λ3889. Suppose that each λ3889 resonance-like photon created travels an effective (1/e) distance, in the absence of dust, $f^*_{38}R \equiv Q^*\ell_{38}$ (cf., equation [II-10]) before it is degraded to 4.29μ, λλ7065, 10830. If it were not so degraded, it would travel a distance $f_{38}R = Q_{38}\ell_{38}$ before escaping the nebula. Since the ratio of the mean-free-path to the radius, ℓ_{38}/R, enters both these expressions, one may solve for $f^*_{38} = Q^*_{38}f_{38}/Q_{38}$. Given τ_0(λ3889) and V(R)/V(TH), we use Capriotti's (1965) escape probabilities for $1/Q_{38}$, and the values of f computed in Appendix 2. For Q^*_{38} we note that the λ3889 branching ratio $T = A(3\,^3P \rightarrow 2\,^3S)/[A(3\,^3P \rightarrow 2\,^3S) + A(3\,^3P \rightarrow 3\,^3S)]$ is related to the emergent λ3889 flux from Robbins' models by

$$T^{Q^*_{38}} = I(\lambda3889)/I(\lambda3889;\ \tau_0 = 0).$$

Thus f^*_{38} is found, and the mean λ3889 energy density is reduced by $\{1-\exp[-f^*_{38}\tau_d(\lambda3889)]\}/f^*_{38}\tau_d(\lambda3889)$.

If $\tau_0(\lambda3889)$ is large, the λ3889 photons will be converted to λ7065 (plus 4.29μ, plus λ10830) before they can be significantly attenuated by the dust. This was found to be the case for parts of the Orion Nebula studied by Münch and Persson (1971). Since $\tau_0(\lambda3889)$ will be < 50 for most nebulae, we find, for example, for $\tau_0(\lambda3889) = 10$, λ3889 decreases by 22% for $\tau_d(\lambda3889) = 0.10$, and the loss to λ7065 (V[R]/V[TH] = 3, $T_4 = 1$) is ∿ 10%. This effect is included in the prediction of D_2 from R_2.

(f) Summary of Chapter II

The aim of this chapter has been to set down the equations and arguments which pertain to the interpretation of the observations used in deriving D_t, D_1 and D_2 for homogeneous isothermal model nebulae. Inhomogeneous models are considered in Chapter VI. Simple models used to predict f_1 and f_{38} are explored in Appendix 2, and further comments on the nature of the postulated grains and the derived color temperatures for objects observed in the infrared are given in Chapter IV.

III. OBSERVATIONS

(a) Introduction

In order to extend the number of observed planetary nebulae used in a comparison of the depopulation rates D_1, D_2 and D_t, observations of over 30 objects were made during the summers of 1969 and 1970. Due to the faintness of the nebular He I lines (and the low quantum efficiency of photo-surfaces in the $\lambda\lambda$7065, 10830 spectral regions) interference filters rather than a grating scanner were used. All observations were made with filters mounted in the X-Y photometer base attached to the f/16 Cassegrain focus of either the 100-inch or 60-inch Mt. Wilson reflectors. At the outset it was hoped that the fluxes F(λ5876) and F(λ7065) measured as functions of radial distance from the centers of the nebulae would give insight into the spatial trend of the depopulation rates D_2 and D_t. The results of this work are interesting, and can be interpreted in terms of schematic nebular models; but quantitative analysis is subject to over-interpretation in view of the nebular velocity field, variations in N_e and T_e, and morphology. The integrated line fluxes F(λ5876), F(λ7065) and F(λ10830) and the integrated continuum fluxes at $\lambda\lambda$6067, 6950 (used to correct the $\lambda\lambda$5876, 7065 measures for the radiation of the underlying continuum plus central star, if present) were obtained for over twenty nebulae.

For some objects a sky chopping system was used, but for most objects the chopper entrance apertures were too small to include the entire nebula at the scale of the 100-inch Cassegrain focus; and since a chopper could not be used on the 60-inch, the sky was measured several times during the observation of a particular object, and interpolations (usually small) for the sky counting rates at the times of the nebular observations were made. Reduction of the raw counts into units of erg cm^{-2} sec^{-1} Hz^{-1} was accomplished in the usual manner, viz., by the observation of a number of standard stars, and correction for atmospheric attenuation. The standard star fluxes were provided by Oke (1969, 1970; private communication) and conform to Oke and Schild's (1970) calibration of Vega. The "standard atmosphere" was also provided by Oke. Since the observations are in the red, the atmospheric attenuation is not overly important; the accuracy was reduced more by temporal changes in the extinction, impossible to correct for completely, than by the dependence of the attenuation on zenith secant distance. Whenever possible, objects were observed near the meridian, and for these reasons, second-order corrections to the attenuation were not made. Repeatability of fluxes showed that this was a reasonable procedure. Tables 1 and 2 give the details on the phototubes and filters used. Columns 1 through 5 of Table 2 give, respectively, the wavelength, bandwidth (BW in Ang-

TABLE 1

PHOTOTUBES

λ	TYPE	PHOTOSURFACE	MT WILSON COLD BOX	DATE
5876	ITT FW130	S-20	V9	1969
5876	ITT FW130	S-20	V1	1970
10830	RCA 7102	S-1	V2	1970

TABLE 2

FILTERS

λ	BW (A)	%T	FWHM (A)	1 + f(λ)
5876	33.5	61	50	0.766
6067	91.6	60	145	0.728
6950	24.7	68	33	0.563
7065	29.9	45	55	0.542
10830	23.6	72	29	0.142

TABLE 3

SPECIAL APERTURES

NAME	ARC SEC I. R. (100-INCH CASS)	ARC SEC O. R.
Q	12.4	14.0
R	10.3	12.0
S	8.3	10.0
T	6.2	8.0
U	4.2	6.0
V	2.2	4.0
SKY		18.0

TABLE 4

SPECIAL APERTURES FOR NGC 6720

NAME	ARC SEC I. R. (60-INCH CASS)	ARC SEC O. R.
K2	(VIGNETTED)	
M2	30.6	37.0
O2	23.7	30.1
Q2	17.2	23.4
S2	10.0	16.7

stroms equivalent width), the percent transmission at λ (T), the full-width at half maximum, and the interstellar absorption parameter [1 + f(λ)] taken from Seaton (1960). The intrinsic flux is found by multiplying the observed flux by $10^{C[1 + f(\lambda)]}$ where C is $\Delta \log_{10}(H\beta)$, the logarithmic extinction at Hβ. The values of C are from Kaler (1970). The λ7065 filter is actually a λ7090 filter tipped $8^{\circ}.85$ to shift the peak. The transmissions of all filters were measured several times on a Cary 14 spectrometer. A precision micrometer laser mirror/filter holder (Oriel Optics Corp.) was mounted in the light path to check the effect of the non-parallel (f/16) incident light, and to duplicate the beam incident on the λ7065 filter. Measurements at several angles of incidence were used to integrate (over the primary mirror surface) each line filter response. This procedure is unnecessary for the continuum filters; and since only the ratio BW/T is important for line filters, a λ-independent change in the filter response does not affect the results. Since the $\lambda\lambda$5876 and and 7065 filters were almost flat and smoothly varying at the relevant wavelengths, shifts of the lines or filter responses were unimportant. (The λ10830 filter is discussed in Section III-[e]). The reduction of the line fluxes was effected in the following manner: the net counts in each color were converted to fluxes and corrected for interstellar extinction. For the range of nebular

electron temperatures encountered, the theoretical atomic continuum flux is smoothly varying and nearly flat between λλ5876 and 7065. The observations confirm this behavior for most objects and thus a linear extrapolation of the λλ6067, 6950 fluxes (star plus continuum) to the wavelengths λλ5876, 7065 was made. Subtraction of this continuum, conversion to erg $cm^{-2}sec^{-1}$ A^{-1} and multiplication by BW/T then gives the line fluxes in erg cm^{-2} sec^{-1} required for D_1 and D_2. This procedure is equivalent to the reduction of scanner observations of nebular emission lines. The line fluxes include central star emission lines, and for a few objects (e.g., BD+30°3639, NGC 40) this limits the reliability of the R_1 and R_2 determinations. The continuum in the λ10830 band was not subtracted due to the strength of the λ10830 line and the weakness of the underlying continuum beyond the Paschen jump. This correction amounts to ∿ 1% in most cases; the correction to F(λ5876) due to the continuum was typically 25-30%.

The weather was found to be a major source of annoyance: water vapor and smog from Los Angeles, and forest fire ash reduced the number of usable nights considerably below that to be expected given only natural observing hazards. The observations are thus neither as extensive nor as accurate as had been hoped. In the following sections are given the results and details of the observations.

(b) Special Aperture Observations

A set of special apertures was constructed so that the radial dependence of R_2 could be determined for large approximately circular planetaries. The apertures were made by supporting a circular stop inside a larger circular aperture by means of narrow struts. The outside radius of the annular aperture thus formed was approximately equal to the inner radius of the next larger one. Both the apertures and stops were punched out of 0".010 bronze sheet, and were assembled using a Grant measuring engine to insure proper centering. It was found that the resulting apertures had clean edges and that the supporting struts obscured less than 3% of the light in all cases. The relative open areas were determined by measuring the night sky brightness, and were found to agree well with the computed areas. This method is preferable to the measurement of difference in the flux admitted through a series of open circular apertures, since the central star is always eliminated; and the 1% photon-statistical confidence level is reached in less time, especially for sources brighter at the center. In a typical observation, the object was centered and a field star was located for offset guiding. Periodically the sky brightness in each color was measured with a circular aperture, and the relative areas were calibrated on open sky. The total integration time was chosen

to insure that the accuracy was not limited by counting statistics.

The surface brightnesses $I(\lambda)$, (erg cm^{-2} sec^{-1} [arc sec]$^{-2}$), were than found using the known aperture areas and the method of reduction described in Section III-(a). At the end of all observations the values of $I(\lambda)$ were averaged together weighting each measurement by the inverse square of its associated standard error. The objects NGC 6826 and NGC 7662 were measured most often, and a plot of the observations of NGC 6826 is given in Figure 3 to illustrate the degree of repeatability attained. Much of the noise is caused by seeing variations.

If it is assumed that the nebulae are spherically symmetric (this is implicit in the averaging by the annular apertures) and that the emissivity $E(\lambda,r)$ depends only upon r, the radial distance to the center, then the surface brightness observations may be inverted to yield $E(\lambda,r)$. The procedure used depends upon the fact that the intersection of a sphere and a cylinder whose axis passes through the center of the sphere is an analytic function of two variables, their respective radii. If $E(\lambda,e)$ is assumed constant in concentric shells e of radii e_1, e_2 ($e_1 < e_2$), the volume common to a particular shell and a cylindrical shell defined by the inner and outer radii d_1, d_2 of the aperture projected on the sphere, multiplied by

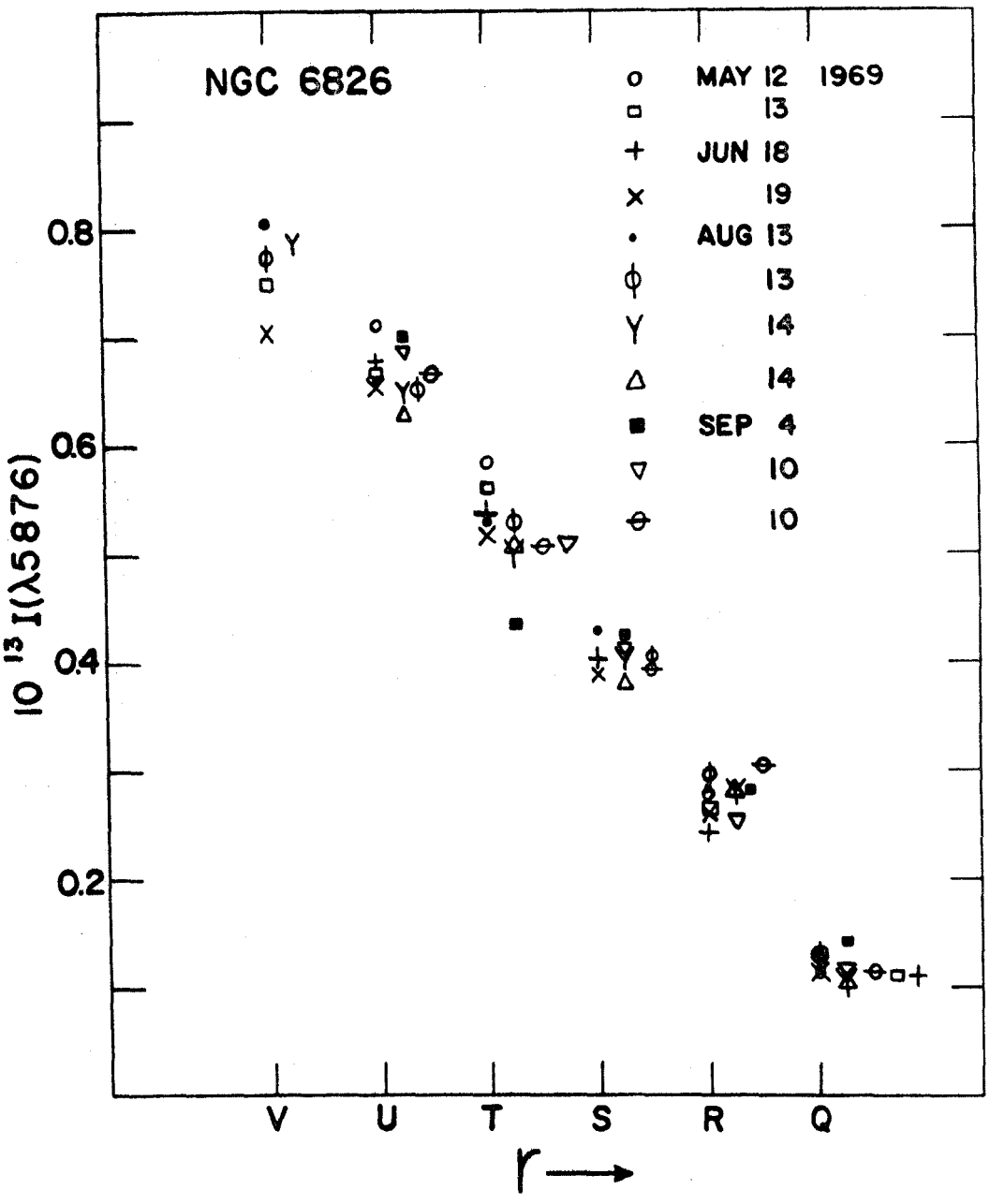

Fig. 3. - Plots of λλ5876, 7065 surface brightnesses in erg cm^{-2} sec^{-1}(arc sec)$^{-2}$ vs. projected radius for NGC 6826, illustrating degree of repeatability. Symbols have been displaced horizontally for clarity. Aperture Q is at r = 13 arc sec.

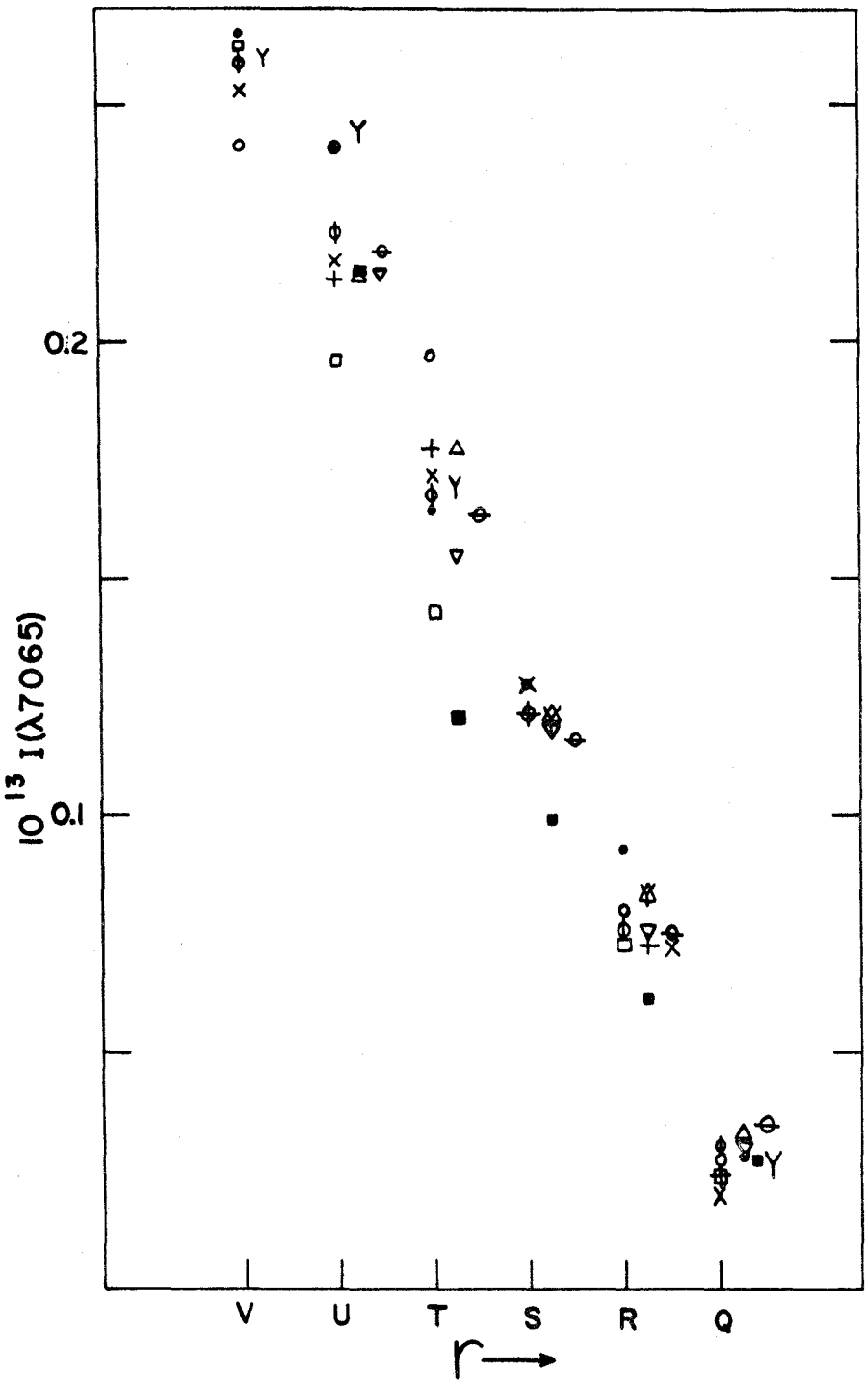

Fig. 3. - Continued.

$E(\lambda,e)$ gives the flux contribution of that shell to the surface brightness measured by the aperture. If this volume is $G(d,e)$, then

$$G(d,e) = \sum_{i,j=1,2} G(d_i,e_j)\ (-1)^{i+j}$$

where

$$G(d_i,e_j) = \frac{4\pi d_i^3}{3}\left\{1-[1-(e_j/d_i)^2]^{3/2}\right\} \quad \text{if } e_j \le d_i$$

$$= \frac{4\pi d_i^3}{3}, \qquad \text{if } d_i \le e_j,$$

and the surface brightness $I(\lambda,d)$ is found from

$$\pi(d_2^2-d_1^2)\ I(\lambda,d) = \sum_e G(d,e)\ E(\lambda,e).$$

This tridiagonal matrix equation is easily solved for $E(\lambda,e)$. No further refinements have been made due to the uncertainty of assuming spherical symmetry. Nebulae with clearly toroidal components cannot be inverted (e.g.: NGC 7662, NGC 6720) and only the uninverted results are given. The results are shown in Figure 4 for all nebulae observed in 1969. The units are erg cm^{-2} sec^{-1} $(arc\ sec)^{-3}$, since the coefficients G were computed in $(arc\ sec)^3$, and can be converted to erg cm^{-3} sec^{-1} if the distance s is known, by multiplying $E(\lambda,e)$ by $4\pi(206265)^3/s$.

The measures of the continuum show much the same be-

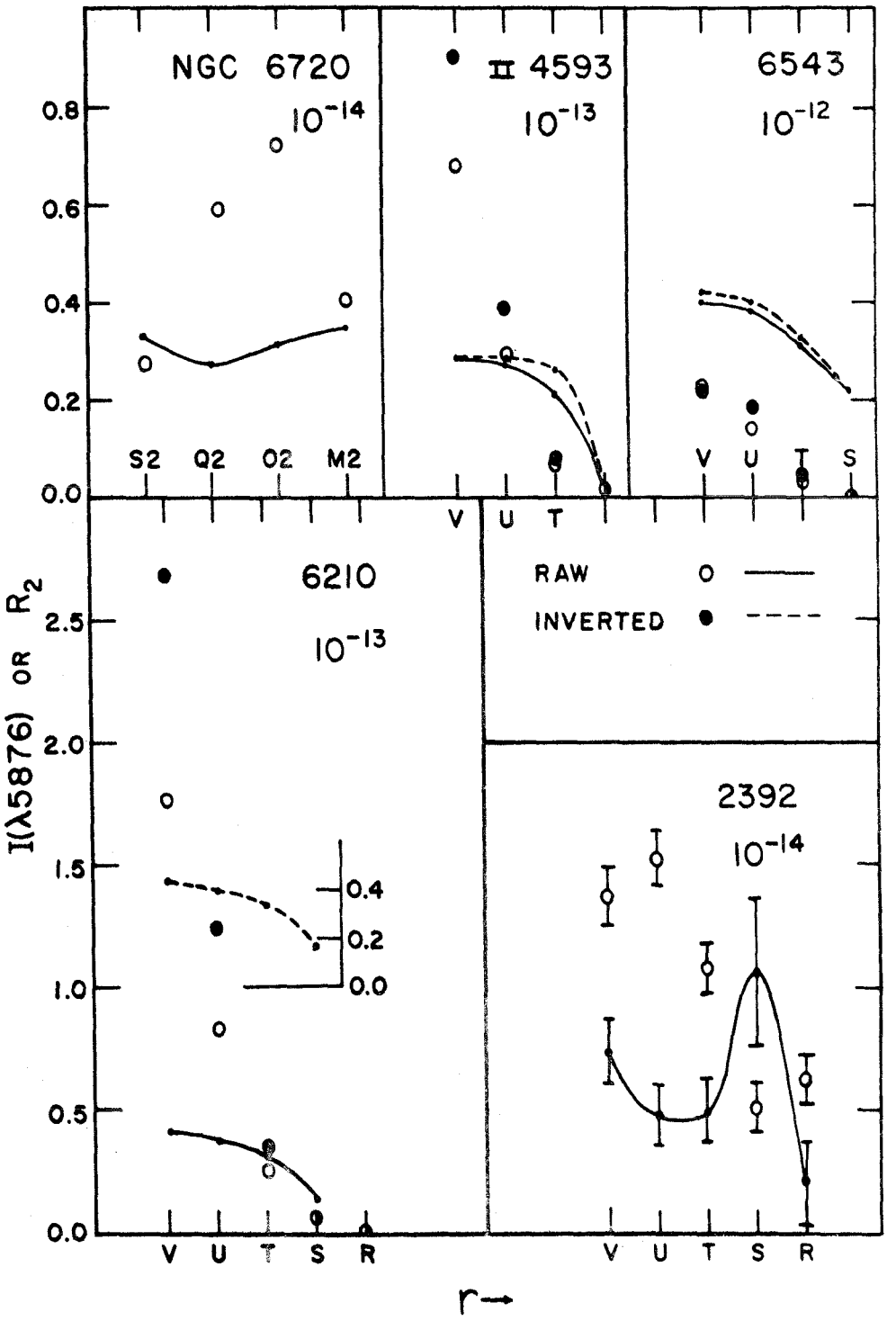

Fig. 4. - Plots of λ5876 surface brightness in units of erg cm^{-2} sec^{-1} $(arc\ sec)^{-2}$ and R_2 vs. projected radius for objects observed in 1969. Factor by which I(λ5876) scale is to be multi-

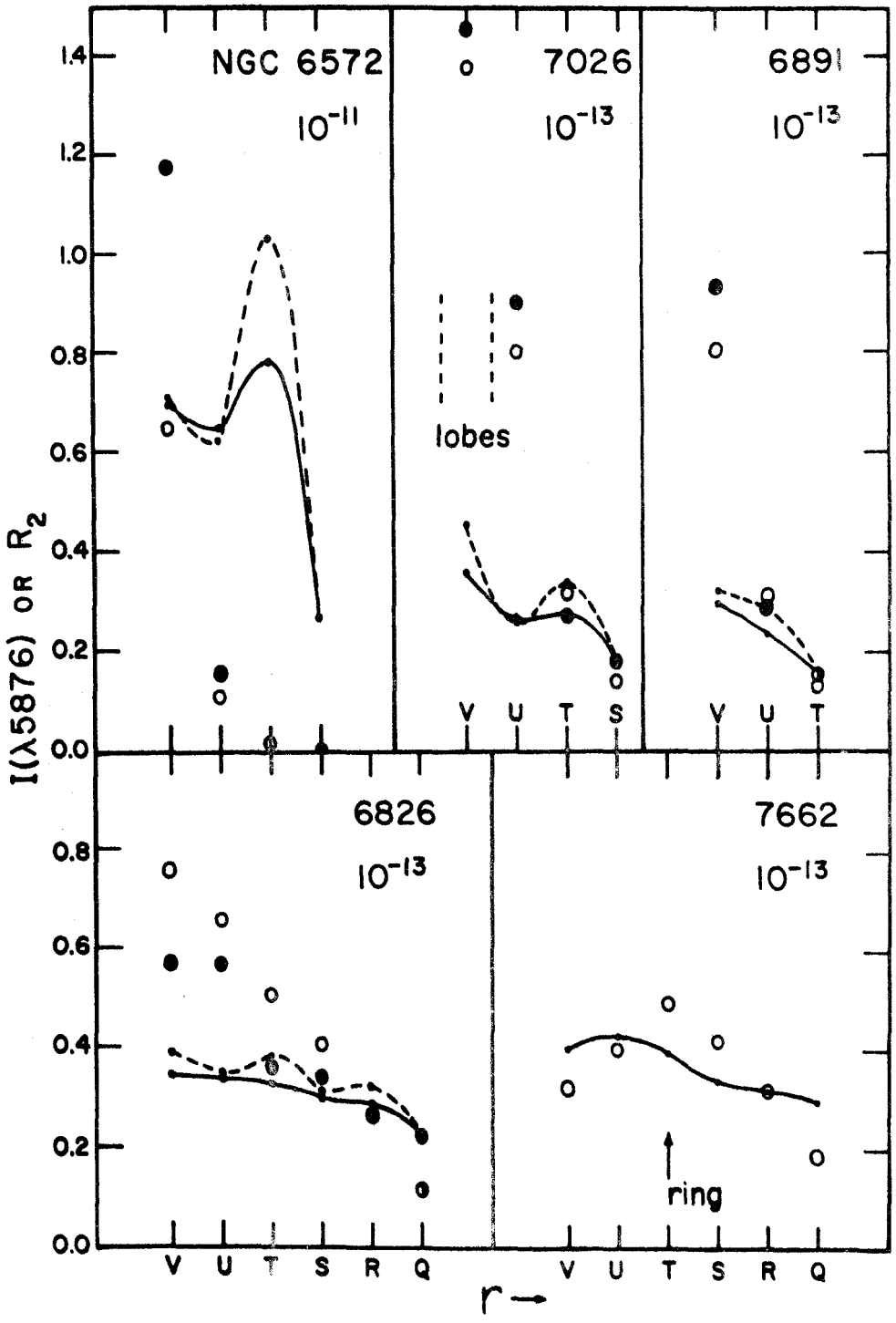

plied is given below each NGC number. [A III] contamination has not been removed. 1σ errors are 3% for all objects except NGC 2392, where 1σ error bars are given. See text for I(λ5876; inverted) scale.

havior as those of λ5876. They will not be considered further as they do not bear directly on the He I line problem. The curves I(λ,e) and E(λ,e) of Figure 4 are self-explanatory; the trend of R_2 is explained qualitatively as follows: in the outer parts of the nebulae the expansion velocities are large enough to allow the easier escape of λ3889 photons and hence a reduction in the λ7065 emissivity. The λ3889 → λ7065 conversion process and the trend of Robbins' models are thus confirmed. R_2 (i, inverted) tends to be flatter than R_2 (o, observed) but "bumps" in R_2 (o) are exaggerated in R_2 (i). Thus the presence of toroidal components in nebulae such as NGC 7662 and NGC 6572 introduces spurious features. We return to a discussion of these features in Chapters VI and VII.

Preliminary observations of the high excitation planetary NGC 2392 were obtained with the special apertures (see Figure 4). The trend of R_2 is interesting and is interpreted as follows. The peak in I(λ5876) corresponds to the bright inner toroidal ring, and the outer upward trend corresponds to the outer, fainter ring of the nebula (see Curtis 1918). The peak in R_2 at r = 11 arc sec may be overestimated due to an uncertainty in the λ6067 continuum flux. The peak could be lower by as much as 30%, but in this case R_2 is still significantly larger just outside the bright inner ring than in adjacent regions. Wilson

(1948, 1950) has reported the expansion velocities of ions emitting lines of various degrees of excitation, and concluded that all the lines he measured arise in the inner ring and have V $\sim$ 50 km/sec. If the outer ring has V(R) < 50 km/sec, then a considerable transfer of energy from H8 (H I λ3889.05) to He I λ3889 (actually λ3888.65) can occur due to the aproach of the H I emitters relative to the He I ($2\,^3S$) absorbers. Robbins (1968b) includes this effect for expanding spheres and finds an increase in I(λ7065) of $\sim$ 3.5% for V(R) = 0, $\tau_0(\lambda 3889) = 75$. It is clear, however, that if the relative velocity is negative and in addition T_e is large ($T_4 \sim 2$ for NGC 2392) considerably more conversion of H8 radiation will occur.

The data presented here are too rough to permit a more detailed analysis. An observation of the outer shell expansion velocity would be most useful.

(c) Chopper Observations of NGC 7027 and BD+30°3639

(i) NGC 7027

Due to its intrinsic brightness, this enigmatic, amorphous nebula could be observed with fairly high spatial resolution using a sky chopper. Offset guiding was employed to measure the brightness in the four regions shown in Figure 5. The results are given in Table 5. Due to the high excitation of this object there is some spurious

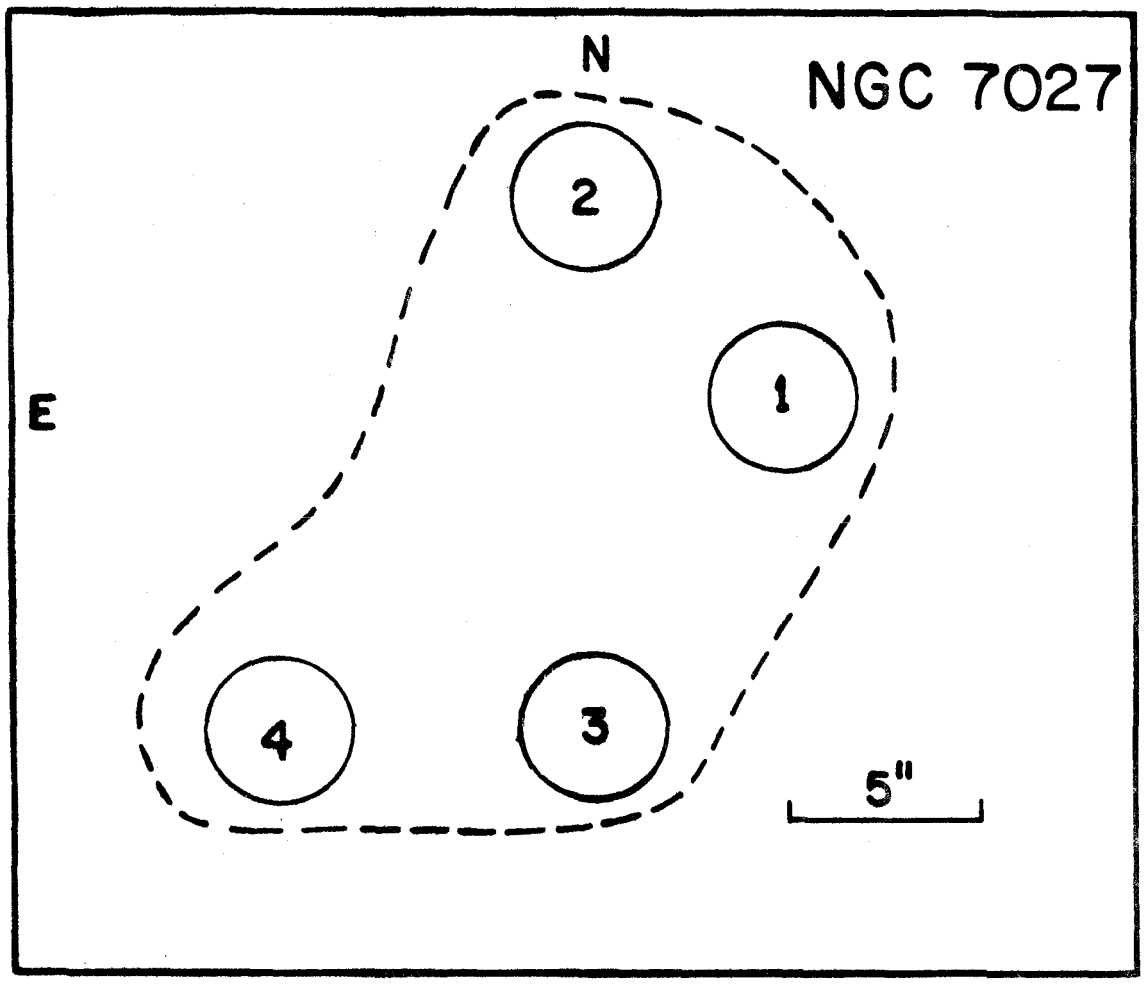

Fig. 5. - Map (to scale) of regions measured on NGC 7027. Chopper diaphragm diameter is 3.56 arc sec. Region 1 is brightest part of nebula. Dashed line is approximate optical boundary.

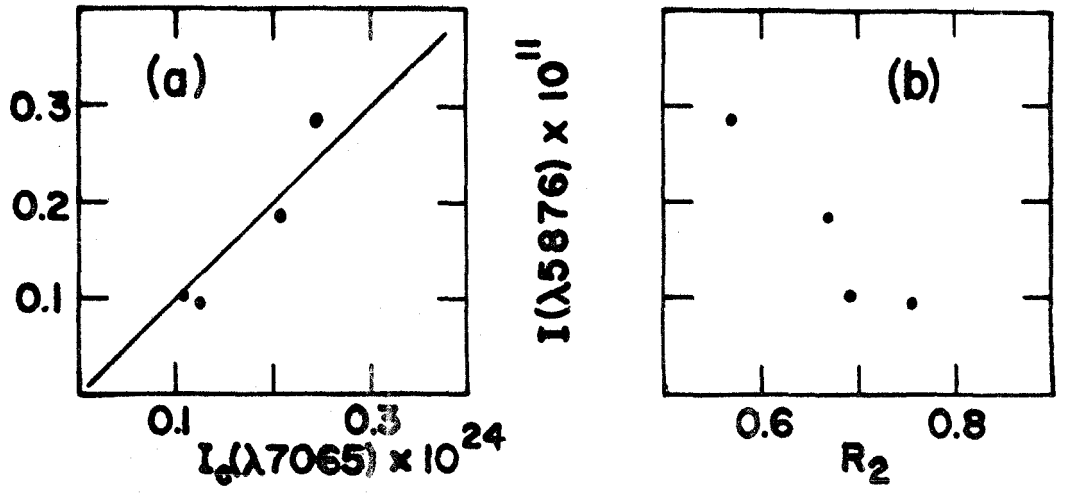

Fig. 6. - NGC 7027: λ5876 line surface brightness vs. (a) λ7065 continuum surface brightness (extrapolated from λ6950), (b) R_2, for the four regions studied. Units as per Table 5. R_2 is not corrected for contamination.

TABLE 5

CHOPPER OBSERVATIONS OF NGC 7027[†]

REGION	DIST	I(λ5876)	I_c (λ7065)	CONT. COLOR	CONT. %5876	CONT. %7065	R_2
1	0.0	0.282	0.244	1.0	28	37	0.571
2	7.2	0.183	0.208	1.0	35	38	0.670
3	9.5	0.093	0.124	1.37	35	40	0.756
4	14.9	0.101	0.108	1.26	29	38	0.693

[†]See notes on p. 60.

Units for I(λ5876): 10^{-11} erg cm^{-2} sec^{-1} (arc sec)$^{-2}$;
for I_c(λ7065): 10^{-24} erg cm^{-2} sec^{-1} Hz^{-1} (arc sec)$^{-2}$.

TABLE 6

CHOPPER OBSERVATIONS OF BD+30°3639

AP	λ5876	λ6067	λ6950	λ7065	ENTRY
CS	0.119-22[†]	0.615-23	0.503-23	0.817-23	FLUX[**]
CL	0.160-22	0.851-23	0.732-23	0.116-22	FLUX
CL-CS	0.409-23	0.236-23	0.229-23	0.340-23	FLUX
CL-CS	0.815-11			0.443-11	LINE FLUX[*]
CS	0.265-10			0.132-10	LINE FLUX
CL	0.347-10			0.175-10	LINE FLUX

	R_2
CS	0.496
CL	0.504
CL-CS	0.543

[†]Power of 10.

[**]erg cm^{-2} sec^{-1} Hz^{-1}(arc sec)$^{-2}$

[*]erg cm^{-2} sec^{-1}(arc sec)$^{-2}$

line contamination of the fluxes. Consulting the spectrum of NGC 7027 given by Aller, Bowen and Minkowski (1955, hereinafter referred to as ABM), we can estimate the degree of contamination for each filter (we shall return to these corrections in Section III-[e]). There is $\sim$ 1% contamination of λ5876 from measured lines and an estimated maximum of 3.5% due to tabulated but unmeasured lines. The λ6067 filter is contaminated by $\sim$ 20% (ABM); thus I(λ5876) should be raised by $\sim 0.3 \times 0.2 \sim 6\%$. The λ6950 filter is almost completely ($\sim$ 1.6%) free, and the λ7065 filter has $\sim$ 17% contamination due to the lines [A III] λ7135 and [A V] λ7005. Correction for these effects will probably lower R_2 for all four regions, but if anything R_2 will be reduced more in the brightest region. Some of the results in Table 5 are plotted in Figure 6 to emphasize the striking fact that R_2 appears to be systematically <u>lower</u> in the brighter regions of NGC 7027 than in the outer, fainter regions.

These results are accounted for as follows. The trend in Figure 6(a) is reasonable; the slight upward curvature could be due to the collisional loss of the two-photon continuum in the higher density bright region, although $N(He^+)/N(H^+)$ is undoubtedly involved also. The continuum color variation in Table 5 may be due to a combination of differing contamination and temperature differences. Table

5 shows that in Regions 1 and 2 a combination of (i) a higher expansion velocity or chaotic velocity field and (ii) a concentration of grains is destroying the λ3889 photons and hence reducing I(λ7065).

The data presented here illustrate the complexity of this nebula, and lead us to question seriously the application of spherical homogeneous model calculations to the interpretation of measured line ratios. Clearly more observations are needed to confirm and expand upon these results.

(ii) BD+30°3639

This very low excitation object has been the subject of much investigation recently. O'Dell and Terzian (1970) described some of its optical properties, and Aller (1968) has published a spectrum of its central star. The broad emission-line character of the WC nucleus might lead us to suspect that O'Dell's values of R_1 and R_2 are meaningless. I(λ10830) is certainly weak, however (Vaughan 1968).

Since this object is too small to be observed with the special apertures, it was observed with two chopper apertures (denoted CS and CL) having diameters (at the 100-inch Cass) 3.56 and 8.95 arc sec; and areas 9.88 and 62.85 (arc sec)^2 respectively. In each case the object was centered in the aperture. Table 6 gives the results of observations

made on two nights. The interpretation of these results is as follows: (1) The underlying continuum flux is partly stellar, and hence is ν-dependent for CS and CL. The continuum flux from the outer regions is nearly ν-independent as expected, but is strong compared to the He I line intensities and may thus be due to (real) scattered starlight; (2) R_2 appears to be relatively insensitive to the presence of the central star, although the difference between CS and (CL-CS) indicates that I(λ5876) is proportionately greater near the star. The value of R_2 is in good agreement with that of O'Dell (1963b).

We shall return to further discussion of this object in Chapters IV and VI.

(d) 1970 F(λ5876) and F(λ7065) Observations of 26 Nebulae

Integrated fluxes at λλ5876, 6067, 6950 and 7065 were obtained for a number of planetary nebulae selected from the Perek-Kohoutek (1967) catalog. The methods of observation and data reduction were the same as those used for the special aperture measurements except the sky brightness was always measured with the aperture used for the object. The aperture radii were always chosen to include the entire object (except for NGC 6720). The selection of objects depended on surface brightness, accessibility and the weather, and for this last reason several important nebulae

(e.g.: NGC 3242, 2440) have been omitted. In addition to those objects listed here, the following were found to be too faint to allow measurement in a reasonable length of time: NGC's 6894, 6905, 7008, 7048 and 7139. The fluxes reported here are calibrated absolutely by Oke and Schild's (1970) energy distribution of Vega, and all results published by other authors have been adjusted to this system. The fluxes are averages of two or more separate observations, where possible; rather than give formal standard errors for each entry, we estimate the one-sigma error for all fluxes and R_2 to be 3% (except where noted) since the flux ratio is less sensitive to extinction vagaries when the fluxes are measured many times in sequence. This figure of 3% does not include the uncertainty due to contamination of the λ7065 filter (see below). The results obtained on different nights and with different telescopes were found to agree quite well.

(i) Line Contamination of Filter Response

As indicated in Section III-(c) high excitation lines (mainly He II) contaminate the $\lambda\lambda$5876 and 6067 filters in a few nebulae. These effects work in opposite directions, partially cancelling each other out for NGC 7027. We thus ignore line contamination for F(λ5876). The λ6950 filter is essentially free from contamination, but unfortunately the available λ7065 filter has rather broad wings and trans-

mits $\sim$ 3% at [A V] λ7005 and 2% at [A III] λ7135. Since only the very highest excitation nebulae show [A V] lines, since I(λ7005) is much less than I(λ7135), and the λ6950 filter takes half of this line out, we attempt to remove only the effect of [A III] λ7135 by the following empirical procedure. Several methods were tried, and this seemed to be the most reasonable and consistent. Aller and Czyzak (1968) give

$$\frac{N(A^{++})}{N(O^{++})} \sim 79\times10^{8050/T_e}\frac{I(\lambda5191)}{I_o} ,$$

where I_o = I(λ4959) + I(λ5007) of [O III] and λ5191 is the auroral line of [A III]. (Recent spectrophotometry does not include this line.) Also,

$$\frac{I(\lambda5191)}{I_s} \simeq 0.091\times10^{-12000/T_e} ,$$

where I_s = I(λ7135) + I(λ7751), ([A III] nebular lines), so we write

$$\log\left[\frac{N(A^{++})}{N(O^{++})}\right] = -\frac{3950}{T_e} + \log\left[\frac{I(\lambda7135)}{I(\lambda4959)}\right] + [\text{const.} \equiv P]. \qquad \text{(III-1)}$$

Assuming a constant O/A abundance ratio, and noting the run of ionization potentials for O and A, we would expect a general decrease in P with excitation class followed by an increase for the highest excitation classes since $N(O^{++})$ then decreases faster than $N(A^{++})$. The parameter [-P] is

plotted in Figure 7 for the available λ7135, 4959 observations of O'Dell (1963b); and for NGC 7009, a rough estimate was made by combining the photometry of Liller and Aller (1963) and Osterbrock, Capriotti and Bautz (1963). The latter authors note that the measurements are somewhat uncertain. The excitation classes, listed by Perek and Kohoutek (1967), are taken from Aller (1964). The correlation is seen to be fairly good for lower and intermediate excitation class objects, and quite uncertain for others. The scatter is due to observational uncertainties, N(O)/N(A) differences and vagueness of the excitation class parameter.

The measured flux (corrected for interstellar absorption) $F_o(\lambda 7065)$ is related to the intrinsic fluxes (uncorrected) $F_u(\lambda 7065)$, $F_u(\lambda 7135)$ by

$$F_o(\lambda 7065) = \frac{10^{0.542C}}{T} \left\{F_u(\lambda 7065)T + 0.02F_u(\lambda 7135)\right\},$$

where T = 0.45 is the filter transmission at λ7065 and 0.02 is the transmission at λ7135. Thus the flux corrected for [A III] and reddening is

$$F(\lambda 7065) = F_o(\lambda 7065) - 10^{0.014C} \times 0.0445F(\lambda 7135), \quad \text{(III-2)}$$

where F(λ7135) is the corrected [A III] flux found from Figure 7, equation (III-1) and the [O III] fluxes reported by Collins, Daub and O'Dell (1961) or O'Dell (1963a).

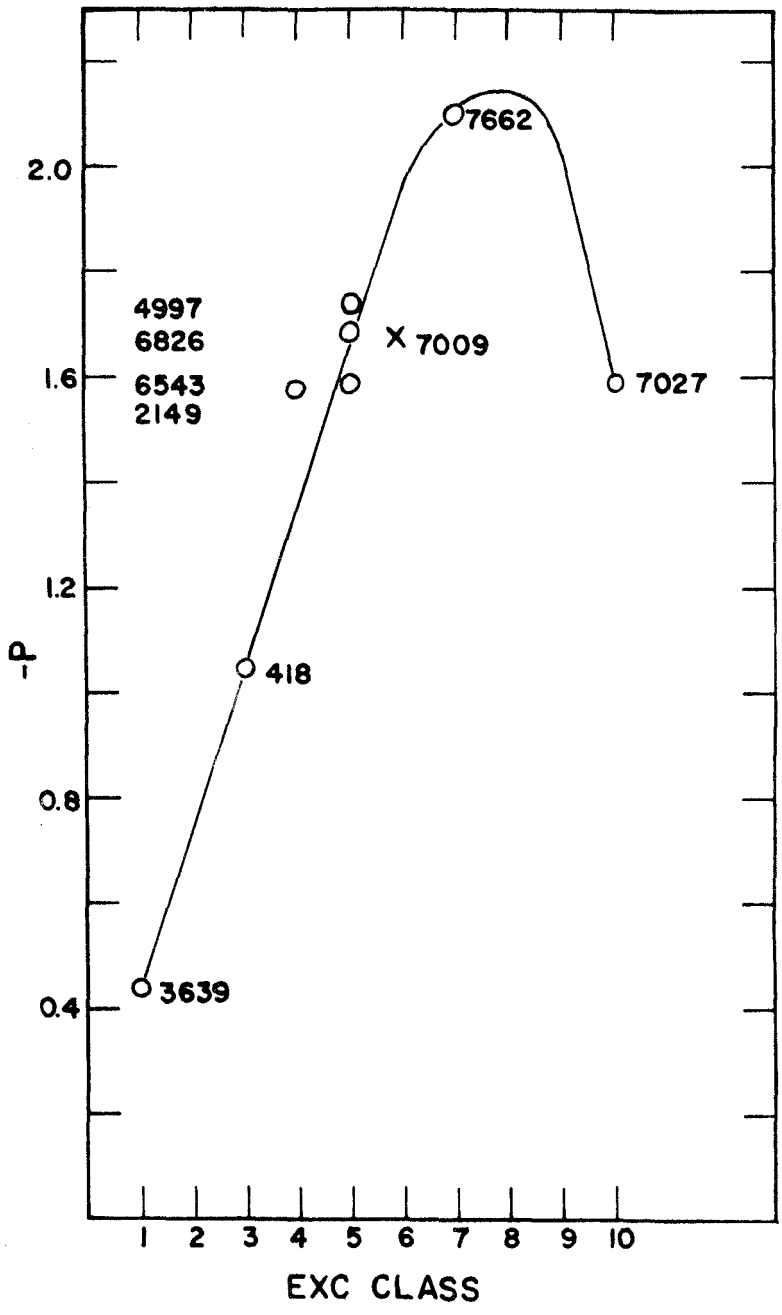

Fig. 7. - Parameter [-P] vs. Aller's (1964) excitation class. Figure is used to correct R_2 for [A III] contamination.

Table 7 gives the results of the observations, where F (λ7065) has been corrected using equation (III-2). This correction procedure is probably accurate to 50%, which gives an RMS error in the values of R_2 of $\sim$ 10%. For some objects this figure may be $\sim$ 3%, but for others it may be $\sim$ 20%. The forbidden-line electron temperatures are taken from Kaler (1970) unless noted otherwise (in Chapter V). The required values of F(λ4959) are found using F(λ5007) = 3×F(λ4959).

(ii) Comments on Individual Nebulae in Table 7.

(1) NGC 40. Central star has λ5876 emission (Aller 1968); data therefore uncertain. R_1 very low - arbitrarily set = 2.

(2) NGC 2392. R_2 is obtained from 1969 special aperture data, (Section III-[c]) assuming surface brightnesses near the central star are the same as for innermost annular aperture.

(3) NGC 4593. [A III] correction is largest, $\sim$ 27%; therefore R_2 is uncertain by $\sim$ 20%.

(4) NGC 6543. Adding special aperture fluxes gives agreement for R_2. O'Dell (1963b) gets R_2 = 0.438, but may have measured only inner regions. Central star is bright, and probably influences results.

(5) NGC 6572. 1969, 1970 data agree.

(6) NGC 6720. Cannot measure entire nebula; therefore

R_2 is quite uncertain.

(7) BD+30°3639. Data agrees with chopper data. O'Dell (1963b) gets R_2 = 0.493. C has been corrected.

(8) NGC 4997. Possible variable nebula (Aller and Kaler (1964). Nebula is located in a very crowded field so both O'Dell's (1963b) results and these are suspect. He gets R_2 = 0.66.

(9) NGC 7009. Sky brightness was very noisy during observation. Both R_1 and R_2 values very uncertain.

(10) NGC 7027. O'Dell (1963b) gets R_2 = 0.585 (well-determined). Consistent with chopper observations (cf. Section III-[c]).

(11) NGC 7662. O'Dell (1963b) appears to have used an incorrect value for ϕ. The nebula is at least as big as NGC 6826 (Curtis 1918). His observations probably refer only to the inner regions. See Section VI-(f).

(e) 1970 F(λ10830) Observations of 25 Nebulae

We have attempted to measure F(λ10830) for those nebulae listed in Table 7. A combination of bad weather and regrettable circumstances have rendered much of this work somewhat uncertain. First, one cannot measure F(λ10830) at the same time as F(λ5876) due to the efficiency of the S-1 tube response at λ5876. Since these two measurements require different standard stars for cali-

TABLE 7

OBSERVATIONAL DATA - LINE FLUXES

OBJECT	EXC	C	5876 ADOPT	7065 RAW	7065 ADOPT	10830 ADOPT	%	10830 OD	ϕ	LOG S(λ5876)	NOTES
40	2	0.97	38.6	13.70	13.3	0.580	10		18.2	-2.305	6,7
1535	7	0.13	4.88	1.44	1.34	0.214	15		9.2	-2.608	
418	2	0.33				4.40	10	4.40	6.2	-1.132	3
2149	4	0.54				0.484	10	0.484	4.2	-1.471	3
2392	8	0.43	4.67	2.68	2.52	0.224	15		22.4	-3.401	4,6,7
3568	5	0.24	3.57	1.87	1.51	0.200	10		9.0	-2.724	
4593	4	0.27	6.64	2.13	1.55	0.206	10		6.4	-2.161	6,7
6210	5	0.16	17.6	7.16	6.09	0.959	5		8.1	-1.945	
6309	8	1.04	4.19	1.19	1.02	0.110	10		6.9	-2.427	
6439	5	1.40	6.18	2.18	1.78	0.193	15		2.5	-1.376	1
6543	5	0.22	61.0	26.2	23.1	3.00	10	3.22:	9.4	-1.531	6,7
6572	5	0.31	56.0	42.3	39.3	4.34	5		7.2	-1.334	7
6567	5	0.69	8.81	4.24	3.84	0.484	15		4.4	-1.716	
208	5	0.53	6.84	4.19	4.03	0.428	10		1.5	-0.889	1,8
6720	6	0.29	13.4	3.48	3.07	0.300	25		34.6	-3.315	7
6790	6	0.33	36.1	23.1	22.1	1.11	10		1.0	0.186	1
3639	1	0.70	35.5	17.9	17.8	0.419	5	0.404	2.5	-0.617	2,6,7
6818	9	0.24	3.90	2.16	1.93	0.295	15		9.1	-2.696	
6826	5	0.18	22.0	7.43	6.53	0.903	5	0.88:	12.7	-2.237	6
6891	5	0.41	7.16	2.39	2.04	0.216	10		5.1	-1.932	6
4997	5	0.54	17.3	13.5	13.2	1.22	5	1.240	0.5	0.469	5,6,7
7009	6	0.24	39.5	15.3	12.8	2.10	10		14.1	-2.074	7
7026	6	0.99	17.0	5.75	5.43	0.525	15		5.6	-1.637	6
7027	10	1.22	130.	89.6	77.8	10.04		10.04	7.1	-0.961	7
5217	6	0.96	6.17	2.00	1.81	0.210	20		3.4	-1.653	
7354	7	1.96	23.2	7.45	6.76	0.494	20		10.0	-2.006	1
7662	7	0.40	21.4	7.96	7.21	0.914	15	1.130	12.7	-2.248	9

Notes to Table 7

Columns:

1. Object NGC or IC number. 3639 ≡ BD+30°3639; 208 ≡ VV208 ≡ Hu-2-1 ≡ M H 78(1).
2. Aller's (1964) excitation class.
3. Kaler's (1970) interstellar absorption constant $C \equiv \Delta \log F(H\beta)$.
4. Reduced $F(\lambda 5876)$, units 10^{-12}erg $cm^{-2}sec^{-1}$.
5. Raw $F(\lambda 7065)$, units 10^{-12}erg $cm^{-2}sec^{-1}$.
6. $F(\lambda 7065)$ corrected for [A III] $\lambda 7135$.
7. $F(\lambda 10830)$ adopted, units 10^{-10}erg $cm^{-2}sec^{-1}$.
8. 1σ uncertainty in $F(\lambda 10830)$.
9. O'Dell's (1963b) results. Colons indicate his estimated uncertainty of ±0.15 in logarithm.
10. Angular radius in arc sec.
11. Log ($\lambda 5876$ surface brightness), erg $cm^{-2}sec^{-1}$

Notes:

1. $F(\lambda 4959)$ from O'Dell (1963a).
2. Recalibrated; O'Dell and Terzian (1970).
3. All data from O'Dell (1963b).
4. Special aperture averaged flux.
5. $F(\lambda 4959)$ from O'Dell (1963b).
6. Central star either Of or WR type. Only brightest nuclei may affect integrated fluxes.
7. See Section III-(d) for comments.
8. Measured in 1969.
9. ϕ altered. See comments in Section III-(d).

bration, one is tied to some uncertainty through the Vega calibration. Second, since both the standard stars' energy distributions and the tube response are very much higher at λ8000 A than at λ10830 A, a filter leak which is undetectable with the Cary 14, spread over several hundred Angstroms, will contaminate the standards' observed counting rates. This leak was discovered and eliminated with a Wratten #87A infrared cut-on filter. (The other filters were checked for similar leakage and found to have none.) Third, the λ10830 filter obtained was really too narrow for this work, and displayed some temporal changes in peak transmission position. Also, the λ10830 line fell on the red side of the peak, and thus temperature shifts (Blifford 1966) had an important effect upon BW/T. For these reasons we were forced to calibrate the λ10830 data (obtained on only two good nights, two fair nights and one marginal night) using the work of other observers. We chose the scanner observations of NGC 7027 reported by O'Dell (1963b) for this purpose since this nebula is small and bright, and O'Dell estimates high accuracy for his observation of I(λ10830). Also, profiles I_ν(λ10830) exist (Vaughan 1968, Robbins 1970b). Using the planetary radial velocities of Vaughan (1968) or Perek-Kohoutek (1967), we have employed a process of fitting fluxes and nightly transmission curves to work through all the data to achieve consistency and check the values of F(λ10830) for other

objects against those of O'Dell. The agreement for other objects is seen to be satisfactory. In Table 7, we report the adopted fluxes and dispersion in measured values. We defer to Chapter VI (Table 12) the values of R_1 and R_2 and the comments for each nebula. The one-sigma percent errors are estimates based upon the results of the fitting procedure, agreement with O'Dell's values of $F(\lambda 10830)$ and R_1 (cf. Table 12), the number of observations made, and the prevailing observing conditions. The uncertainties are unfortunately large, but one should be able to distinguish a factor of two in D_t vs. D_1 for most of the objects.

(f) Comment Upon Uncertainties

The results presented in Table 7 are quite uncertain for a number of objects. We have outlined the reasons for this, and in the comments following Table 12 we summarize additional sources of observational uncertainty, e.g., the presence of central star He I emission lines. We note also that the interstellar absorption coefficients (Kaler 1970) present a further obstacle to the proper solution of the depopulation rate anomaly. Gull (1971), in studying this problem, has raised doubts about the validity of some of the constants C. Figure 8 illustrates the factor error made in R_1 for values of C and possible errors in C. The dispersion in quoted values of C (Radio: Terzian 1968, Thompson 1968a; Optical: Kaler 1970, Gull 1971) and the

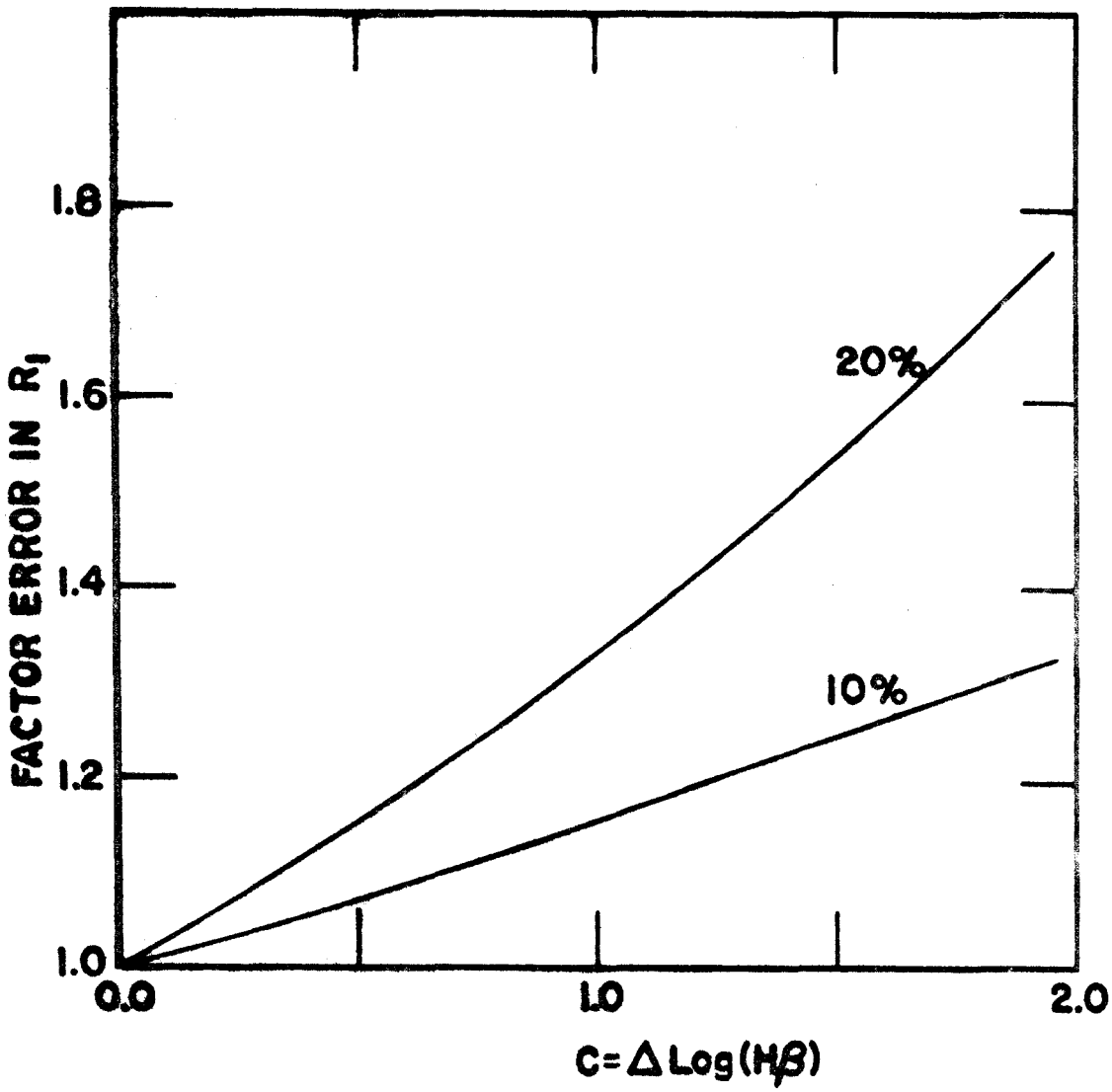

Fig. 8. - Factor error made in $R_1 \equiv I(\lambda 10830)/I(\lambda 5876)$ as a function of C, for 10% or 20% error in C.

use of a unique reddening law indicate that the adopted values of R_1 should be used only in a statistical sense.

IV. INFRARED EMISSION FROM PLANETARY NEBULAE

(a) Introduction

The first 7.5-14μ observation of a planetary nebula was reported by Gillett, Low, and Stein (1967), who measured the flux at different wavelengths from NGC 7027, and found a considerable continuum excess over that expected from free-free emission alone. Further work by Gillett and Stein (1969) on IC 418, Gillett and Stein (1970; hereinafter referred to as GS), Woolf (1969), Gillett, Knacke and Stein (1971), Neugebauer and Garmire (1970), Willner et al (1972), and several others has confirmed the existence of an IR excess for many of the objects studied. Krishna Swamy and O'Dell (1968) discussed a graphite grain emission mechanism for NGC 7027 in response to the new measurements. Far infrared (45-750μ) measures of K3-50 and NGC 7027 were reported by Harper and Low (1971), and high wavelength resolution studies by Rank et al (1970) and Holtz et al (1971) have confirmed the continuous nature of the excess. Woolf (1969) and GS also reach this conclusion. The theoretical infrared line fluxes (Petrosian 1970) are apparently higher than are observed (cf. Gillett and Stein 1969) and a correction for the weak lines is thus uncertain. Recent observations of peculiar objects such as K3-50, FG Sagittae, IRC +10216 and the high IR excess late-type stars are discussed in Chapter

VII.

Let us assume that the infrared excess is continuous, and that it arises from solid grains within the H II region. This assumption now appears to be generally accepted, and the discussion presented here will lend support to it. The exact nature of the grains is very uncertain, but graphite and silicates are two strong possibilities for the bulk constituent. Graphite was chosen for BD+30°3639 by Persson (1970) since the star has a WC spectrum.

(b) Color Temperatures from Observations

Using the graph of log(Flux) vs. log(ν) for the three objects studied by GS we derive the apparent color temperatures of the dust from several pairs of fluxes, after correcting each flux for the expected free-free continuum contribution given by GS. No correction has been made for line contamination, and the nebulae are assumed to be optically thin in the dust at the infrared wavelengths. The values of T_c derived using equation (II-23) are given in Table 8 (the value of 300°K given by Persson [1970] for BD+30°3639 is in error). The compilation of data for $\lambda < 3.5\mu$ by Willner et al (1972) has not been used to derive T_c since the excesses at short wavelengths are very uncertain, although they appear to be real. It is clear

TABLE 8

INFRARED FLUXES AND COLORS

OBJECT	λ_μ	$F_\nu(\lambda_\mu)$	T_c (°K)	$\tau_d(\lambda 10830)$
NGC 7027	12.5	176	181 (10)	0.133
			210 (8)	0.055
			319 (5)	0.008
	10.0	110	241 (8)	0.027
			377 (5)	0.005
	8.0	75	233 (5)	0.032
	5.0	7.7		
BD+30 3639 (3639)	11.5	78	238 (8.5)	0.104
			227 (5)	0.134
			250 (3.5)	0.081
	8.5	55	230 (5)	0.125
			253 (3.5)	0.076
	5.0	3.3	304 (3.5)	0.033
	3.5	0.33		
NGC 6572	11.5	23	144 (8.5)	0.115
			198 (5)	0.011:
	8.5	4.8	233 (5)	0.044:
	5.0	1.0:		

TABLE 9

DUST SHELL MODELS, $\tau_d(\lambda 10830) = 0.1$

OBJECT	T_c (°K)		$F_\nu(11.5\mu)$			$F_\nu(3.5\mu)$			Lyα / TOTAL
	Z_1	Z_3	Z_1	Z_3		Z_1	Z_3		
418	158	147	0.68	0.60	-21	0.12	0.015	-25	0.58
2392	119	109	0.36	0.25	-21	0.39	0.02	-28	0.04
6210	106	96	0.16	0.10	-22	0.81	0.03	-31	0.82
6543	141	130	0.48	0.39	-21	0.14	0.014	-26	0.38
6572	156	146	0.73	0.63	-21	0.13	0.018	-26	0.30
3639	261	248	0.30	0.33	-20	0.35	0.17	-22	0.09
6826	132	122	0.41	0.32	-21	0.40	0.03	-27	0.13
4997	242	229	0.90	0.93	-22	0.39	0.15	-24	1.00
7009	119	109	0.17	0.12	-21	0.19	0.01	-28	0.34
7026	159	148	0.45	0.40	-21	0.10	0.01	-25	0.16
7027	169	158	0.16	0.15	-20	0.78	0.13	-25	0.55
7354	111	101	0.43	0.28	-22	0.73	0.03	-30	0.78
7662	132	122	0.43	0.33	-21	0.40	0.03	-27	0.29

Notes to Table 8.

1. $F_\nu(\lambda_\mu)$ is in f.u.. 1 f.u. = 10^{-23}erg $cm^{-2}sec^{-1}Hz^{-1}$.
2. Number in parentheses following T_c is other λ_μ used in T_c determination.
3. All data are from GS.
4. Uncertain 5μ point for NGC 6572 is from curve of GS, not upper limit.

Notes to Table 9.

1. Shell model has same grain density as homogeneous sphere with $\tau_d(\lambda 10830) = 0.1$.
2. Last column gives fractional heating by trapped Ly α.
3. Flux units: erg $cm^{-2}sec^{-1}Hz^{-1}$; power of 10 follows each column.

that the best determined (excess) fluxes at longer λ's give consistently lower temperatures. This may be due to the underlying line contamination, or to a grain temperature or grain density gradient within the nebulae. We list also the values of $\tau_d(\lambda 10830)$ found using equation (II-26). These values are discussed in later chapters.

(c) Theoretical Grain Temperatures and Fluxes

The large infrared excesses of the nebulae apparently represent a sizable fraction of the total energy output. The fact that the objects with the largest values of S(Hβ) have the largest excesses suggests that Lyα provides a significant fraction of the total energy input to the grains since both depend upon N_e^2 (see below). There is also heating by collisions with electrons and protons, and by absorption of light from the central star. The collisional heating rate per cm^3 by particles p (ions, atoms or electrons) is

$$\Gamma_p = N_d N_p \pi a^2 \frac{m_p}{2} \langle v_p^3 \rangle$$

$$= 4\left(\frac{2}{\pi m_p}\right)^{1/2} \times N_d N_p \pi a^2 (kT_p)^{3/2} \qquad \text{(IV-1)}$$

$$= 10^8 N_d N_p \pi a^2 T_4^{3/2} \text{ eV cm sec}^{-1}\text{(electrons)},$$

where N_p, m_p and v_p are the number density, mass, and

relative velocity, respectively, of the particles; πa^2 is the grain cross section; N_d is the grain number density; and the angular brackets indicate an average over a Maxwell-Boltzmann distribution. This equation (Spitzer 1968) assumes a unit probability of sticking to uncharged grains, and total conversion of electron or ion energy into thermal energy. If the grains become negatively charged in order to balance the number of electron and proton impacts, Spitzer has shown that the rate will be (electron rate)/6; i.e., the proton rate increases by a factor ~ 3.5 for $T_4 = 1$. Mathews (1967, 1969) has studied the erosion of grains by photoejection of electrons and sputtering by ions in H II regions, and concludes that the grains will become positively charged. Fortunately the poorly determined heating rate is small compared to the other rates. The energy gained due to recombination of protons with electrons on the grain surfaces (13.6eV) will be

$$\sim N_d N_e \pi a^2 T_4^{1/2} \times 0.3 \times 10^6 \text{eV cm sec}^{-1},$$

where it is assumed that half the energy available is radiated away.

After Q scatterings, a Lyα photon has travelled a distance $f_\alpha R$ in escaping the nebula, and thus the energy input to the grains,

$$\Gamma_\alpha = \alpha(\mathrm{Ly}\alpha)N_e N(H+)h\nu_\alpha(1-\exp[-f_\alpha\tau_d]),$$

(where $\tau_d \equiv \tau_d[\lambda 1216]$) depends only weakly upon f_α or τ_d as long as $f_\alpha\tau_d > 2$. The values of f_α(Table 11) and (post facto) values of τ_d show that this is nearly always true. Comparing the two heating rates Γ_p and Γ_α, using S(Hβ) to eliminate $N_e N(H^+)$, we find that at $T_4 = 1.5$, $\Gamma_\alpha/\Gamma_p \sim 25/\tau_d$ for S(Hβ) = 1 erg cm^{-2} sec^{-1}. Including the factor of 6 shielding (Spitzer) and the increase in Γ_p due to H^+-e^- recombination, we find $\Gamma_\alpha/\Gamma_p \geq 100$ for $\tau_d \leq 0.5$, in the brightest planetaries.

So far, this picture is nearly model independent, but the stellar heating rate complicates the expected emission. At a distance r from the star, the stellar heating rate Γ_s is given by

$$\Gamma_s(r) = N_d\pi a^2 \int_0^\infty Q(a,\lambda)E_\nu(T_s)d\nu \times \frac{4\pi^2 R_s^2}{4\pi r^2} \quad , \qquad \text{(IV-2)}$$

where R_s and T_s are the stellar radius and effective temperature and $E_\nu(T_s)$ is the stellar emission rate, $= B_\nu(T_s)$ for a black-body star. Recent calculations by Cassinelli (1971; and references cited therein) demonstrate the non-black-body character of the stars. The luminosities and radii derived by Seaton (1966) are computed using the black-body star assumption, so we shall use it also. Since the grain cross sections at high

frequencies are probably $\sim \pi a^2$, this is a safe assumption; i.e., the incident flux distribution with ν is unimportant.

Suppose the nebula is optically thick in the (H I) Lyman continuum (Lyc). Böhm (1968) has given solutions for the neutral hydrogen density $N_H(r)$ inside an optically thick nebula, assuming black-body stars and "model atmosphere"stars. The density $N_H(r)$ can be fitted reasonably well in both cases by a power law $N_H(r) \propto r^p$ with $p \sim 6.3$. It is easily shown that the optical depth (at position r) to Lyc stellar photons is $\tau_\nu(r) = \tau_c(r/R)^{p+1} \times (\nu_c/\nu)^3$, where a ν^3 opacity law is assumed, and τ_c is the total Lyman continuum (λ912) optical depth. Reduction of the stellar flux beyond λ912 may thus be included in equation (IV-2). He^{++} exists in only a small volume around the central star, so that all stellar flux beyond λ228 may be neglected. Between λ505 and λ228 (He I and He II Lyc) there may be a reduction of the stellar flux in the outer layers if the nebulae are assumed to be optically thick in the He I Lyc. The reduction throughout most of the nebula is negligible, however, since (as for H) both the $(r/R)^{p+1}$ and $(\nu_c/\nu)^3$ factors are very strong. Böhm's black-body solution for $N(He^\circ)$ with $T_s \simeq 46000^\circ K$ shows that essentially no flux reaches the outer 10% of the nebula; but for the "model atmosphere" star, the

ionization boundaries of H and He coincide.

The diffuse continua of H, He, and He^+ are neglected in computing the heating rates. Assuming the on-the-spot approximation, the effect of Lyα will be more important than that of the Lyc photons which spend a negligible time as continuum photons before conversion to Lyα + Balmer + higher order photons. He II Lyα(λ303) is created near the central star, and diffuses out through the He^+ gas, ionizing hydrogen and exciting the Bowen Fluorescent lines of O III. The apparent discrepancy in the Bowen conversion efficiency (Weymann and Williams 1969) as it may relate to grain absorption will be discussed in Chapter VII. The effect of He II Lyα is neglected due to the low abundance of He^{++} ions in most objects. He I Lyα(λ584) is also trapped inside the nebula, and may contribute to heating of the grains. The maximum effective recombination coefficient leading to He I Lyα will be

$$\alpha_{eff} = 1/4\alpha_{He} + 3/4\alpha_{He}F_c/D,$$

where $\alpha_{He} = 4/3\alpha(2^3S)$, and F_c/D is the fractional depopulation rate of He I 2^3S due to collisions. For most nebulae $F_c/D \sim 0.7$, and therefore $\alpha_{eff} \simeq \alpha$(H I Ly$\alpha$). The total energy available in He I Lyα compared to that for H I Lyα will be given by

$$\frac{h\nu_{584}}{h\nu_{1216}}\frac{\alpha_{eff}\, N_e N(He^+)}{\alpha(H\ I\ Ly\alpha) N_e N(H^+)}\ \frac{\tau_d(1-\exp[-f_t\tau_{tot}])}{\tau_{tot}(1-\exp[-f_\alpha\tau_d])}\ ,$$

where f_t is the number of nebular radii traversed by a He I Lyα photon before destruction or escape, and τ_{tot} is the total optical depth to a He I Lyα photon due to absorption by $H^o(\tau_c\times[584/912]^3)$, dust ($\tau_d$) and conversion to the He I 2-photon continuum (cf. Appendix 1); i.e.

$$\tau_{tot} = \tau_c\times 0.263 + \tau_d + \ln[(1-B)^Q]$$

where the $2^1P \rightarrow 2^1S$ or 1^1S branching ratio $B \sim 0.001$, and Q is now the total number of He I Lyα scatterings. The nebulae are assumed to be optically thick in the He I Lyϵ, so τ_0(He I Lyα) is probably large enough that $BQ \sim 1$. The He I Lyα heating rate is then $\sim 10\%$ that of H I Lyα and will be ignored.

The energy balance equation (per cm^3) for grains having a unique radius a, at a distance r from the central star is then

$$4\pi^2 a^2 N_d \int_0^\infty Q(a,\lambda) B_\nu(T)\, d\nu = \Gamma_\alpha + \Gamma_p + \Gamma_s(r),$$

which may be rewritten in terms of S(Hβ), τ_d and the expressions given above as

$$\frac{4\pi\tau_d}{Q(a,\lambda 1216)}\int_0^\infty Q(a,\lambda) B_\nu(T)\, d\nu = 3S(H\beta)\ \frac{\alpha(Ly\alpha)}{\alpha(H\beta)}$$

$$\times \frac{h\nu_\alpha}{h\nu_\beta}(1-\exp[-f_\alpha\tau_d]) + \frac{1.6\times10^{-4}}{6}\frac{\tau_d N_e T_4^{3/2}}{Q(a,\lambda 1216)} \quad \text{erg cm sec}^{-1}$$

$$+ 0.5\times10^{-4}\frac{\tau_d N_e T_4^{1/2}}{Q(a,\lambda 1216)} \quad \text{erg cm sec}^{-1}$$

$$+ \tau_d\left(\frac{R_S}{r}\right)^2 \frac{\pi\bar{Q}}{Q(a,\lambda 1216)}\int_0^{\nu_{228}} E_\nu(T_S)\,d\nu \ . \qquad \text{(IV-3)}$$

For simplicity, we put $E_\nu(T_S) = B_\nu(T_S)$ since $Q(a,\lambda)$ should be flat in this region, and since the values of L_S are derived on the black-body assumption. The last term of equation (IV-3) may be written in terms of Seaton's (1966) derived values of $\Lambda \equiv L_S/L_\odot d^2$, where d is the nebular distance in kpc. We have

$$\Gamma_S(r) = \left[\frac{206265}{3.086\times10^{21}}\right]^2 \times \frac{\tau_d}{4\pi} \times \frac{L_\odot}{\phi^2} \times \frac{\Lambda G}{\bar{y}^2} \ , \qquad \text{(IV-4)}$$

where ϕ is the nebular angular radius in arc sec, $Q(a,\lambda 1216) \simeq \bar{Q}$, G is a factor near unity which takes account of the diminution of the photons in the Lyc of H°, He° and He^+, and y is the fractional radius, i.e., $y = r/R$. Equation (IV-4) represents the most direct method of estimating the stellar heating rate, and should be about as well determined as Λ, which is probably good to 50% judging by Harman and Seaton's (1966) curves of

$\log\Lambda$ vs. $\log T_s$.

In order to predict values of $F_\nu(\lambda)$, one assumes values of $S(H\beta)$, N_e T_e, f_α, a grain size distribution function $Z(a)$, where $\sum_a Z(a) = 1$, and some spatial density distribution of grains. First, equation (IV-3) is solved (using equation [IV-4]) for $T(a,r)$, the equilibrium grain temperature for each value of a and r, where the fraction of the total Lyα energy available used up on each grain size $\propto Z(a)a^2$. The total flux as a function of λ and τ_d is then found by integrating $Q(a,\lambda)B_\nu(T[a,r])\pi a^2 Z(a)N_d$ over a and r. We choose $Q(a,\lambda) = 2\pi a_\mu p/\lambda_\mu^2$ at long wavelengths where p is a factor $\simeq 1.5$ which does not depend too strongly upon grain composition. This form for $Q(a,\lambda)$ is found from equation (II-19) and is probably reasonable for graphite (cf. Kinchin 1953) but there is no intent to specify the grain composition or shape. Silicates, which have emission peaks throughout the 3.5 - 20μ region, do not follow this law, and the derivation of optical depths τ_d for that class of grains is not warranted at this time. We take $Q(a,\lambda) = 1$ at the absorption wavelengths ($\lambda < 0.1\mu$) since the short wavelength photons encounter essentially the geometrical cross section. A range, $0.01\mu < a < 1\mu$, is thus allowed, wherein both these conditions are satisfied. We emphasize that the value of a does not affect the determination of $\tau_d(\lambda 10830)$ when it is computed from

equation (II-26), as long as the factor $Q(a,1.083\mu)/Q(a,11.5\mu) \simeq (11.5/1.083)^2$.

Equation (IV-3) may be written in schematic form:

$$\Psi a T^6(a,y) = \frac{P}{\tau_d} + \Phi + \frac{\Pi}{y^2} , \qquad \text{(IV-5)}$$

where the parameters Ψ, P, Φ, and Π have obvious definitions, and the sixth power of T arises from the λ^{-2} factor in $Q(a,\lambda)$ at the emission wavelengths. Different sized particles equilibrate at different temperatures, because of the linear dependence of $Q(a,\lambda)$ upon a. Near the star (if any dust exists there) the grains emit more, and have higher color temperatures; while if Lyα is dominant, the emission will not increase linearly with τ_d, because a limited amount of Lyα will be used up on a larger number of grains, thus lowering their mean temperature. Suppose a given mass M of grains is available, and that only the stellar heating is important. Then $T^6(a,y) \propto a^{-1}y^{-2}$, and the emission $\propto Z(a)N_d a^2 y^{-2}$. Since the mass $M \propto Z(a)N_d a^3$, the volume-averaged emission per unit mass $\propto a^{-1}$. Thus, for a given total grain mass, nebulae with generally smaller particles will radiate a greater integrated flux at a slightly higher color temperature $T \propto a^{-1/6}$. If only Lyα is important, the emission per unit mass is constant.

What difference does the gross structure make? Con-

sider a dust shell rather than a sphere. If the star does all the heating, $T \propto y^{-1/3}$, and the total flux will be reduced by the factor

$$1 - \frac{\int_o^{r_i} r^2 T^6 dr}{\int_o^R r^2 T^6 dr} = 1 - (r_i/R).$$

The largest reduction attainable for $r_i = 0.5R$ is thus a factor of 2, and if Lyα is non-negligible, the factor will be less than 2, as long as all the Lyα is destroyed.

Using the values of N_e, $\log(L_S/L_\odot)$, T_e, $S(H\beta)$ and f_α given in Tables 10 and 11, or the values of Λ given by Harman and Seaton (1966) when available, or calculated where necessary, we derive the theoretical fluxes and apparent color temperatures $T_c(\lambda_1, \lambda_2)$ for homogeneous dust spheres and spherical shells. Three different (step) size distributions $Z_j(a)$ have been assumed. For particle sizes (in μ) of 0.04, 0.08, 0.12, 0.16, and 0.20, they are: Z_1(small): 0.5, 0.2, 0.15, 0.1, 0.05; Z_2(medium): all 0.2; Z_3(large): 0.05, 0.10, 0.15, 0.20, 0.50, respectively. Clearly one could generate a large number of models with density gradients, very large or very small particles, etc. Typically, the fluxes at short wavelengths are very sensitive to Λ, ϕ, and $Z_j(a)$, since they lie on the strongly exponential part of the black-body curve.

Some of the results are summarized in Figures 9 and 10 and in Table 9. In Figure 10 we plot partial results for BD+30°3639. Since the central star does most of the heating in this object, the color temperatures are insensitive to τ_d. For each model generated, the flux at any wavelength may be used to estimate τ_d. For the example given, comparison of Table 9 and the recent 3.5μ flux measurement (Willner et al 1972) with Figure 10 gives τ_d = 0.02, 0.02, 0.01, and 0.1 for λ_μ = 11.5, 8.5, 5.0 and 3.5 respectively. There appears to exist an excess of $3.5 \times F_\nu$ (predicted continuum) at 1.65μ also, implying either a much larger value of τ_d for a shell model, or some particles very close to the central star. This example shows the great indeterminancy of the method of finding τ_d from theoretical fluxes.

Table 9 gives some parameters for shell models of nebulae observed by Willner et al (1972) at 3.5μ. In every case the values of τ_d deduced from 11.5μ measurements (Woolf 1969 or GS) are considerably smaller than those found from 3.5μ excesses. Although these short wavelength excesses are very uncertain, there appears to be an increasing (with λ) excess for all nebulae observed at 1.65, 2.2 and 3.5μ. The values of τ_d deduced from 11.5μ fluxes will be seen to be smaller (except for NGC 6543 and NGC 7027) by a factor $\geq$ 2 than the values of

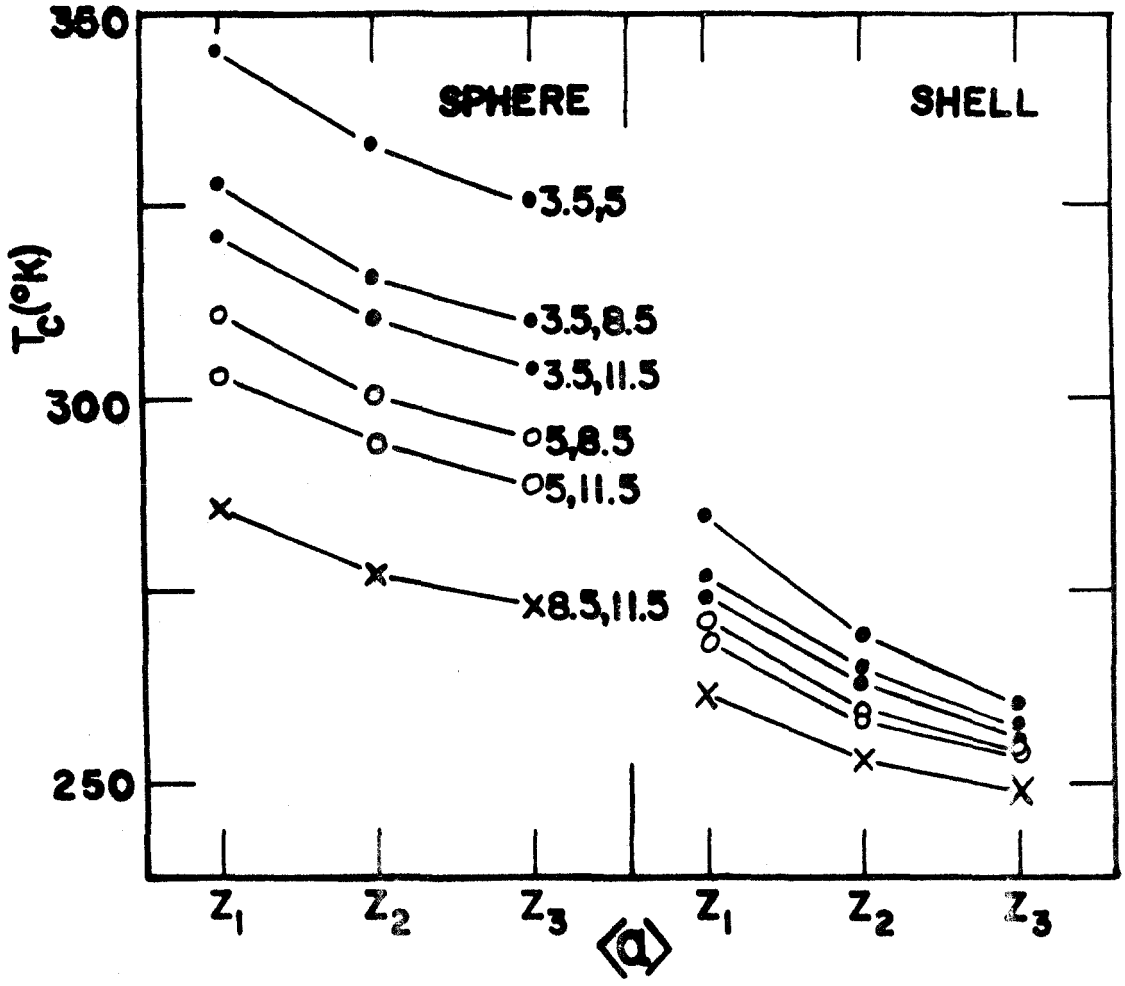

Fig. 9. - Apparent IR color temperatures for homogeneous dust spheres and shells (r_1 = 0.5R) as functions of particle size distribution Z, and wavelengths λ_1, λ_2 which could be used to measure T_c. Object is BD+30°3639, with τ_d = 0.1. For the shell, the same grain density is assumed.

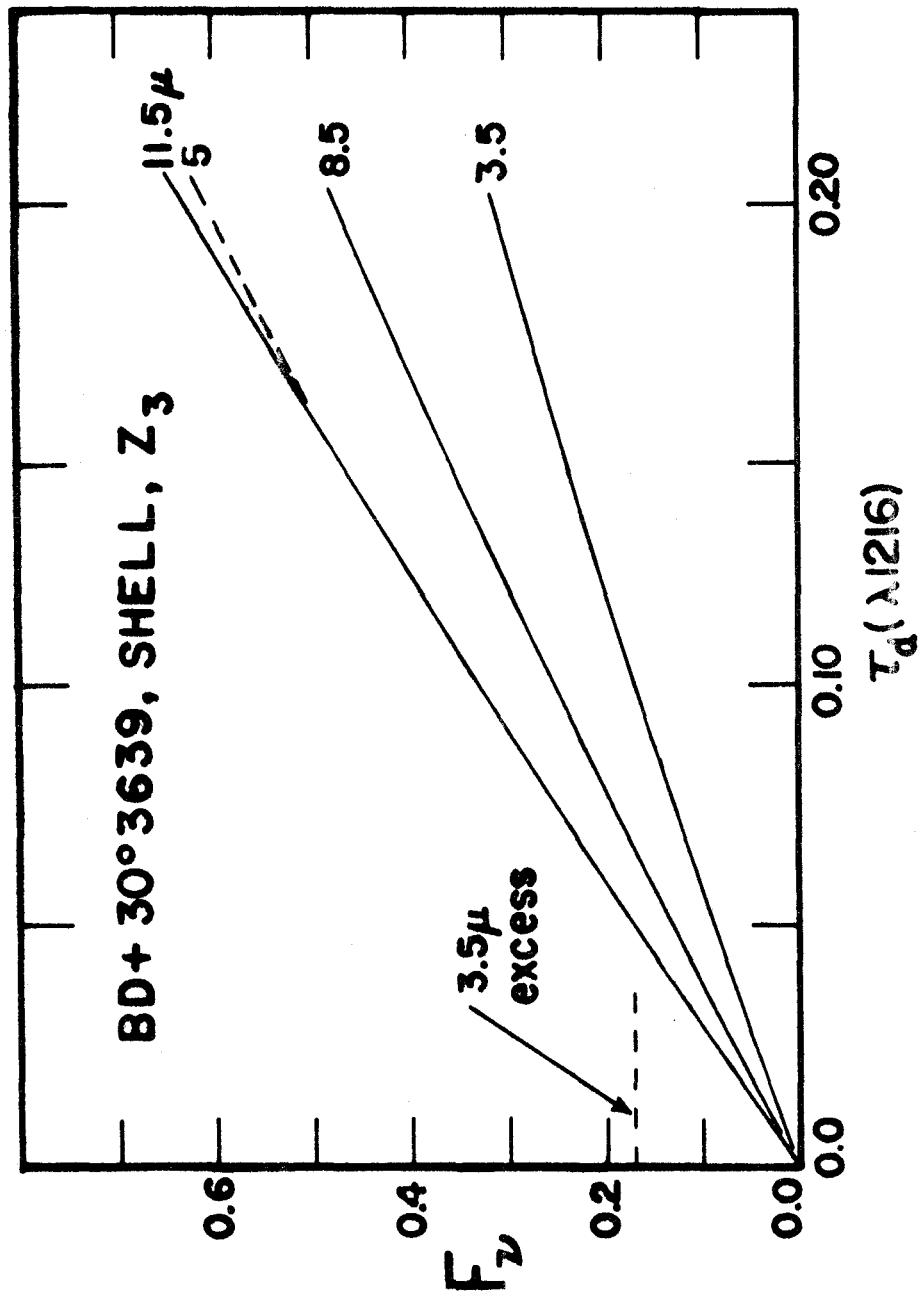

Fig. 10. - F_ν vs. $\tau_d(\lambda 1216)$. Units for different λ_μ's (erg cm^{-2} sec^{-1} Hz^{-1}): 11.5μ, $\times 10^{-20}$; 8.5μ, $\times 10^{-20}$; 5μ, $\times 10^{-21}$; 3.5μ, $\times 10^{-22}$. τ_d is the optical depth a sphere would have at the same grain density.

$\tau_d(\lambda 10830)$ deduced from the He I depopulation rates, if the discrepancy is due solely to dust.

(d) Summary of Chapter IV

Grain color temperatures from observations and from energy balance considerations are shown to be in fair agreement, cf. Tables 8 and 9. The excess continua at short wavelengths, 1.65, 2.2 and 3.5μ, imply the presence of either some very hot dust, or a large number of grains. For example, in the object NGC 2392, 0.04μ grains should equilibrate at 196°K for $y = r/R = 0.24$, or 260°K at $y = 0.1$. The observation of an excess of $\sim$ a factor of 2 at 2.2μ implies either a large number of very small grains, or some particles well within $y = 0.1$ of the central star. This does not mean that $\tau_d(\lambda 10830)$ must necessarily be small, for what matters is $Q(a,\lambda_\mu)/Q(a,1.083\mu)$, which for very small particles still behaves like λ^{-2}.

Silicates have not been considered in any detail since their emission properties may be quite complicated functions of λ, and may cause equilibration at very low temperatures. Martin (1971) plots $Q_{abs}(a,\lambda)$ for a spherical quartz grain of $a = 0.1\mu$ illustrating this point.

The calculations described in this chapter are meant only to illustrate the indeterminancy and complexity of the grain equilibrium problem. The differing measured

color temperatures may be accounted for by a spatial dust distribution, but the number of adjustable parameters is so large as to render any more than order-of-magnitude comparisons meaningless.

V. COMPILATION

In this chapter the theory and data given in Chapters I - IV are combined to derive values of the depopulation rates D_1, D_2 and D_t. Before this is done, values of N_e, T_e and V(R) must be assumed.

(a) Values of N_e and T_e

The problem of determining N_e and T_e for planetaries is fundamental since different methods of simultaneous determination measure different regions of the nebulae. This becomes especially noticeable for filamentary objects, where the reported densities may vary by factors of 10. Seaton and Osterbrock (1957) give the formulae required for finding N_e from the [O II] λλ3726, 3729 doublet ratio, and compare their values with those derived from the Balmer discontinuity B and from the surface brightness S(Hβ). In each case, the [O II] method measures the lower, and B and other forbidden line ratios measure the higher density regions. Kaler (1970) has collected the data for a large number of objects in order to derive N_e using standard methods.

Somewhat the same type of uncertainties arise in the determination of T_e observationally. For example, since the H I recombination rates are higher in regions of lower T_e, while the [O III] emission rates are greater in

regions of higher T_e, different regions of the nebulae may be emphasized in temperature measurements. Peimbert (1967) has demonstrated the effects of fluctuations in N_e and T_e upon the determination of T_e by radio measurements of lines and continuum, [O III] line ratios, Hβ and the Balmer continuum, and has compared his findings with observations of H II regions. Kaler (1970) has discussed the so-called H - temperatures, and reports forbidden line temperatures as well for many objects. On the theoretical side, Gurzadyan (1969) discusses several methods of determining T_e, and also considers temperature gradients and determinations of T_e in the inner regions of nebulae. Seaton (1960) has given an approximate method for finding T_e once the central star temperature T_s is known. These methods depend, in general, upon an energy balance equation, the (cooling) terms of which are uncertain, and T_s, which may be poorly determined.

In Tables 10 and 11 are given the values of N_e and T_e for our list of objects, as determined by different authors, using different methods. We regard the range in these values to be primary evidence for the presence of density fluctuations. The effect of fluctuations upon the derived rates is treated in the next chapter, where the meaning of the lower H - temperatures of Kaler (1968, 1970), Lee (1968), and Thompson (1967, 1968b) is discussed. The

TABLE 10

ELECTRON DENSITIES N_e X 10^{-4}; MISC. DATA

OBJECT	(2)	(3)	(4)	(5)	(6)	(7)	(8)	(9)	(10)	CLASS	ID	LOG $L_S/L_\odot$	LOG R(PC)
40									0.163	I	A	2.060	-1.510
1535	0.25	0.38	0.46	0.26	0.36	0.46			0.448	R	B	4.370	-0.086
418	0.87			1.62	1.59	2.40			4.17	S	C	3.220	-1.640
2149				0.29	0.29				1.47	R	D	5.010	-0.490
2392				0.11	0.07				0.959	R	E	4.510	-0.700
3568									0.567	S	F	3.700	-0.950
4593				0.30	0.22			0.27	0.264	S	G	3.950	-1.100
6210				0.87	1.15				0.655	S	H	2.390	-1.730
6309		0.08	0.42						0.406	I	I	4.480	-0.780
6439									0.592	I	J	4.010	-1.100
6543				0.65	0.56		1.50	0.60	0.779	I	K	4.270	-1.030
6572	0.89			1.05	0.57	4.0	1.90	1.00	0.946	I	L	4.380	-1.140
6567									0.596	I	M	3.140	-1.220
208									3.17		N	2.930	-1.900
6720		0.10	0.08						0.099	R	O	2.780	-0.950
6790									8.60	I	P		-1.360
3639									0.80	S	Q	5.670	-1.250
6818	0.30			0.30	0.32				0.427	I	R	4.170	-0.910
6826				0.23	0.20				0.241	I	S	4.400	-0.910
6891									0.367	R	T	4.480	-0.910
4997									69.0	I	U		-1.240
7009	0.30			0.66	0.65	2.8	1.00	0.60	0.613	I	V	4.040	-0.900
7026									0.506	I	W	4.700	-1.040
7027	1.86			0.50	0.56	4.5	1.70	0.85	1.47	I	X		-1.210
5217									0.868	S	Y	4.190	-0.880
7354									0.581	R	Z	3.750	-0.760
7662	0.72			0.69	0.60	5.0	1.10		0.469	R	Λ	4.590	-1.020

Notes to Table 10

Column:

2. Aller and Liller (1968) p. 540; Radio data.
3. Ibid., p. 527; F(Hβ).
4. Ibid., p. 527; [O II].
5. Aller (1956) p. 149; F(Hβ).
6. Ibid., p. 149; Balmer continuum.
7. Seaton and Osterbrock (1957); Balmer + [lines]†
8. Ibid., S(Hβ).
9. Ibid., [O II] doublet ratio.
10. Kaler (1970); mean value (best estimate).
11. Structural class: I = irregular; S = smooth; R = ring. See Chapter VII.
12. Identification for figures in Chapter VII.
13. Harman and Seaton (1966).
14. Ibid.

† Forbidden lines.

Note: N_e for BD+30°3639 is from O'Dell and Terzian (1970).

TABLE 11

ELECTRON TEMPERATURES T_e X 10^{-3}, EXPANSION VELOCITIES (KM/SEC), Lyα DATA

OBJECT	(2)	(3)	(4)	(5)	(6)	(7)	V(R)	LOG S(Hβ)	τ_c	f_α	NOTES
40					12.0		20	-2.402		50	4
1535	16.0	14.3			13.5		20	-0.690	0.33	17	4
418	12.5		10.4		11.0	4.8	25	-0.157		50	3
2149		14.2	9.2		12.4		20	-0.578		50	1
2392		19.6	18.0		18.8		53	-2.032	0.08	12	1,2
3568			13.4		10.2	8.1	12	-1.860	0.30	17	5
4593		7.7	9.1	10.0	7.7		5	-1.264	0.55	22	4
6210		10.8	11.5		10.2		35	-1.089	1.07	26	1
6309		12.2			12.2		20	-1.300	0.45	18	4
6439					12.0		15	-0.398	0.42	18	4
6543		9.5	7.4	11.0	8.2	3.7	30	-0.698	4.70	40	7
6572	13.0	13.5	12.2	13.0	10.5	6.1	17,20	-0.517	4.50	40	1,6
6567					10.6		35	-0.899		50	1
208					9.8		15	0.016	4.00	40	4
6720		14.9			13.2		30	-2.220		50	2
6790					11.9	2.6	20	0.208		50	4
3639					11.0		30	0.522	0.20	16	1
6818	20.0	15.7	11.6		17.0		30	-1.180	45.0	46	1
6826		11.2	10.6	9.0	10.5		10	-1.320	0.89	23	6
6891					10.2	2.1	15	-0.977	0.89	24	4
4997		10.0			18.8	12.0	15	1.280		50	8
7009	12.0	13.9	13.6	10.0	10.6	9.7	20	-1.210	1.30	28	1
7026					11.2		40	-0.778	2.00	35	3
7027	16.0	16.8	16.5		14.3		23	0.025		50	1
5217			16.5		12.9		20	-0.655	0.73	21	4
7354					12.0		20	-0.962	0.89	22	4
7662	14.0	15.0	20.4	14.0	13.0	5.8	29	-1.159	1.00	23	1

Notes to Table 11.

Column:

2. Aller and Liller (1968) p. 540; [lines].
3. Gurzadyan (1969) p. 122; Aller and Liller (1968) p. 527; Aller (1956) p. 149; [lines].
4. Andrillat (1954); [lines].
5. Sobolev (1960); energy balance and Zanstra T_s.
6. Kaler (1970); best estimate.
7. Ibid., hydrogen temperatures.
8. Hβ surface brightness from, e.g., O'Dell (1962).
9. Lyc optical depth from Capriotti (1967a).
10. Lyα trapping parameter computed per Capriotti (1967b).

NOTES for expansion velocities, etc.

1. Wilson (1950); [O II] or [N II].
2. Ibid., [O III] or [N_e III].
3. Ibid., H or [O I].
4. Derived from Stoy (1939); [O III].
5. Münch (1971; private communication); [O I].
6. Osterbrock, Miller and Weedman (1966); [O III] or [N II].
7. Münch (1968); [O II].
8. Wilson and O'Dell (1962); mean of several lines.

values of Kaler (1970) will be used for N_e, and T_e(F; forbidden lines). The lower hydrogen temperatures T_e(H) are also employed, where possible; otherwise T_e(F)/2 is used to illustrate the effect of assuming a lower temperature. Other determinations of N_e and T_e exist in the literature; we have chosen to collect the values given in the tables to illustrate the ranges in values.

(b) Values of V(R)

Essentially the only data available are the values measured by Wilson (1950). In order to employ the expanding models, one should presumably use the line splittings of the ions of lowest ionization potential. We thus use the [O II] lines when available, and since V([O II]) $\geq$ V([O III]), the [O III] results are lower limits to the expansion velocities and thus give lower limits to $\tau_0(\lambda 3889)$. For those nebulae we have studied, which for one reason or another were not observed by Wilson, we use a rough procedure to estimate the expansion velocity. Stoy (1939) has studied the early spectrograms of Campbell and Moore (1918) and gives verbal descriptions of the line shapes, doublings, etc. Stoy does not make numerical estimates of the degree of broadening, but a plot of Wilson's 2V([OIII]) against a number assigned to each of Stoy's classes exhibits a fair correlation for those planetaries common to both authors' lists. The RMS

deviation of a point from the least-squares straight line through the points is $\sim$ 6 km/sec so the RMS error in V(R) is $\sim$ 3 km/sec. The values of V(R) obtained from this plot for the other objects are thus as well determined as those given by Wilson, since for some objects only a few lines are available, and in any case the values of V([O III]) are probably underestimates. In Table 11 are listed the values of V(R) adopted for this work. The notes to this table give the source and ion for each entry. The Lyman continuum optical depths (λ912) of Capriotti (1967a) and the corresponding values of f_α(Capriotti 1967b) are also listed. If τ_c is unavailable, f_α = 50 is assumed.

(c) Solution for D_1, D_2 and D_t

Using the equations of Chapter II, and the collisional and radiative rates given in Chapter II and Figure 2, we employ power law interpolations to find the depopulation rates implied by Robbins' (1968b) models. The values of N_e are those in column 10 of Table 10; the values of T_e are the forbidden line temperatures in column 6 of Table 11. The results of the solution for the "standard" densities and temperatures are given in Table 12 and Figure 11 where plots of the derived rates are given. The notes appended to Table 7 give the details of the data used for several objects.

TABLE 12

HOMOGENEOUS NEBULA SOLUTION FOR D_1, D_2, AND D_t

OBJECT	R_1	R_2	A	COLL	Lyα	STAR	-LOG D_t	-LOG D_1	-LOG D_2	R_1 REQ	R_2 REQ
40	2.00	0.346	0.564	0.424	0.006	0.005	3.672	2.459	3.961	6.68	0.274
1535	4.38	0.275	0.294	0.646	0.061	0.000	3.388	2.862	3.702	10.59	0.232
418	6.60	0.485	0.046	0.832	0.114	0.009	2.580	2.332	3.159	10.36	0.263
2149	3.45	0.354	0.113	0.783	0.098	0.006	2.975	2.231	3.110	11.26	0.313
2392	4.80	0.575	0.159	0.836	0.001	0.004	3.121	2.353	4.154	18.91	0.242
3568	5.60	0.422	0.295	0.695	0.004	0.006	3.391	3.171	4.388	8.21	0.196
4593	3.10	0.273	0.488	0.420	0.034	0.059	3.609	3.386	3.700	4.15	0.274
6210	5.46	0.346	0.259	0.703	0.033	0.005	3.333	3.093	3.835	8.27	0.225
6309	2.63	0.244	0.337	0.638	0.019	0.006	3.449	2.531	3.521	9.37	0.235
6439	3.13	0.288	0.237	0.647	0.105	0.011	3.295	2.564	2.770	9.16	0.459
6543	4.92	0.379	0.235	0.633	0.116	0.016	3.291	3.181	3.645	5.88	0.273
6572	7.74	0.690	0.168	0.675	0.129	0.028	3.147	3.112	3.827	8.23	0.376
6567	5.50	0.435	0.254	0.645	0.096	0.005	3.325	3.102	3.818	8.06	0.263
208	6.26	0.590	0.059	0.749	0.171	0.022	2.689	2.530	3.230	8.25	0.368
6720	2.24	0.230	0.668	0.321	0.011	0.000	3.745	2.818	4.147	6.02	0.208
6790	3.08	0.837	0.021	0.848	0.130	0.0	2.253	1.387	2.413	11.09	0.619
3639	1.91	0.502	0.077	0.271	0.255	0.396	2.810	1.738	2.957	4.53	0.450
6818	7.55	0.494	0.288	0.660	0.051	0.001	3.381	3.059	4.206	13.79	0.251
6826	4.10	0.304	0.468	0.478	0.030	0.023	3.591	3.306	3.680	6.36	0.282
6891	3.02	0.284	0.363	0.553	0.054	0.031	3.480	2.901	3.409	6.85	0.302
4997	7.03	0.765	0.002	0.830	0.167	0.0	1.261	0.745	1.540	18.35	0.535
7009	5.31	0.324	0.268	0.700	0.028	0.004	3.348	3.067	3.710	8.63	0.242
7026	3.09	0.319	0.271	0.607	0.096	0.026	3.354	2.691	3.442	8.16	0.294
7027	7.72	0.597	0.084	0.623	0.292	0.0	2.846	2.661	3.117	10.79	0.451
5217	3.41	0.294	0.182	0.760	0.053	0.004	3.182	2.414	3.053	11.48	0.326
7354	2.13	0.292	0.261	0.699	0.039	0.001	3.337	2.061	3.439	9.89	0.271
7662	4.27	0.336	0.295	0.666	0.020	0.019	3.390	2.855	3.907	10.43	0.235

Notes to Table 12.

Column:

2. $R_1 \equiv F(\lambda 10830)/F(\lambda 5876)$ corrected for reddening, from Table 7. †

3. $R_2 \equiv F(\lambda 7065)/F(\lambda 5876)$ corrected for reddening, from Table 7.

4-7. Fractional parts of the theoretical depopulation rate, Section II-(c).

A: radiative decay
COLL: collisional deactivation
Lyα: H I Lyα ionization
STAR: central star ionization

8. $-\log D_t$: theoretical He I 2^3S depopulation rate in sec^{-1}.

9. $-\log D_1$: depopulation rate inferred from R_1, equation (II-2).

10. $-\log D_2$: depopulation rate inferred from R_2, Section II-(b).

11. Value of R_1 required to satisfy $D_1 = D_t$.

12. Value of R_2 required to satisfy $D_2 = D_t$.

† R_1 for BD+30°3639 from O'Dell (1963b).

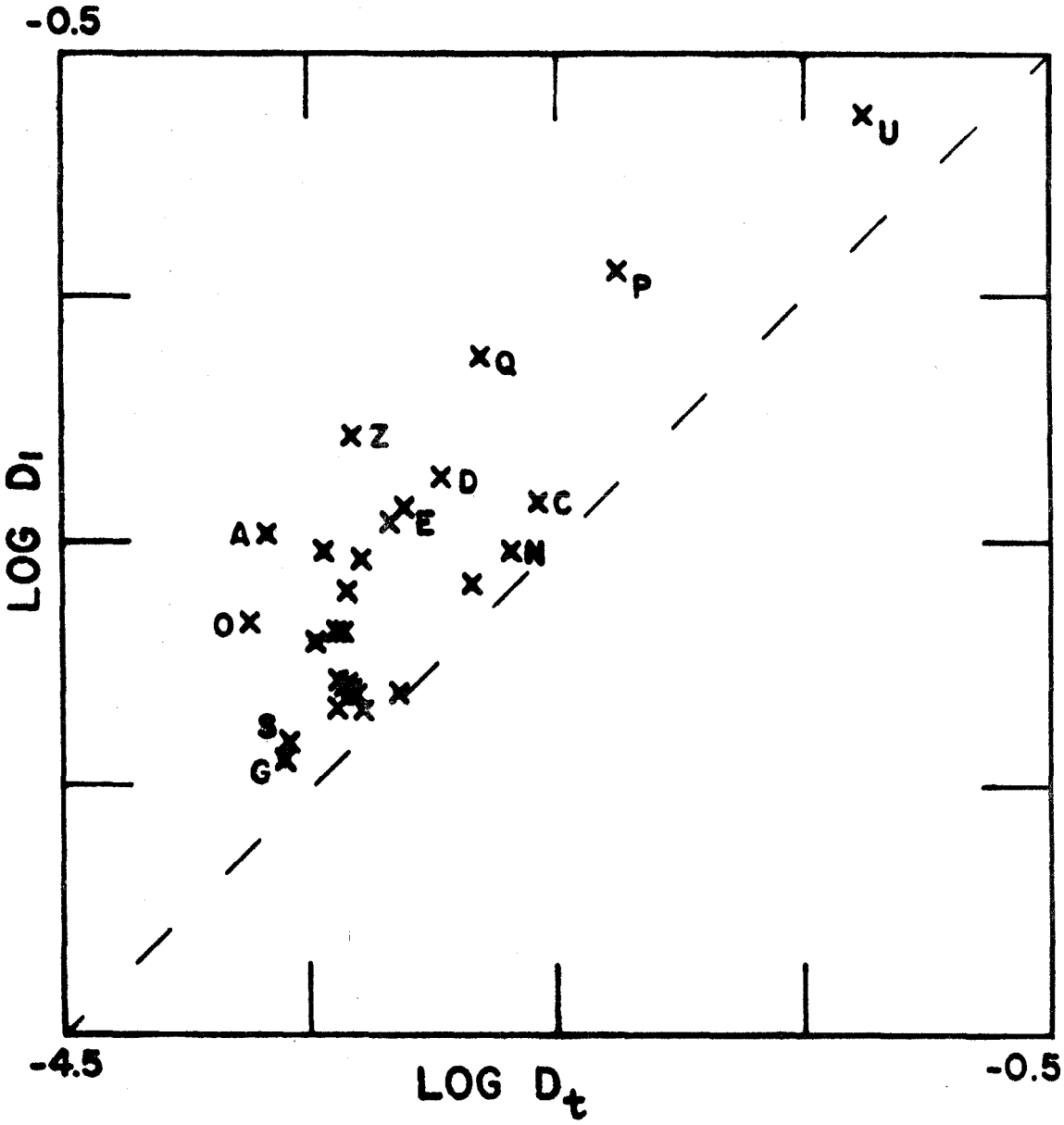

Fig. 11. - Theoretical and observationally inferred 2^3S depopulation rates from Table 12 (no dust model). Identification letters are from Table 10. Dashed line has unit slope.

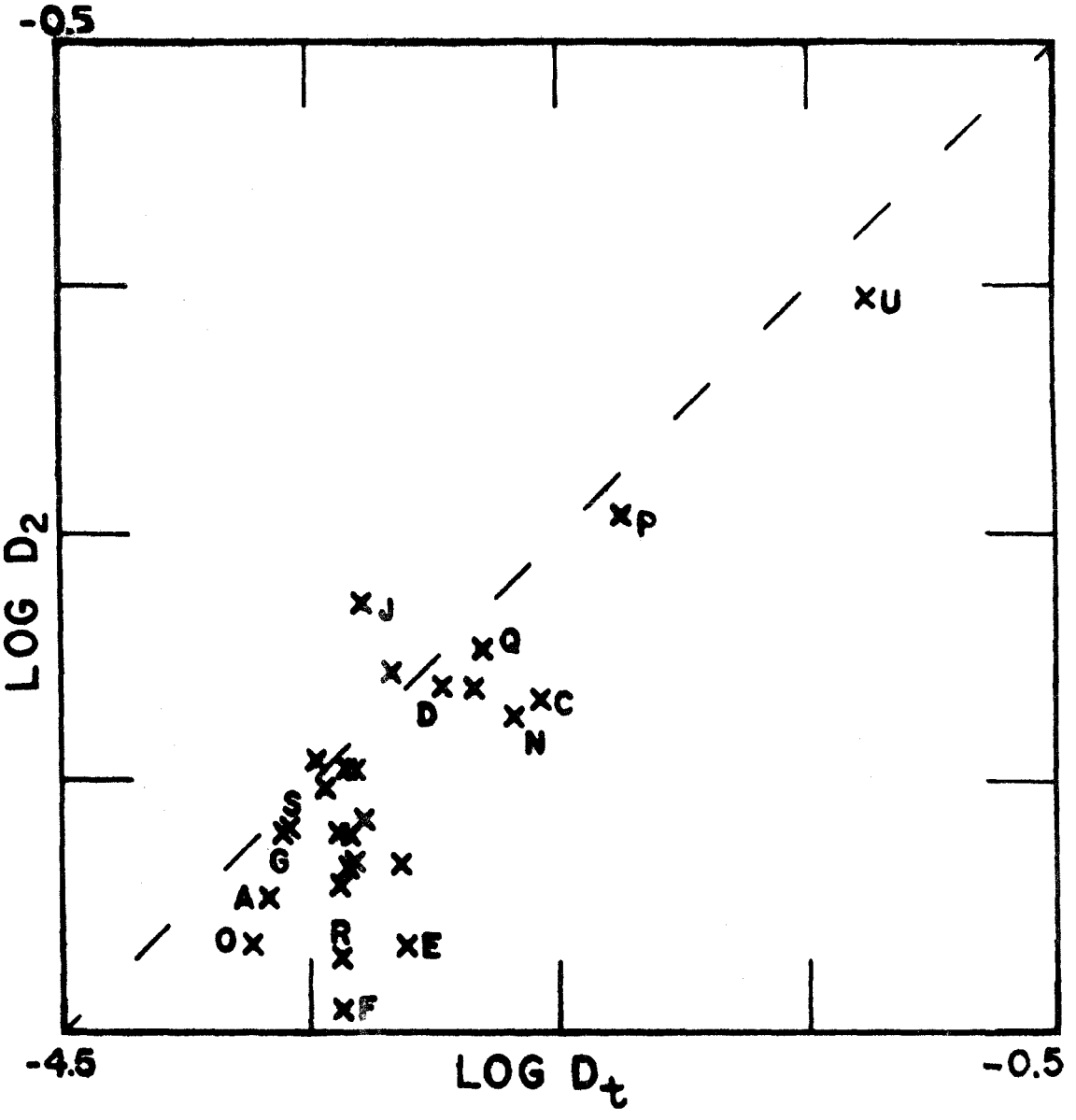

Fig. 11. - Continued.

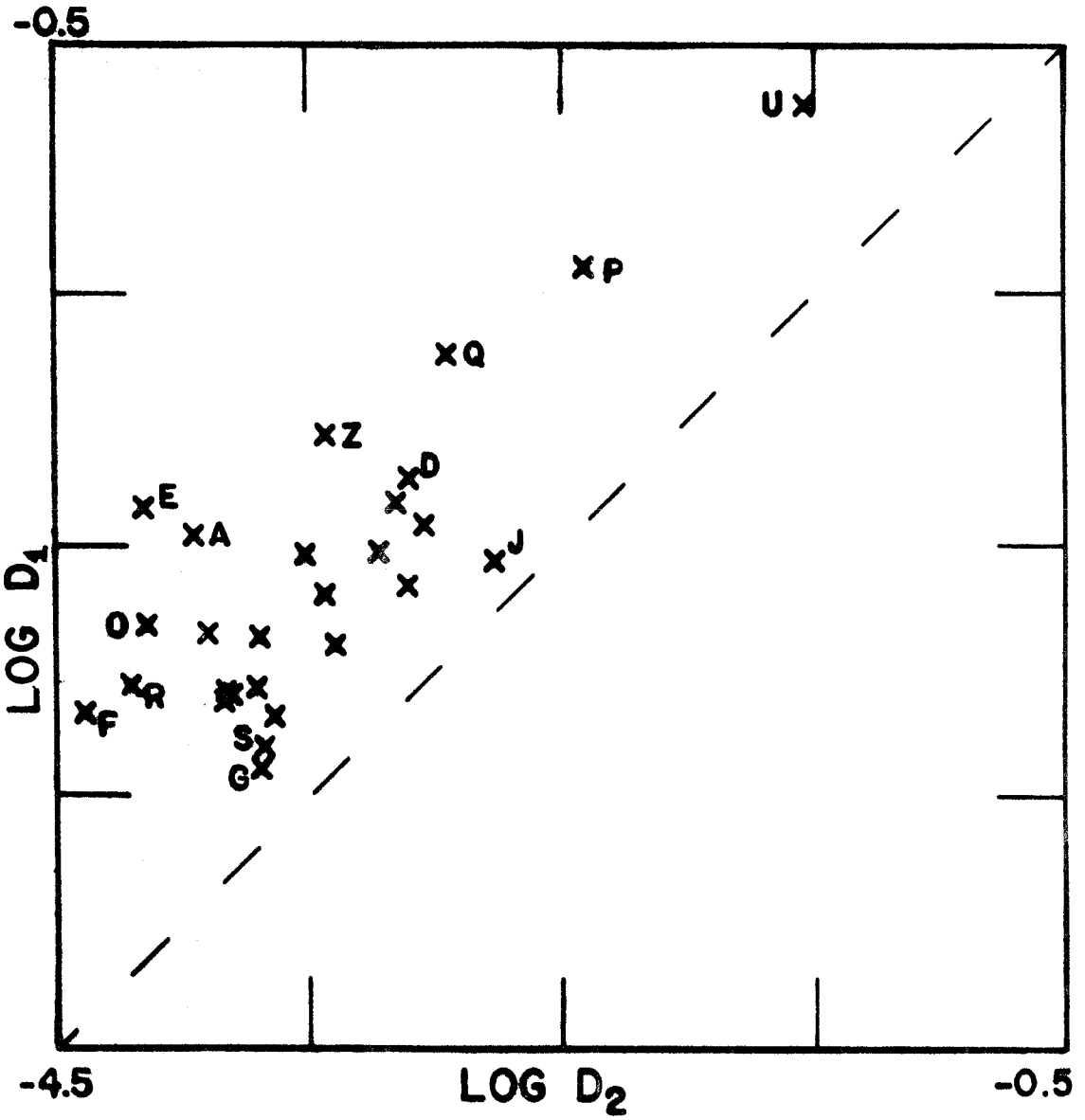

Fig. 11. - Continued.

As indicated by Persson (1970), the lack of agreement between the values of D_t and D_1, and D_t and D_2 goes in the opposite sense, i.e., either the values of R_1 are too low (I[λ10830] is too weak), and the values of R_2 are too high (I[λ7065] is too strong), or the theoretical rates, implied by R_1, are too low, in which case the disagreement for R_2 becomes much worse. The results given here confirm the trends which were apparent in the earlier data studied by Capriotti (1967c). As shown in Chapter VI, this isothermal, homogeneous solution is far too simple to allow a more quantitative analysis.

We have also computed a solution using Kaler's (1970) hydrogen T_e's, or $T_e(F)/2$. The results are not reported since the values of $\tau_0(\lambda 3889)$ tend to be greater than 75. This is due to the dependence of $\xi = V(R)/V(TH)$ on T_e; i.e., the already large values of R_2 imply even larger τ_0's and smaller D_2's if the expansion parameters are increased by $\sqrt{2}$, say.

(d) Sensitivity of the Homogeneous Solution to Uncertainties in the Input Parameters

In order to study the effect of uncertainties in the derived rates due to uncertainties in the parameters entering the determinations, we have chosen to compute a series of solutions for a fictitious object, in which each

parameter is varied in turn. Standard values of the parameters are chosen to represent the "typical" planetary in the list (approximately NGC 6543). The results are shown in Table 13, where the values of $\Delta_1 = \log (D_1/D_t)$ and $\Delta_2 = \log(D_2/D_t)$ are listed with the nominal parameter values and the changing parameters R_2, N_e, etc. The notation "A", "Coll", etc., is explained in the notes to Table 12.

The results of this test are clear: both methods of determining the relative discrepancy between the depopulation rates are quite sensitive to the input parameter values. The relative changes in Δ_1 and Δ_2 with each parameter depend upon the fractional makeup of the theoretical rate, and will thus not be the same for each real object. The dependence of Δ_1 upon C (cf. section III-[f]) is strong because of the large wavelength difference; but for Δ_2, not only is R_2 affected, but S(λ5876) changes with C, and these effects work in the same direction. The use of purely observational parameters is the best one can do, however. As V(R) increases, a larger $\tau_0(\lambda 3889)$ is required to produce the observed R_2, and D_2 decreases accordingly. As N_e increases, Δ_1 increases because only the collisional part of D_t varies linearly with N_e, and thus D_1 (which $\propto N_e$) overtakes D_t. On the other hand, D_2 depends only weakly upon N_e and so Δ_2 decreases as N_e

increases. The most interesting feature of Table 13 is the similar dependence of Δ_1 and Δ_2 upon T_e. The extreme sensitivity of Δ_1 to T_e results from the fact that the cross sections $\sigma(2^3S \rightarrow 2^3P)$ and $\sigma(2^3S \rightarrow$ singlets) have a dissimilar energy dependence (Burke et al 1967), which results in the collisional rates given in Figure 2. Thus despite the conclusion that the collisional part of D_t is often the most important depopulation mode, the T_e dependences in D_1 and D_2 do not cancel out in Δ_1. For D_2, an increase in T_e is a decrease in V(R)/V(TH) so that the λ3889 photons are more severely trapped. An observed value of R_2 must then be produced by a lower value of $\tau_0(\lambda 3889)$; i.e., a higher value of D_2. The increase in D_2 rapidly overtakes the increase in D_t with T_e, especially at higher temperatures. The collisional excitation of 3^3P works in the same direction.

The N_e, T_e sensitivity of the solutions provides the stimulus for Chapter VI, in which density and temperature inhomogeneities are studied.

An estimate of the RMS uncertainties in Δ_1 and Δ_2 for this representative case can be made with the help of Table 13. Allowing the following uncertainties in the parameters: $R_1(\pm 1.0)$, $R_2(\pm 0.06)$, $C(\pm 0.05)$, V(R)(±5km/sec), N_e(factor of 2), $T_e(\pm 1000°K)$, we find the total RMS uncertainties in Δ_1 and Δ_2 to be ±0.2 and ±0.28 respectively.

TABLE 13

SENSITIVITY OF THE SOLUTION

NOMINAL PARAMETER VALUES

R_1	5.00	V(R)	20	A	0.156
R_2	0.35	LOG S(λ5876)	-1.300	COLL	0.683
N_e	10000	LOG S(Hβ)	-0.418	Lyα	0.150
T_e	11000	f_α	40	STAR	0.011
C	0.50	Δ_1	+0.333	Δ_2	+0.064

PARAM.	VALUE	Δ_1	Δ_2	PARAM.	VALUE	Δ_1	Δ_2
R_1	4.0	+0.489	+0.064	V(R)	15	+0.334	+0.139
R_1	6.0	+0.218	+0.064	V(R)	25	+0.333	-0.004
R_2	0.3	+0.333	+0.235	V(R)	30	+0.332	-0.063
R_2	0.4	+0.337	-0.073	N_e	5000	+0.220	+0.237
C	0.3	+0.181	-0.156	N_e	20000	+0.405	-0.136
C	0.4	+0.258	-0.044	T_e	7000	-0.050	-0.144
C	0.6	+0.416	+0.173	T_e	9000	+0.178	-0.030
C	0.7	+0.503	+0.287	T_e	13000	+0.450	+0.151
				T_e	15000	+0.543	+0.237

As stated previously, the models will thus distinguish a factor of two discrepancy between the derived rates.

(e) Inclusion of a Dust Optical Depth

In order to include the possible effect of dust upon the triplet line intensities, equations (II-18) for D_α, and Sections II-(d) and II-(e) are used to revise the expected values of R_1 and R_2. The values of D_1, D_2 and D_t are then found, as for Table 12, as functions of $\tau_d(\lambda 10830)$, assuming the same color dependence $Q(a,\lambda)$ as in Chapter IV to find the expected attenuation of $\lambda 3889$ and Lyα. The condition $D_1 = D_t$ then specifies $\tau_d(\lambda 10830)$, the $\lambda 10830$ dust optical depth along a radius, which forces agreement between D_1 and D_t. In Table 14 are given the results of this solution. The dependence of R_2 upon $\tau_d(\lambda 3889)$ is seen to be slight (cf. Table 12; log $(D_t = D_1)$ vs. log D_2 is replotted in Figure 12). This is because the two effects of dust work upon Δ_2 in opposite directions: (a) $\lambda 3889$ is attenuated, reducing $I(\lambda 7065)$, thus requiring a larger $\tau_0(\lambda 3889)$ and lower D_2, and (b) Lyα is attenuated, lowering D_t. From the compilation of infrared fluxes and apparent dust color temperatures given in Chapter IV, it is seen that better than order-of-magnitude agreement between $\tau_d(\lambda 10830)$ and $\tau_d(\lambda 1216)$ occurs for NGC 7027, BD+30°3639, NGC 6543, NGC 6572 and IC 418, at least, depending very sensitively upon the proposed particle

TABLE 14

SOLUTION FOR $\tau_d(\lambda 10830)$

OBJECT	τ_d 10830	RED 10830	RED 7065	A	COLL	Lyα	STAR	-LOG D_t	-LOG D_2	R_2 REQ	τ_o (λ3889)
40	0.37	3.91	1.09	0.568	0.427	0.000	0.005	3.675	3.976	0.275	5.7
1535	0.52	2.58	1.05	0.310	0.681	0.009	0.000	3.412	3.728	0.235	1.6
418	0.15	1.73	1.06	0.051	0.923	0.018	0.009	2.625	3.183	0.272	6.9
2149	0.31	3.78	1.07	0.125	0.862	0.008	0.005	3.017	3.121	0.323	8.2
2392	1.30	3.97	1.16	0.159	0.839	0.000	0.002	3.123	4.418	0.244	0.2
3568	0.24	1.49	1.07	0.296	0.697	0.001	0.005	3.392	4.402	0.196	1.1
4593	0.07	1.35	1.02	0.494	0.425	0.023	0.058	3.615	3.707	0.275	6.5
6210	0.16	1.55	1.04	0.265	0.721	0.009	0.005	3.344	3.868	0.221	5.7
6309	0.57	4.55	1.05	0.343	0.650	0.002	0.005	3.457	3.518	0.237	2.9
6439	0.19	3.09	1.03	0.256	0.698	0.036	0.010	3.328	2.778	0.457	19.3
6543	0.05	1.25	1.02	0.250	0.675	0.058	0.017	3.319	3.656	0.279	13.7
6572	0.01	1.06	1.01	0.168	0.675	0.129	0.027	3.147	3.835	0.376	13.4
6567	0.13	1.57	1.05	0.276	0.702	0.017	0.005	3.362	3.863	0.263	9.8
208	0.07	1.44	1.04	0.066	0.838	0.073	0.023	2.738	3.268	0.382	15.1
6720	0.77	2.79	1.03	0.675	0.324	0.000	0.000	3.750	4.181	0.210	0.8
6790	0.21	3.97	1.14	0.024	0.960	0.016	0.0	2.306	2.368	0.572	65.5
3639	0.20	2.72	1.12	0.097	0.341	0.110	0.452	2.909	3.097	0.456	42.9
6818	0.42	1.93	1.10	0.303	0.693	0.003	0.001	3.402	4.237	0.255	1.2
6826	0.13	1.59	1.02	0.478	0.489	0.011	0.022	3.600	3.684	0.284	5.1
6891	0.19	2.38	1.03	0.379	0.578	0.013	0.030	3.500	3.414	0.306	8.4
4997	0.19	3.00	1.09	0.003	0.975	0.022	0.0	1.331	1.577	0.569	12.6
7009	0.17	1.67	1.04	0.274	0.716	0.006	0.004	3.358	3.715	0.245	4.4
7026	0.29	2.82	1.06	0.297	0.666	0.012	0.024	3.394	3.530	0.280	13.5
7027	0.11	1.75	1.05	0.110	0.815	0.075	0.0	2.962	3.148	0.502	20.1
5217	0.30	3.77	1.04	0.191	0.795	0.010	0.004	3.202	3.051	0.331	8.1
7354	0.48	8.14	1.08	0.270	0.725	0.005	0.001	3.352	3.440	0.275	5.7
7662	0.43	2.57	1.08	0.301	0.681	0.002	0.016	3.400	3.916	0.238	2.5

Notes to Table 14

Column:

2. Derived $\tau_d(\lambda 10830)$ required to fit D_1 and D_t.
3. Implied I(λ10830) reduction factor.
4. Implied I(λ7065) reduction factor.
5-8. Fractional parts of D_t due to radiative decay, collisions, Lyα, central star; as for Table 12.
9. -log D_t forced = -log D_1.
10. -log D_2 implied for $\tau_d(\lambda 10830)$ included.
11. Required value of R_2 for $\tau_d(\lambda 10830)$ included.
12. Line center optical depth in the λ3889 transition.

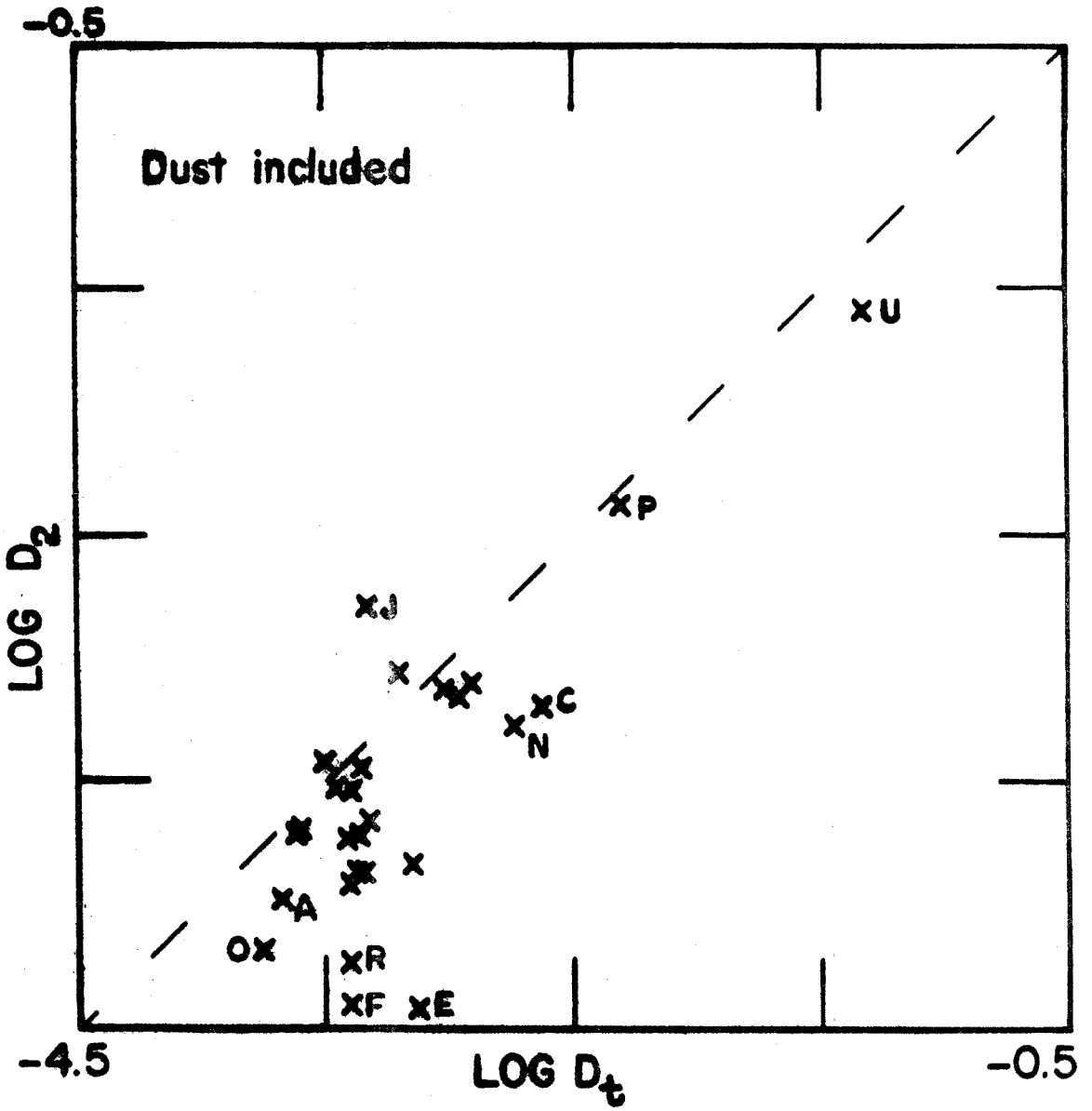

Fig. 12. - Log D_2 vs. Log D_t from Table 14. Enough dust is now included to force $D_1 = D_t$. There is marginal improvement over corresponding plot of Figure 11.

characteristics (for fluxes), and upon the adopted value of T_c (observed) for the best observed objects.

The fractional parts of D_t are listed again to illustrate the effect upon the separate rates. The destruction of Lyα generally raises $\tau_0(\lambda 3889)$, and thus for several objects a greater value of $\tau_d(\lambda 10830)$ is required than would be necessary if Lyα were unimportant.

The main conclusion to be drawn from these tables is that the orders-of-magnitude (if not better) of the values of $\tau_d(\lambda 10830)$ derived by two (or three) independent methods are the same for this highly idealized model fitting procedure. In a statistical sense, the values of τ_d found by these methods provide a reasonable argument supporting the interaction of the resonance-like $\lambda 10830$ photons with grains inside the nebulae. The discussion of the theoretical grain temperatures in Chapter IV indicates that the fluxes can be accounted for by the presence of dust, and also that the range in color temperatures may be produced by particles with smoothly varying functions $Q(a,\lambda)$. In addition, appreciable amounts of dust may be present inside some nebulae, but at very low temperatures, due to a combination of shielding effects which are discussed in Chapter VII.

VI. NEBULAR STRUCTURE

(a) Introduction

In this chapter we consider one of the most striking and least understood aspects of planetary nebulae, namely the presence of widely diverse structural features such as bright toroidal rings, mottled surfaces, sharp filaments, and faint outer envelopes. Since the depopulation rate of He I (2^3S) seems to be mainly collisional, one would not expect a large alteration of the deduced rates D_1 and D_t in an isothermal nebula. Despite the apparent difficulty in driving thermal instabilities in plasmas which have very effective thermostatic agents such as the O^{++} ions which emit $\lambda\lambda$4959, 5007 radiation after collisional excitation (Mathis 1968, Harrington 1968), we shall see that in real objects, lower temperature regions can and perhaps do exist, as the so-called "H-temperatures" (Kaler 1970) seem to suggest.

In this chapter several different problems are considered. The discussion is motiviated by a brief review of some observational material. The rates D_1, D_2 and D_t are then rederived for simple model nebulae which have high and low density phases. Further observations by the author are then presented which strongly support the ideas presented in the preceding chapters, and suggest a

mechanism for the production of toroidal features which seem to be common to $\sim$ 70% of all planetaries. The discussion of structural effects and causal agents is then compiled to examine the problem of the maintenance and spectral emission of a model filament.

(b) Motivation

The main reason for studying the effects of density (and temperature) fluctuations upon the He I problem is simply that they exist. Numerous authors have commented upon these features; the photographs and drawings of Curtis (1918) and the catalogue of Perek and Kohoutek (1967) eloquently summarize the situation. Tables 10 and 11 are regarded as strong evidence for fluctuations, since determinations of N_e by different methods often give very different results. Seaton and Osterbrock (1957) and Seaton (1960) have discussed simple two-phase (high and low N_e) models for NGC 7027; Weedman (1968) has presented observations and descriptions of several objects with a view to studying the brightness fluctuations, and Peimbert (1967) has considered in some detail the determination of T_e in fluctuating media. The general morphology of planetary nebulae has been discussed by several authors in the I.A.U. Symposium 34 (1968).

The fact that inhomogeneities are observed to occur

in practically all planetaries argues either for long lifetimes or continuing rapid evolution and decay. Since toroidal features are observed in so many objects, however, the latter case is possible only for fine scale structures. We shall show that it is reasonable to attribute both types of inhomogeneity to the same cause.

In connection with the observations of filamentary structure in the nebular light, observations of the central star of BD+30°3639 should also be mentioned. Wilson (1950) has shown that two very sharp absorption features to the blue of λ3889 exist. The apparent lack of λ3889 absorption components in planetaries (Münch; private communication) may be due in part to filamentary structure (cf. Münch and Wilson 1962). Vaughan (1968) has observed blue absorption features in the λ10830 line of several objects.

Two other problems are almost certainly related to this study. First, the appearance of [O I] λλ6300, 6363 lines in several objects (Campbell 1968) implies the existence of a phase in a state of somewhat lower-than-average ionization, but with enough free electrons to excite the lines (Williams 1970, but see Field and Steigman 1971). One immediately thinks of transition regions (neutral to ionized) which occur at the nebular surface for ionization bounded objects - of which there may be only a few - or around the surfaces of individual

filaments. Second, recent determinations of the electron temperatures from Balmer decrements (Kaler 1968), from continuum to line ratios (Lee 1968) and for the Orion Nebula (Hjellming and Gordon 1971 and references cited therein) seem to indicate that lower temperatures (a difference of a few thousand °K) exist somewhere in the vicinity of planetary nebulae and H II regions. More work will be required to settle this problem, but if the interpretation is correct, one again thinks of the filaments as the probable location of the lower temperature gas. Confirmation of this statement would considerably aid in understanding the maintenance of the higher density filaments, since filaments in an isothermal nebula would lose their identity (suppose the density is twice as high in the filaments as in the intervening gas) on a time scale of $\sim 2X/V(TH)$, where X is the characteristic dimension of a filament, say 1/20 the nebular radius. For typical objects this is $\sim$ 1000 years, during which time the object will have expanded by $\sim$ 20%. While this is possible for small filaments, it is highly improbable for the toroids, and renders more difficult the problem of filamentary origins.

It will be shown that given the presence of grains around the progenitor stars, it is reasonable to expect all the aforementioned effects, viz.: toroidal and

filamentary structure, higher values of R_2 and lower values of R_1 than expected, higher and lower temperature regions, and [O I] emission.

We first demonstrate the effect of structure upon the observed value of R_1, and show that a solution for D_1 may be meaningless in certain situations. Ad hoc assumptions about the pressure equilibrium are made at this point, but are reconsidered later. A different model is used to study the rate D_2.

(c) Effect of Fluctuations Upon R_1 and D_1

Suppose that only two discrete densities coexist in the emitting volume. For definiteness, we assume that a number of high density clumps is embedded in a low density medium. Let all parameters for the high density phase have the subscript 2, and those for the lower density phase, 1. Let the ratios (high N_e/low N_e) of densities be x, volumes y, and Hβ recombination coefficients ω. Table 15 summarizes the convention. The Hβ flux is proportional to

$$\alpha_2(H\beta)N_{e_2}^2 V_2 + \alpha_1(H\beta)N_{e_1}^2 V_1,$$

and the mean-square density determined from Hβ photometry is thus

TABLE 15

INHOMOGENEOUS MODEL - NOTATION

Parameter	High density phase	Low density phase	Ratio or Note
Density	N_{e2}	N_{e1}	$x \equiv N_{e2}/N_{e1}$
Volume	V_2	V_1	$y \equiv V_2/V_1$
Temperature	T_{e2}	T_{e1}	$T_1 \equiv T_{e1} \times 10^{-4}$ etc.
Recombination coefficient	$\alpha_2(\lambda)$	$\alpha_1(\lambda)$	$\omega \equiv \alpha_2(H\beta)/\alpha_1(H\beta)$
$N(2^3S)$	$N_2(2^3S)$	$N_1(2^3S)$	
$N(He^+)$	N_2^+	N_1^+	$\beta_{1,2} \equiv N^+_{1,2}/N_{e_{1,2}}$
2^3S Depopulation rate	$D(1)^\dagger$	$D(2)$	
λ10830 Collisional rate	$q_2(2^3S \rightarrow 2^3P)$	$q_1(2^3S \rightarrow 2^3P)$	$\equiv q_{2,1}$

† Observed or observationally inferred values have superscript (°). Subscript c denotes clouds.

$$\overline{N_e^2} = \frac{\alpha_2(H\beta)N_{e2}^2V_2 + \alpha_1(H\beta)N_{e1}^2V_1}{\alpha_2(H\beta)V_2 + \alpha_2(H\beta)V_2} . \qquad \text{(VI-I)}$$

Dividing this equation by $\alpha_1(H\beta)V_1$ and using Table 15, we have

$$\overline{N_e^2} = N_{e1}^2\frac{(1 + x^2\omega y)}{(1 + \omega y)} ,$$

or

$$N_{e1} = \left[\frac{1 + \omega y}{1 + x^2\omega y}\right]^{1/2}(\overline{N_e^2})^{1/2} . \qquad \text{(VI-2)}$$

Of course the density may be found by other methods which will produce other expressions involving collisional rates for forbidden lines. The $N(2^3S)$ balance condition holds for any part of the nebula, so the equations of Chapter I can be modified for the two-phase medium, and with the definition $\gamma = \frac{\beta_2\alpha_2(\lambda5876)}{\beta_1\alpha_1(\lambda5876)}$ we have

$$R_1 = \frac{2.43q_1N_{e1}}{(1 + \gamma x^2y)D(1)} + \frac{2.43q_2N_{e2}\gamma x^2y}{(1 + \gamma x^2y)D(2)} + 1.63, \qquad \text{(VI-3)}$$

where R_1 is the observed ratio $I(\lambda10830)/I(\lambda5876)$ corrected for reddening. The results of Chapter V show that collisional excitation of the He I singlet levels is the main 2^3S depopulation agent. Letting $D(1,2) = c_{1,2}N_{e1,2}$ where

$c_{1,2}$ are the rates presented in Figure 2, equation (VI-3) may be rewritten as

$$(R_1-1.63) = \frac{2.43}{(1 + \gamma x^2 y)}\left[\frac{q_1}{c_1} + \frac{q_2 \gamma x^2 y}{c_2}\right] \qquad \text{(VI-4)}$$

Note that the ratio q/c increases steadily with T_e.

There are two extreme cases to consider: (a) if the temperature is constant $q_1/c_1 = q_2/c_2$ and $(R_1-1.63)$ will correspond to the adopted temperature, and (b) if there is pressure equilibrium, then $q_1/c_1 > q_2/c_2$. For case (b), we make the approximation (from Figure 2) that $q/c \simeq dT_e$, where d is a constant. If all the gas is ionized, N^+/N_e is constant, $\beta_1 = \beta_2$, and γ is the ratio of the λ5876 recombination coefficients, so that $\gamma \sim (T_{e1}/T_{e2})^{1/2}$, and equation (VI-4) becomes

$$(R_1-1.63)_p = 2.43 dT_{e1} \frac{[1 + x^{3/2} y]}{[1 + x^{5/2} y]} . \qquad \text{(VI-5)}$$

A large enough value of x will thus begin to affect $(R_1-1.63)$ if an appreciable volume of the nebula is in the higher density phase.

Now, only three quantities are observed, viz., R_1°, $(\overline{N_e^2})^{1/2}$ and T_e, from which the inferred $2\,^3S$ depopulation rate D° is formed:

$$D_1^\circ = \frac{2.43q(\overline{T_e})\ (\overline{N_e^2})^{1/2}}{(R_1^\circ - 1.63)} \quad . \qquad \text{(VI-6)}$$

The mean electron temperature $\overline{T_e}$ is usually found from observations of [O III] lines, whose intensities are given by

$$I_o \equiv I(\lambda 4959 + \lambda 5007) \propto \frac{\exp(-2.97/T_4)}{T_4^{1/2}} N(O^{++})N_e,$$

and

$$I(\lambda 4363) \propto \frac{\exp(-3.3/T_4)}{T_4^{1/2}} N(O^{++})N_e \ .$$

Assuming with Seaton (1960) that most O is O^{+++}, the ionization equilibrium between O^{++} and O^{+++} is $N(O^{++})\mathcal{A} \propto \alpha(O^{++})N(O^{+++})N_e$ where $\mathcal{A}$ is the O^{++} ionization rate. If $\mathcal{A}$ is $\sim$ constant, $N(O^{++}) \propto N_e^{5/2}$ (approximately) in pressure equilibrium. Using the above equations and Table 15, we write

$$\frac{I_o}{I(\lambda 4363)} \propto \exp(0.33/T_1) \qquad \text{(VI-7)}$$

$$\times \frac{(1 + x^4 y \exp[-2.97\{1/T_2 - 1/T_1\}])}{(1 + x^4 y \exp[-3.30\{1/T_2 - 1/T_1\}])},$$

where the subscripts 4 are suppressed from T, and the T subscripts identify the phases.

The presence of the exponentials insures that the measured ratio gives the temperature of the low N_e, high T_e phase, for any reasonable combination of x, $T_{e1,2}$ and y. Since this means that $\overline{T_e} = T_{e1}$, combining equations (VI-2), (VI-5), and (VI-6) gives

$$D^\circ = \frac{(1 + x^2\omega y)}{(1 + \omega y)} \times \frac{(1 + x^{5/2}\, y)}{(1 + x^{3/2}\, y)} \times D(1). \quad \text{(VI-8)}$$

Now $\omega > 1$, and $\gamma \sim \omega > 1$, and $x > 1$, so the "observed" depopulation rate is larger than the true depopulation rate in the hotter phase, and for most cases, larger than that in the cooler phase. Equivalently, since most of the λ5876 flux is from the cooler regions, R_1° will be too small and D° will appear to be too large, since the λ10830 production is very temperature-dependent.

Equation (VI-8) represents the extreme case of pressure equilibrium, and thus gives an upper limit to the real rate discrepancy $D^\circ/D(1)$, for the R_1-derived $2\,^3S$ depopulation rate D_1. In Section VI-(f) the above result is shown to have a small effect upon R_1 and D_1 in two nebulae, but not nearly the effect that would be observed in the (impossible) pressure equilibrium (as it has been used here, $N_{e_1}T_{e_1} = N_{e_2}T_{e_2}$) case.

(d) Effect of Fluctuations Upon R_2 and D_2

One cannot use such a simple model as in Section VI-(c) to study structural effects upon R_2. Capriotti (1967c) mentions the effect of shell structure briefly in his treatment of the 2^3S rate anomaly, but does not pursue the point. As shown in Chapter V, for many objects the theoretical 2^3S depopulation rates are larger than those deduced from measured values of R_2 and $S(\lambda 5876)$, and assumed values of T_e and $V(R)$; i.e., $D_t > D_2$ or R_2 appears to be too high ($\lambda 7065$ is too strong).

Consider two hypothetical nebular models, the first being a homogeneous, uniformly expanding sphere with $S \equiv S(\lambda 5876)$ and $\tau_0 \equiv \tau_0(\lambda 3889)$, i.e., Robbins' model. Let the other nebula be filled with randomly distributed, uniform, spherical clouds expanding away from the central star. For the moment, we suppose that the space between the clouds is empty. Let there be N clouds, each with radius r_c, so that the cloud optical depth at line center is defined by

$$\tau_c \equiv r_c \frac{\alpha_c(2^3S) N_{ec} N_c(He^+)}{D_c} \frac{\kappa_0(\lambda 3889)}{T_4^{1/2}} \qquad \text{(VI-9)}$$

and $\kappa_0(\lambda 3889)$ does not involve T_e. The mean optical depth of this model nebula is

$$\langle \tau_c \rangle = \frac{R \kappa_0(\lambda 3889)}{T_4^{1/2}} \times \frac{\alpha_c(2^3S) N_{ec} N_c(He^+)}{D_c} \times \frac{N \times (4/3)\pi r_c^3}{(4/3)\pi R^3} \cdot \qquad \text{(VI-10)}$$

As usual R is the nebular radius and D_c the theoretical depopulation rate. The surface brightness (λ5876) is

$$S \simeq N \times \frac{4\pi r_c^3}{3} \times \frac{\alpha_c(\lambda 5876) N_{ec} N_c(He^+)}{4\pi R^2} \qquad \text{(VI-11)}$$

so that

$$\langle \tau_c \rangle = \frac{\kappa_0(\lambda 3889)}{T_4^{1/2}} \frac{3S}{D_c} \frac{\alpha_c(2^3S)}{\alpha_c(\lambda 5876)} \qquad \text{(VI-12)}$$

as before. Let us compare the line emission for a given $\langle \tau_c \rangle$ and S. Combining equations (VI-9) and (VI-10) gives

$$\tau_c = \frac{\langle \tau_c \rangle}{N} \left(\frac{R}{r_c} \right)^2 \qquad \text{(VI-13)}$$

Keeping the same S for the two models requires that S from equation (VI-11) be just

$$\alpha(\lambda 5876) N_e N(He^+) \times (4/3)\pi R^3 / 4\pi R^2 ,$$

where now the densities and α's are for the homogeneous model. This gives

$$N = \left(\frac{R}{r_c} \right)^3 \times \left(\frac{Ne}{N_{ec}} \right)^2 \times \frac{\alpha(\lambda 5876)}{\alpha_c(\lambda 5876)} \quad , \qquad \text{(VI-14)}$$

so that

$$\tau_c = \langle \tau_c \rangle \frac{r_c}{R} \frac{\alpha_c(\lambda 5876)}{\alpha(\lambda 5876)} \left(\frac{N_{ec}}{N_e} \right)^2 . \qquad \text{(VI-15)}$$

Suppose $N_{ec} \sim 3N_e$, and $\alpha_c(\lambda 5876) \sim \sqrt{3} \times \alpha(\lambda 5876)$ in analogy with the pressure equilibrium case. For N = 1000, equation (VI-14) gives $(R/r_c) \sim 26$, and $\tau_c \sim 0.6\langle\tau_c\rangle$ Smaller, denser clouds may have optical depths even greater than $\langle\tau_c\rangle$. If these clouds are internally static, the λ7065 emission for a given $\tau_0 \leftrightarrow \langle\tau_c\rangle$ may be larger than for the homogeneous case, since we effectively have N model nebulae each with an optical depth $\sim \tau_0$ but <u>zero expansion velocity</u>. For $T_4 = 1$, and $\tau_0 = 20$, the λ7065 enhancement may approach 50%.

These simple considerations show that in filamentary nebulae, the possible enhancement of I(λ7065) may render the rate D_2 useless, insofar as comparison with D_t goes. The effect of each filament upon every other has been neglected in this treatment, but inclusion of the diffuse λ3889 radiation from the other clouds increases I(λ7065) even further. We may estimate the effect of the other clouds as follows: each cloud will radiate a flux of λ3889 which has a double peaked profile symmetric about the particular λ_0 corresponding to its velocity of recession from the nucleus. These peaks are displaced $\sim (\ln\tau_c)^{1/2}$ Doppler widths from λ_0, and for typical nebulae this is between 1.5 and 2.0 $\Delta\lambda_d$. Since each cloud is moving away from every other, the blue emission peak will be preferentially absorbed by other clouds. The mean optical depth

($\equiv \tau_b$) through the randomly distributed clouds will be

$$\tau_b \simeq \frac{N}{(4/3)\pi R^3} \times \pi r_c^2 \times \langle \ell \rangle ,$$

where the geometrical cross section is assumed for each cloud; i.e., a "blue" photon has unit probability of being absorbed by any cloud, and $\langle \ell \rangle$ is the mean distance to the surface of the nebula. Approximating $\langle \ell \rangle$ by R, we have

$$\tau_b \simeq (3/4)N(r_c/R)^2 ,$$

and for the previous example, we have $\tau_b \leq 1$ (upper limit since the cross section of each cloud is $< \pi r_c^2$). The extra probability of absorption given to each λ3889 photon in this way will increase I(λ7065) even further.

(e) Effects of Other Structural Features Upon R_2 and D_2.

In this section two other structural effects which may alter R_2 and D_2 are considered qualitatively. Firm numerical estimates of the magnitudes of these effects cannot be made due to their highly model-dependent nature.

(1) Nebular Shell

The measured value of R_2 will be lower for a shell nebula than a sphere. Not only is the λ7065 emissivity higher in the center of a sphere, but λ3889 photons emitted

from the inside surface of a shell stand a good chance of escaping through the opposite side of the shell since the Doppler shift of the absorbers will be $\gtrsim$ V(R). The observations of E(λ5876) and E(λ7065) presented in Chapter III indicate, however, that many of the nebulae are not shells, insofar as their He I emission is concerned, so shell emission models will not be considered further.

(2) Outer Envelopes

Conspicuous outer envelopes surround the planetaries NGC 6826, 6543 and 6720. Duncan (1937) has reproduced long exposure photographs of several objects and has searched for envelopes around several others. Minkowski and Osterbrock (1960) have taken spectra in [O II] λ3727 of the envelopes surrounding NGC 6720 and NGC 650-1, and O'Dell (1962) has commented upon the possible origin of these features. The objects NGC 6891 and NGC 7662 also appear to have very faint envelopes, judging by the Palomar Sky Survey E plates. One cannot rule out the existence of extremely faint envelopes around all planetaries, nor can one dismiss early ejection as a possible cause. Radial velocity information will be very difficult to obtain except perhaps for objects like NGC 6720, and at present no radial velocity data are available. Early ejected matter cannot be appreciably slowed down by compression of the interstellar gas, but the possibility that the

bright inner regions are actually expanding faster cannot be ruled out. If this is the case, either the envelope itself, the boundary, or the outer regions of the "planetary" itself may be effectively approaching parts of the expanding nebular gas. If this occurs, some of the H8 λ3889.05 emission line 32 km/sec to the red of He I λ3888.65 may be blueshifted onto the He I λ3889 transition thus increasing I(λ7065) and R_2. The increases in I(λ7065) observed at the edges of NGC 2392 and NGC 6572 are not unreasonable if the relative approach velocity ∿ 25 km/sec, in which case ∿ one-half the H8 emission (0.11 times Hβ) may be converted to λ3889 resonance-like radiation.

(f) Further Observations of Planetaries

(1) Results

Immediately preceding and following the observations of the Orion Nebula (in December 1969) reported by Münch and Persson (1971; hereinafter referred to as MP), the objects NGC 7662 and NGC 3242 were scanned in a similar fashion. The observational method, details on data reduction, and consideration of the errors involved will be found in MP. Briefly, the technique consisted of trailing the 200-inch Hale telescope across the source at a uniform rate, and continuously monitoring the count rate in each of four channels of the multichannel (Cassegrain) spec-

trometer (Oke 1969). One "Hydrogen" scan across NGC 3242 was made, the focal plane entrance aperture subtending 2.0 arc sec, with special exit plots centered on Hα, Hβ, Hγ, and a continuum channel at λ4530. The slots had effective widths of 14, 14, 16, and 120 A respectively. Several "Helium" scans were made across both planetaries. In this case the integration time per point was increased, the entrance aperture was 3.6 arc sec in diameter, and the exit slots were centered on λλ5876, 7065, 8060, 10830, and had widths of 19.5, 20.9, 201.6 and 20.0 A respectively. The sky brightness was measured at the end of each scan, and the resulting count rates were converted to absolute intensities using standard methods. The continuum channel was used in each case to correct the line channel intensities for continuum contamination. This correction is small for Hα and Hβ, but is important for the He observations. Due to some line contamination of the λ8060 continuum channel itself in these moderately high excitation objects, accurate photometric line ratios have not been obtained. The λ10830 intensity is not affected, but both I(λ5876) and I(λ7065) have been underestimated (systematically, since the continuum tracing looks very much like either of these two line tracings); R_1 has thus been overestimated, and $\langle R_2 \rangle$ is uncertain. The important results of this work are the relative changes in the line ratios from point to point along a scan. Figure 13 is a

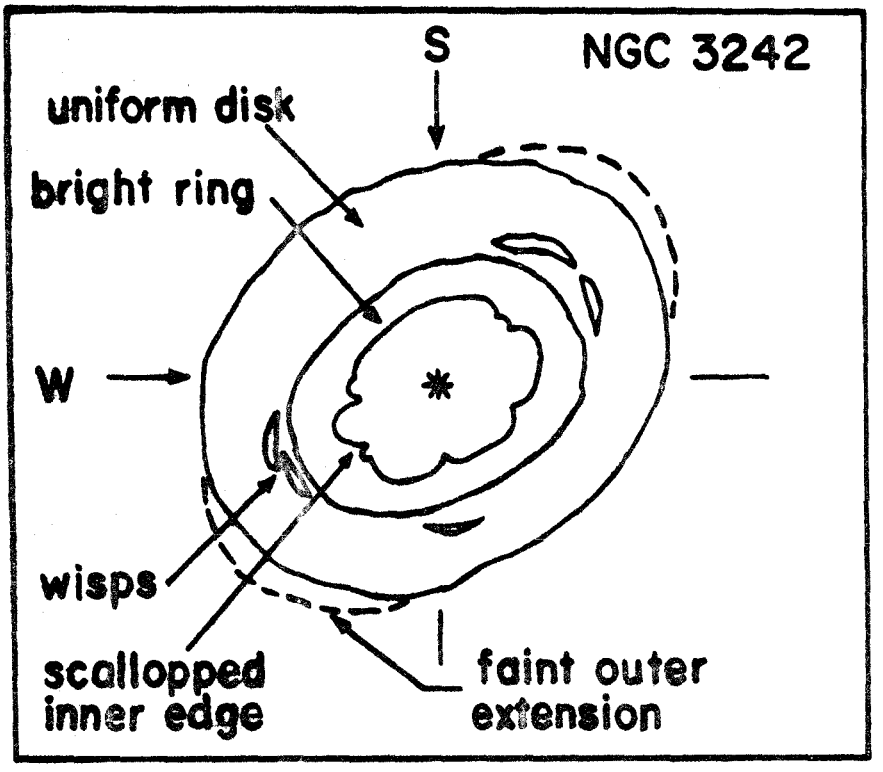

Fig. 13. - Sketch of NGC 3242 showing structural features and orientation of H and He traces. Height of figure corresponds to 60 arc sec.

Fig. 14. - (Next page). Intensity and Log (color) plots for swaths covered on two objects. All Logs are 0.10 per division, 0.0 being measured from the bottom of each plot. I(Hα): 0.10×10^{-12} per division; I(λ10830): 0.25×10^{-13} per division; I(λ5876): 0.5×10^{-14} per division; all units of erg $cm^{-2}sec^{-1}$ $(arc\ sec)^{-2}$. Long tick marks identify 0.'s of intensity traces displaced for clarity. Displaced traces are I(λ10830) except for NGC 3242 W → E, where it is I(λ5876). Crosses indicate position of central star. Reddening correction for NGC 3242 is C = 0.33.

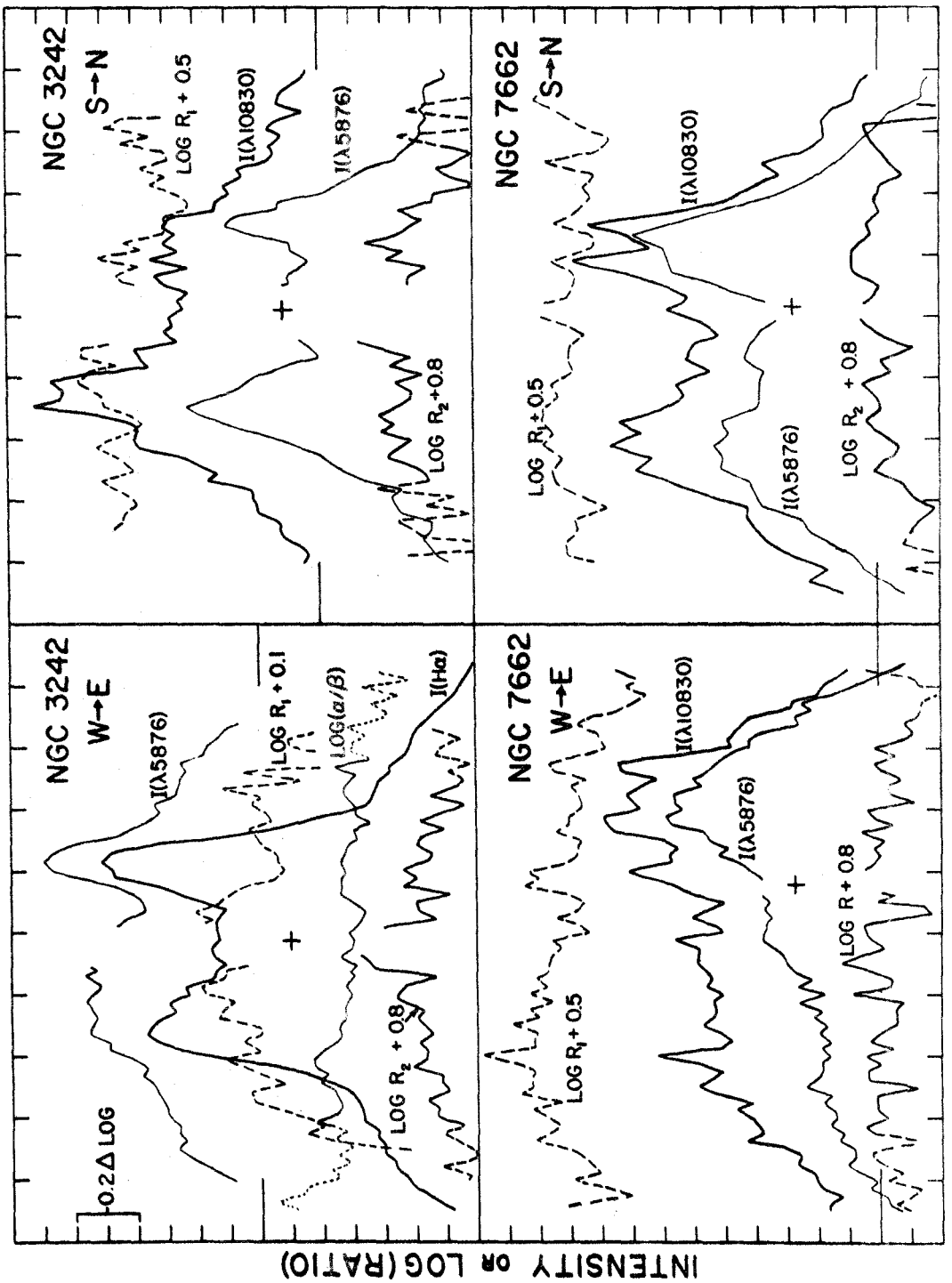
NGC 3242
W→E
NGC 3242
S→N
NGC 7662
W→E
NGC 7662
S→N
I(λ5876)
I(λ10830)
I(Hα)
LOG R1 + 0.1
LOG(α/β)
LOG R2 + 0.8
LOG R1 + 0.5
0.2Δ LOG
INTENSITY OR LOG (RATIO)
1 DIV = 4 ARC SECONDS

sketch of NGC 3242 showing the position of the H and He scans. Figure 14 summarizes the observations of these two objects, where representative intensity tracings and logarithmic color ratios are plotted.

(2) Discussion

The important features of these tracings are the following:

(i) The $I(H\alpha)/I(H\beta)$ fluctuations in NGC 3242 are real, and imply some combination of increased reddening and decreased temperature in the vicinity of the brighter regions of the nebula, viz., the toroid.

(ii) The ratio R_2 decreases systematically to the edges of the nebulae in all tracings studied. This confirms in general the Mt. Wilson results presented in Chapter III, and is independent of the systematic continuum uncertainty.

(iii) $\langle R_1 \rangle$, the average upper limit to the true value of R_1 is consistent with the value quoted in Chapter IV for NGC 7662, and R_1 for both objects is considerably below that required by D_t.

(iv) The $I(\lambda 10830)$ tracings are not as smoothly varying as would be expected for a uniform, optically thick sphere. Sometimes $I(\lambda 10830)$ looks like $I(\lambda 5876)$; often it deviates markedly. Certain regions of the R_1 tracing (NGC 3242 W→E)

are reminiscent of the He tracings presented by Persson (1970) and by MP for the Orion Nebula. While one would expect a decrease in R_1 at a position of increased I(λ5876) for a uniform sphere, it is noted that the changes in R_1 and log [I(Hα)/I(Hβ)] are sometimes nearly mirror images. Also, the λλ10830 and 5876 traces look very similar near the edges, and display similar linear fluctuation scales. This implies that at least some of the λ10830 photons created at any point do not diffuse "slowly" out of the nebula, but escape close to their points of creation. The correlation of R_1 with I(λ5876) changes sense on some regions of the nebula; e.g., NGC 7662 S→N and W→E.

(v) The above effects are noted in all tracings of both objects, including several tracings which covered other parts of the nebulae but which are not reproduced here. Those tracings are consistent with respect to the intensity and color values presented here.

The following schematic interpretation is proposed in view of the above (especially [iv]):

(i) Most of the loss of λ10830 flux documented here and in Chapter III results from trapping of the photons within localized bright regions, specifically in certain parts of the toroidal rings. The loss may be due partially to grains localized within the toroids, or to a temperature

decrease therein (cf. Section IV-[g]). The $H\alpha/H\beta$ color, if it is due to grains alone, implies the presence of some small particles in order that the extinction be frequency-dependent. It also allows the existence of a rather large optical depth in the solid matter, since the gas and dust are well mixed (cf. MP). If much of the solid matter is located within parts of the toroids, most photons arising from the far side of the nebula will propagate freely, thus preserving approximate intensity symmetry in the split lines, as observed (e.g., Wilson 1950).

(ii) The toroids are somewhat decoupled from the rest of the gas, at least as far as the velocity field is concerned. Otherwise, the appearance of the I(λ5876) and I(λ10830) tracings would be very different since the resonance-like photons would escape only from regions close to the nebular boundary, and I(λ10830) would vary smoothly across the nebula.

(iii) The filamentary structure of the nebula is clearly playing a decisive role in the production of the λ10830 line. Recalling the discussion in Section VI-(d), the variability of I(λ10830) can also be accounted for. In Section IV-(h), it is shown that the λ10830 observations of Vaughan (1968) can also be explained in terms of the same simple model of a large number of separate clouds.

(iv) The nebulae having the largest Hβ surface brightness also appear to have the largest IR excesses. It is therefore not unreasonable to expect the brightest regions of any particular planetary to have the largest excesses, and presumably more solid matter.

(g) Comments on Toroids and Filaments

How is the filament (or toroid) maintained against its own expansion? The high surface brightness of these features implies either a large density maximum or a temperature minimum, the latter appearing unlikely at first glance since the main cooling agent, emission of [O III] λλ4959, 5007 increases rapidly with T_e. The question may have been answered in principle by Nordsieck (1971) who has pointed out that the gradient in the H I Lyα energy density which will appear across a localized gradient of grain density (due to resonance trapping and absorption) represents another pressure term acting upon the gas and grains. He considered the onset of fluid instabilities in a series of models, and has predicted time and length scales for the development of density clumps. One does not need to start instability if large density fluctuations in the grain density are present, however. The situation is also aided by the conversion of electron kinetic energy and incident ionizing radiation to (decoupled) infrared flux from the grains. Consider the forbidden line cooling. The

[O III] emission rate is given by Seaton (1960) as

$$\xi = C_1 N_e N(O^{++}) \exp(-E/kT_e)/T_e^{1/2} \quad , \qquad \text{(VI-16)}$$

where $C_1 = 9.5\times10^{-18}$ erg cm^3 sec^{-1}, incorporating the revised value of the O^{++} collision strength (Czyzak et al 1968), and E = 2.49 eV is the excitation energy. The energy gained by the grains, which is lost by the electron gas is given by equation (IV-1) et seq. The ratio of these rates may be written in terms of $\tau_d(Ly\alpha)$ as

$$\frac{\xi}{\Gamma_{ep}} = \frac{2.93\times10^3}{(0.53T_4^2 + T_4)} \times \frac{R_{pc}}{\tau_d} \times \frac{N(O^{++})}{N_e} \times N_e \times \exp(-2.89/T_4) \qquad \text{(VI-17)}$$

when the cooling of the entire nebula is considered. Typically, $R_{pc} \sim 0.1$, $\tau_d \sim 0.1$, $N(O^{++})/N_e \sim 10^{-4}$ (Seaton 1960), $N_e \sim 10^4$, $T_4 \sim 1$, and $\xi/\Gamma_{ep} \sim 10^{-2}$. The grains are thus unimportant as a cooling agent for the nebula as a whole.

Suppose, however, that the filament is optically thick (in H° plus dust) to the stellar ionizing flux. We take, as evidence that this might occur, the photograph of NGC 650-1 reproduced by Seaton and Osterbrock (1957). They postulate that this object is a toroid like NGC 6720, seen directly on edge. While there is emission distributed perpendicular to the plane of the toroid, the emission boundary at each "end" of the toroid is very sharp, giving

the impression that τ(for ionizing photons) > 1. This interpretation is not only reasonable for this object, but may apply in some degree to all toroidal objects. Suppose that the nebula becomes optically thick in the dust over a distance comparable to the width of the ring of NGC 6720. Using O'Dell's (1962) distance estimate, we find from equation (VI-17)

$$\frac{\xi}{\Gamma_{ep}} \sim 4\times10^{-4}N_e \ ,$$

and thus these cooling rates compete.

For an isothermal slab, the ionization balance equation contains an $\exp(-\tau_d)$ term in addition to the H° attenuation factor which leads to the sharpness of the Strömgren edge (ionized → neutral), and thus the edge will be induced to occur closer to the central star. In addition, the ionization structure of the transition region is expected to be altered. This is because the dust is (explicitly) a frequency-and-ionization-independent absorber, unlike H°. The attenuation of the direct Lyc photons will then depend differently upon physical distance, and the resulting changes in the continuous and resonance line energy densities are expected to modify the ionization structures of N and O. Intuitively, one would expect N and O to exist in generally lower states of ionization. The O° density

× pathlength might then be expected to be large enough, where $1 > N_e/N(H) > 0$ to give rise to substantial [O I] λλ6300, 6363 emission. The observations of Campbell (1968) support this qualitative conclusion since both NGC 6720, as the prototype toroidal nebula (with helical structure like NGC 7293) and NGC 2440 and NGC 7027 as the best examples of filamentary objects, have strong [O I] emission. The recent [O I] photographs of nebulae by Capriotti et al (1971) provide especially strong support for this interpretation. Some of the [O I] emitters also have large infrared excesses, e.g.: NGC 7027, 6572, IC 418, and BD+30°3639 (O'Dell [1963] gives the [O I] measure). Correlations between [O I] emission and infrared excess cannot be made without knowledge of the grain temperatures; e.g., the grains in NGC 6720 are expected to be very cool, and poor radiators for $\lambda < 11\mu$.

The exception is IC 418, which is generally recognized as a smooth, symmetric object with [O I] arising near the boundary (Aller 1956). If this is true, then it is presumably legitimate to identify the 20% asymmetry in the [N II] profiles (Osterbrock 1970) with a radial $\tau_d \sim 0.2$, in reasonable agreement with that required for both the λ10830 loss and the infrared emission from a shell. If the nebula is structured, and the combination of low elevation (poorer seeing) and a smaller fluctuation scale

is responsible for the smoothness, the same arguments apply, except that some of the [O I] and infrared emission may arise in filaments.

A rough four-way correlation thus appears to exist between [O I] and [N II] emission, structure, I(λ10830) loss, and IR excess. A calculation of the density and ionization structure, line and IR emission, and stability of a filamentary nebula is a very involved problem, well worth studying in detail.

(h) Comments on λ10830 λ-Resolution Studies of Vaughan

Vaughan (1968) has published λ10830 profiles for eleven planetaries and selected regions of the Orion Nebula. These wavelength profiles were obtained using a pressure scanned Fabry-Perot instrument with a resolution of ∿ 5 km/sec. Briefly, the profiles are redshifted by ∿ 20 km/sec with respect to the center of expansion of each object, and are generally asymmetric, the blue side of the line being stronger, and usually marked by one or more absorption features. For Orion the profiles are symmetric, but redshifted 30-40 km/sec. Resonance line transfer calculations by Hummer and Rybicki (1968) have shown that a P-Cygni type profile is to be expected from expanding, optically thick atmospheres and Robbins (1970b) has invoked this explanation to qualitatively account for

his and Vaughan's observations. The situation is likely to be considerably more complicated however, as the following comments and conclusions indicate:

(1) The high spatial-resolution observations of NGC 3242 and NGC 7662 suggest extreme complexity of the origins of both the λ10830 flux and the λ-dependence of its emission profile. It does not appear to arise solely from the near side of the nebula, but also from a large number of filaments and the toroidal rings.

(2) Resonance line profiles given by Auer (1968), and unpublished calculations by the present author show very deep minima in the center of the λ10830 line for τ_o as low as 10^3. Recalling the argument for the λ3889 line, it is reasonable to suppose that if the emission arises from a large number of internally static filaments, each expanding away from every other, the blue component from each will be preferentially absorbed by another filament (and hence by dust) while the red components will leak out. This would account both for the narrowness and for the large redshifts of the peaks in Orion - a known dusty and filamentary region - since the dust absorption is so much larger. The true case for planetaries will lie between the extreme for Orion, and the idealized case of a homogeneous expanding sphere, consistent with the blue side asymmetry noted above.

(3) The "3889" absorption features noted by Vaughan probably arise from outlying cooler filaments. This is reasonable in view of point (1). The stellar λ3889 features probably arise in the same way.

(4) The positive correlations of λ10830 line width with expansion velocity and with the blue shift of the absorption features are both consistent with looking into the nebula (filaments - points [1] and [2] above), since one would expect the line to be more smeared out by a velocity spread, and one would expect to see larger absorption displacements for larger values of V(R). Correlations of the profile features with IR emission, etc., are too complicated to disentangle at this point.

The profiles of Vaughan are thus qualitatively accounted for in terms of toroidal or filamentary structure, and dust absorption in the filaments.

VII. DISCUSSION

Several of the conclusions derived from this work have been presented in Chapters V and VI. In this chapter some correlations between the properties of the observed He I spectrum and several nebular parameters are made. Further reference is made to recent IR excess results, an outline of some interesting problems is given, and finally, a brief summary of this work is made.

(a) Correlations

The stated purpose of observing a sizable number of objects was to derive correlations between He I line ratios and other nebular parameters. The preceding chapters indicate, however, that the origin of the He I lines is bound up theoretically with infrared emission and structural features in a complicated way. The correlations thus cannot be expected to be very conclusive. The IR data are generally too scarce and so far have no spatial resolution to aid us in this study. The range in IR color temperatures, while qualitatively understandable, depends also upon particle composition (size distribution, absorption bands), and thus detailed models are practically useless. Since it is the depopulation rate discrepancy we are studying, the values $\Delta_1 \equiv \log(D_1/D_t)$, $\Delta_2 \equiv \log(D_2/D_t)$ and $\Delta_{12} \equiv \log(D_1/D_2)$ are used. Also, values of $\tau_d(\lambda 10830)$

given in Table 14 may be employed.

One might expect a dependence of the Δ's upon spectral type, if autoionization of He I (2^3S) by stellar lines (Robbins 1968c) actually contributes another term to the 2^3S depopulation rate. It is emphasized, however, that correlations of this type are bound to be inconclusive, since the production of λλ10830, 7065 depends strongly upon other factors, as shown previously.

First, let us study the observed structure. In view of the lack of quantitative data, e.g., a measure of maximum S(Hβ) relative to average S(Hβ), we divide the nebulae into three broad classes, as judged from personal experience at the telescope and examination of the photographs and drawings of Curtis (1918): smooth (S); toroidal or double-ring (R); and irregular (I), i.e., not fitting into the other two categories. These classes are given for each object in Table 10 (p.88). The average values of τ_d(λ10830) and formal 1σ standard deviations are: S: 0.19±0.07; I: 0.22±0.15; and R: 0.57±0.34. Omitting NGC 2392 from the R category still gives R: 0.47±0.22. It is clear that the toroidal or double-ring nebulae contain either significantly more dust or have lower temperatures in some regions. The Palomar observations of NGC 7662 and NGC 3242 support this view.

Plots have been made of Δ_1, Δ_2, Δ_{12}, Δ_{2t} ($\equiv \log[D_2/D_t]$, for the values of D_2 derived from the force fit of D_1 and D_t- given in Table 14), and $\tau_d(\lambda 10830)$ against the parameters N_e, T_e, V(R)/V(TH), log T_S, $\log(L_S/L_\odot)$, log S(Hβ), distance, radius, age (radius divided by V[R]), $C \equiv \Delta\log(H\beta)$, and stellar spectral type (divided into four categories - W, O or Of, continuous, unknown; all from Perek and Kohoutek 1967). Despite the scatter in these plots, it was found that except for T_e (see below) there was no significant correlation of the first four He I parameters (not $\tau_d[\lambda 10830]$) with any of the nebular parameters. There is a very slight tendency for the emission-line stars to be associated with lower R_2 discrepancies, in the sense to be expected if autoionization is important. It must be emphasized that the values of R_1 and R_2 may be quite uncertain for the emission-line stars. The Δ_1 vs. T_4 correlation is shown in Figure 15. It is seen that the discrepancy is greatest (I[λ10830] is weakest) for a narrow range in T_e, $11000 < T_e < 13500$ °K. The λ10830 observations are not good enough to establish the true magnitude of this effect. Of the six most deviant objects, only BD+30°3639 falls in the "S" category. Of the next four most deviant objects in this range of T_e, NGC 5217 is classified "S", but it is so small that this classification is uncertain. Thus of 10 objects, one, and maybe two are S-type. Statistically we would expect two, and since

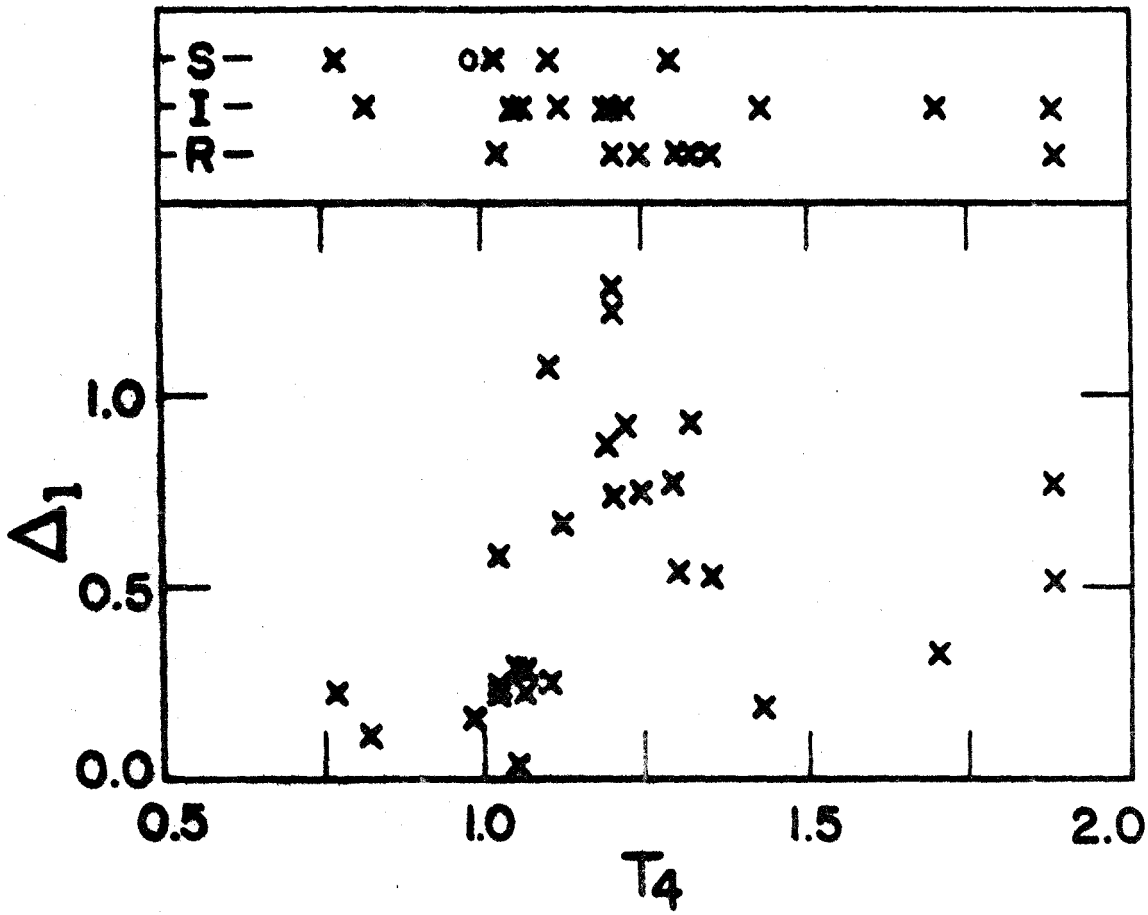

Fig. 15. - Correlation between R_1 derived rate discrepancy, T_4, and structural class. Open circle represents VV 208.

$I(\lambda 10830)$ from BD+30°3639 is almost certainly affected by dust, the separation is suggestive, but not conclusive. A comparison of T_e with structural class reveals a barely significant tendency towards $T_e(S) < T_e(I) < T_e(R)$, cf. Figure 15. Using the structure classification scheme of Curtis (1918), the same trend emerges; but the most one can conclude is that the smooth objects are not hotter than the toroidal ones, and do not tend to cluster between 10,000°K and 13,500°K as much.

Correlations of $\tau_d(\lambda 10830)$ with N_e, T_e, $S(H\beta)$, $V(R)/V(TH)$ (and weakly with T_s but no other parameters) appear to be real, in the sense that the larger values of $\tau_d(\lambda 10830)$ required to force $D_i = D_t$ are associated with smaller values of N_e and $S(H\beta)$ and with larger values of T_e and $V(R)/V(TH)$. Plots of $\tau_d(\lambda 10830)$ vs. log $S(H\beta)$, T_e, and $V(R)/V(TH)$ are shown in Figure 16. The N_e correlation is similar. Part of this effect is due simply to the fact that $\tau_0(\lambda 10830)$, the line center optical depth, increases with $S(H\beta)$ and N_e, and decreases with T_e. The rather large range in $\tau_0(\lambda 10830)$ produces a range in the values of $f(\lambda 10830)$, and since the $\lambda 10830$ destruction varies as $\exp[-f(\lambda 10830)\tau_d(\lambda 10830)]$, the larger values of N_e and $S(H\beta)$ imply larger values of $f(\lambda 10830)$ and hence smaller values of $\tau_d(\lambda 10830)$. The structural effects are noticeable in this correlation also; i.e., two of the lowest

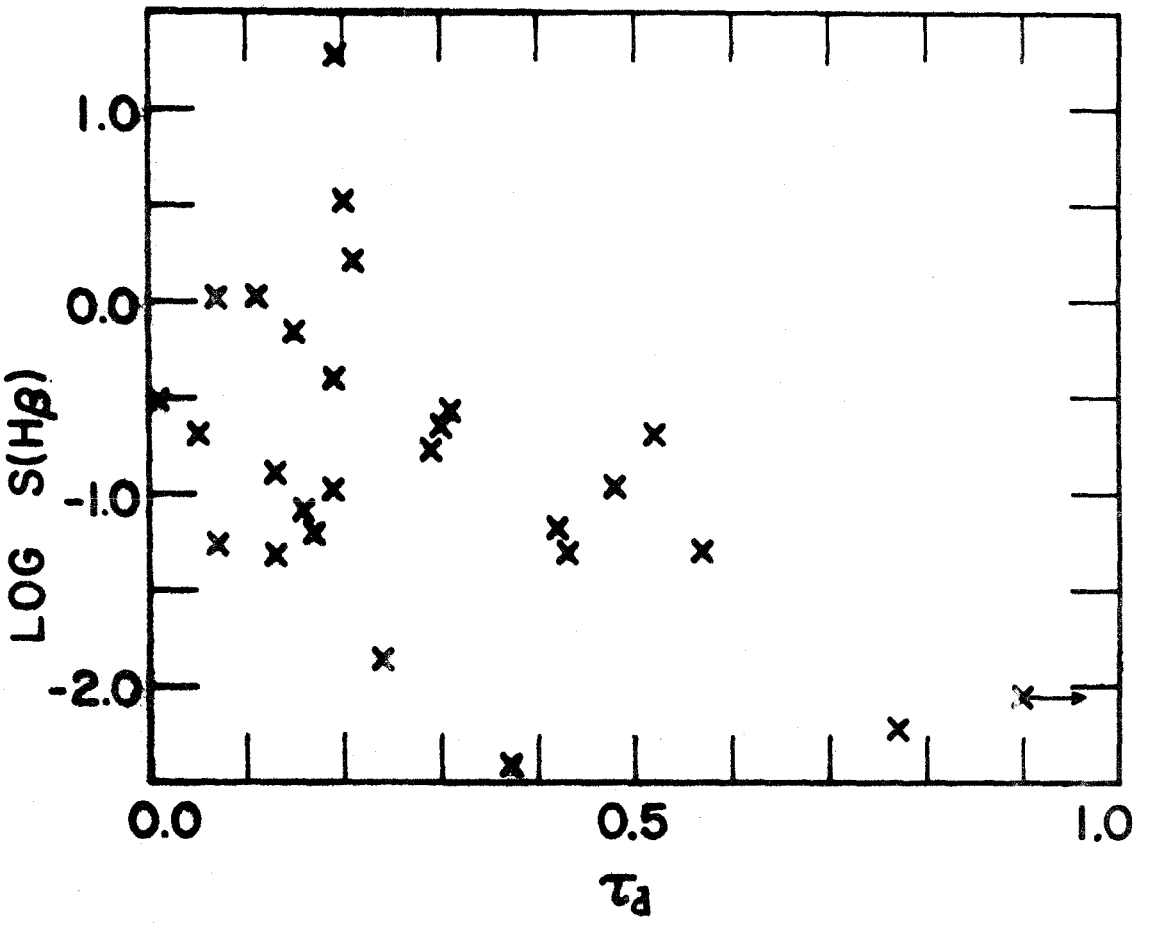

Fig. 16. - Correlations of S(Hβ), T_4, and V(R)/V(TH) with derived values of $\tau_d(\lambda 10830)$ for the objects from Table 14. Open circles in V(R)/V(TH) plot represent removal of $f(\lambda 10830)$ dependence upon V(R)/V(TH). Cross accompanied by an arrow represents NGC 2392, whose value of $\tau_d(\lambda 10830)$ falls off scale at 1.30.

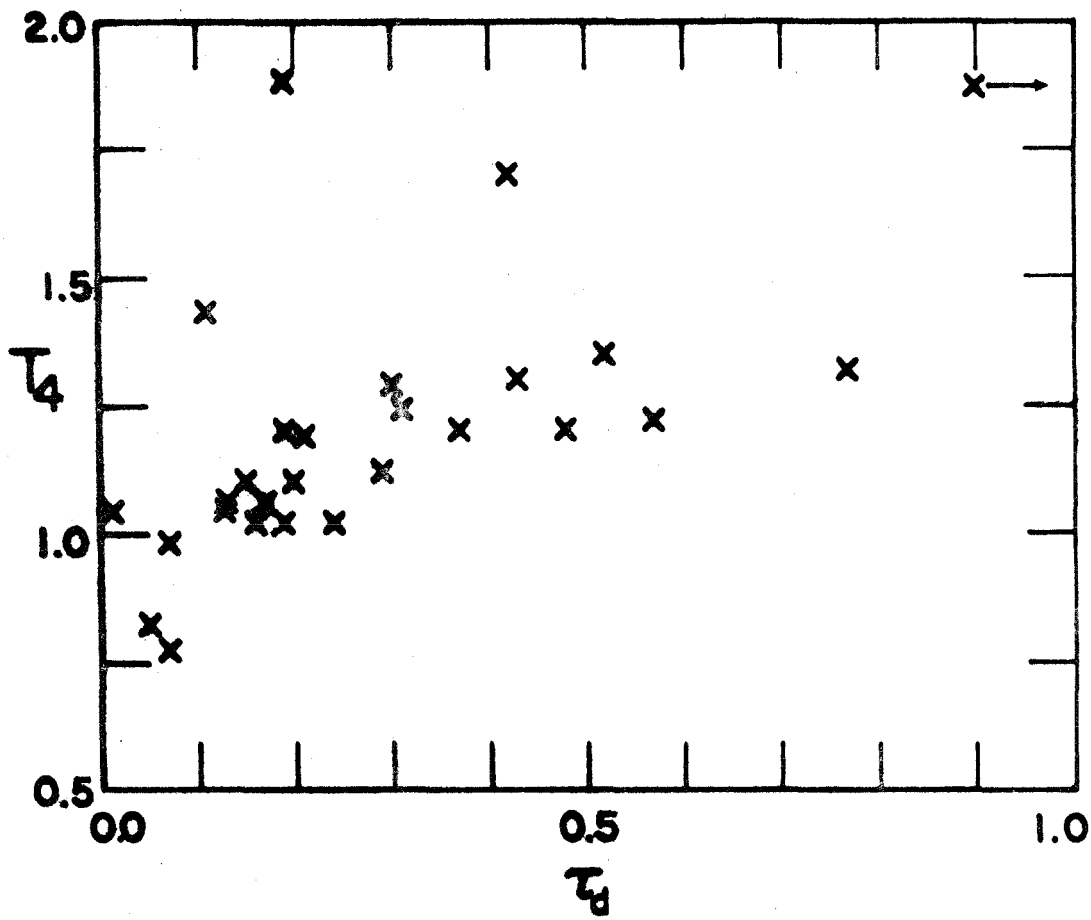

Fig. 16. - Continued.

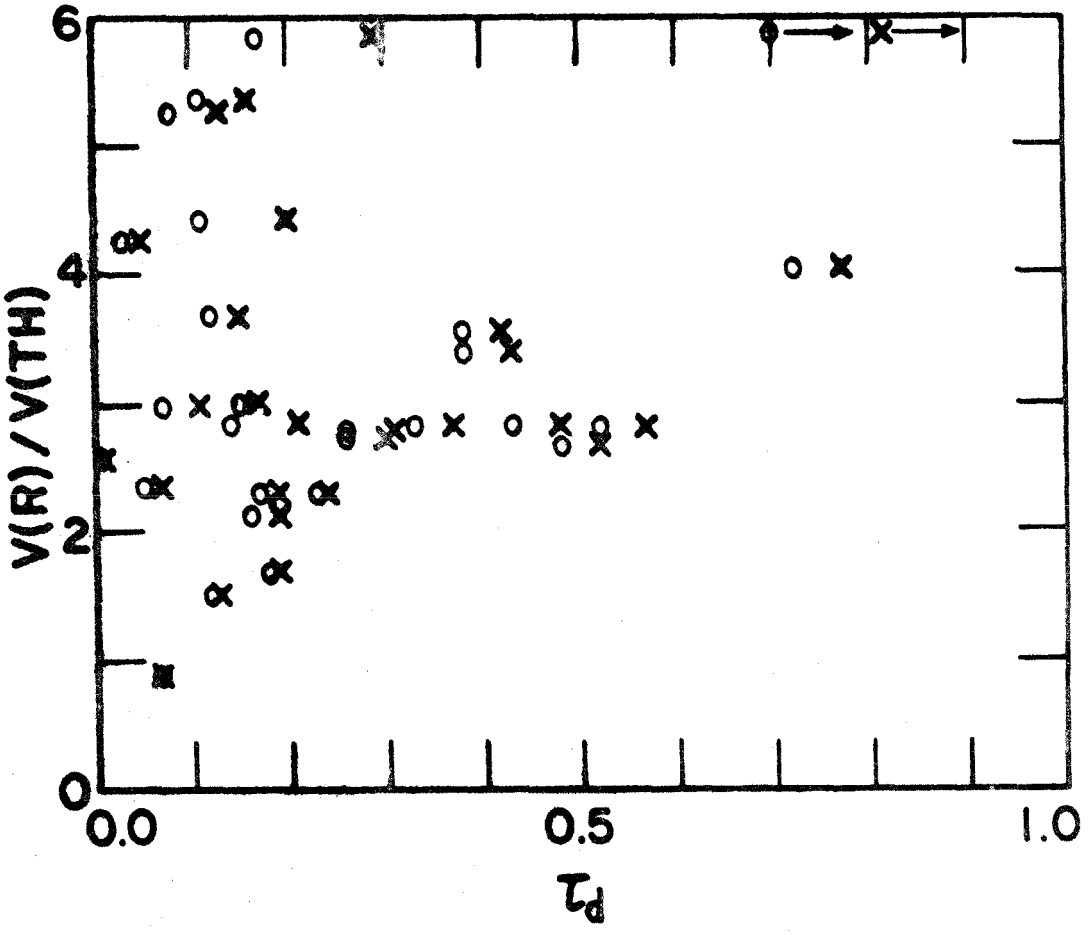

Fig. 16. - Continued.

S(Hβ) objects, NGC 6720 and NGC 2392, are strongly structured, and the higher T_e objects tend to be more irregular (Figure 15). Note that these correlations are not inconsistent with the idea that higher surface brightnesses imply more dust (more IR emission). This is because the large double ring objects, for example, have high S(Hβ) in their rings, but their angular size lowers their effective S(Hβ). The weak correlation of $\tau_d(\lambda 10830)$ with T_s is statistically equivalent to the T_e correlation. The general increase in $\tau_d(\lambda 10830)$ with V(R)/V(TH) is due partially to the adopted decrease in $f(\lambda 10830)$ with V(R)/V(TH), cf. Table A1. To check how much of the effect is due to this specified cause, $\tau_d(\lambda 10830)$ has been computed for values of $f(\lambda 10830)$ which do not vary with V(R)/V(TH), but which retain their dependence upon $\tau_0(\lambda 10830)$; values in column 3 of Table A1 are used. This plot is shown in Figure 16, and is seen to preserve the correlation. We are thus led to the conclusion that larger required values of $\tau_d(\lambda 10830)$ truly are associated with higher expansion parameters V(R)/V(TH).

If the deduced values of $\tau_d(\lambda 10830)$ do actually roughly measure the amount of dust within the planetaries, then this correlation suggests a causal relationship, viz., acceleration of the gas by radiation pressure on the grains.

It must be recalled that a large number of parameters

enter the calculation of $\tau_d(\lambda 10830)$ and that we are using a highly schematic model. It is doubtful that any further properties of the nebulae can be deduced from the data, due to the range in nebular conditions, structure, and observational and other uncertainties.

(b) Further Comments on IR Studies

Recently, many IR studies of early- and late-type stars, novae, transition, and peculiar objects have been made. For a review, see Neugebauer, Becklin, and Hyland (1971) and references cited therein. The consensus of these authors is that most of the IR excess emission from galactic stars and nebulae can be semi-quantitatively explained by thermal reradiation from grains surrounding the objects, and they refer to several specific dust models which have been proposed. The grains would appear to condense on rather short (pulsation) time scales since large, time varying IR excesses are observed from novae (see, e.g., Geisel 1970; Geisel et al 1970). Becklin et al (1969) pointed out the possibility that the object IRC +10216 is in a preplanetary stage. Recalling the succinct and persuasive arguments of Abell and Goldreich (1966), we see that the IR excesses are reasonable and consistent with the idea that the progenitors are mainly M III stars, whose remnant dusty envelopes are carried out by the planetary ejection(s). Gehrz and Woolf (1971) have

postulated radiation pressure on dust both as a mechanism for mass loss from M stars and as a way to replenish the mass of gas and dust in the interstellar medium.

In his study of the unusual IR object VY Canis Majoris, Herbig (1969; 1970) has considered radiation transfer in an optically thick dust shell or ring. Although Herbig considers VY CMa to be a pre-main sequence object, it could as well be an evolved star (Neugebauer et al 1971), the model applying in either case. We might thus identify the dusty rings with the cores of the toroids in the nebulae. NGC's 7293, 6543 and 6720 show distinct helical structure in their rings, so the ejection and formation is undoubtedly very complicated. The role of magnetic fields in the process is not clear, but cannot be very important dynamically, as Menzel (1968) has shown.

In studying filamentary structure in nebulae, Capriotti (1971) has shown that it is difficult to form condensations by the dust-radiation-gravitational instability on a short enough time scale. It is reëmphasized that starting from a nearly smooth mixture of gas and dust is probably unnecessary, and furthermore, unrealistic. Assume for the moment that the solar system is an example of a pre-planetary nebula configuration, on the basis that the sun is in the nominal mass range for progenitor stars. The mass of the planets is 2.7×10^{30}gm, or 1.5×10^{29}gm excluding

Jupiter and Saturn. The mass of spherical dust grains of radii $a = 0.1\mu$, density $\rho = 2$ gm cm^{-3}, and $\tau_d(\text{Ly}\alpha) = 0.1$ uniformly filling a nebula of radius $R = 0.1$ pc is 10^{30} gm. These order-of-magnitude estimates show that stellar system debris may represent a non-negligible fraction of the solid particle mass required for the planetary nebulae, the bulk presumably condensing in the red giant pulsations (cf. Hoyle and Wickramasinghe 1962).

(c) Bowen Fluorescent Mechanism

Unno (1955), Burgess and Seaton (1960), Kaler (1967) and Weymann and Williams (1969; hereinafter referred to as WW) have recently discussed the efficiency of the Bowen Fluorescent Mechanism in planetary nebulae. The conventional definition of the eficiency is

$$\mathcal{R} = \frac{\mathcal{N}(\text{O III})}{\mathcal{N}(\text{He II Ly}\alpha)} \quad ,$$

where $\mathcal{N}$(O III) is the total number of fluorescent O III photons produced by degradation of He II Lyα λ303 photons by branching decay after being absorbed by O III ($2p^2\,{}^3P_2$ - $2p3d\,{}^3P_2$), and $\mathcal{N}$(He II Lyα) is the total number of He II Lyα photons created.

Burgess and Seaton (1960) argued that the close wavelength coincidence ($\lambda\lambda$303.780, 303.799 for He II, O III)

and large optical depths would insure $R \rightarrow 1$. An expansion velocity of 20 km/sec enhances the coincidence but WW have calculated detailed transfer models which predict $R \sim 0.4$. The rest of the He II Lyα photons either escape, ionize H° or He°, or are converted to O III ($2p^2\,{}^3P_1 - 2p3d\,{}^3P_2^\circ$) and escape. The observed values of R are found by measuring the intensities of one or more O III lines, correcting for the recombination contribution, and comparing to I(λ4686). Kaler (1967) has computed R for seven well-observed nebulae and has derived R for nine others using other O III lines. WW have commented upon Kaler's procedure and point out that an error in his calibration factor effectively increases his derived values of R by a factor of 1.5. They also indicate that stellar excitation of the O III levels, and other depopulating mechanisms may be affecting the O III line intensities and hence R. These uncertainties do not remove Kaler's strong correlation of T_e with R however, in the sense that the hotter objects have lower efficiencies (less conversion of He II Lyα to O III emission). Kaler's explanation of this effect as a result of an increased escape probability for He II at higher T_e is incorrect because what counts is V(R)/V(TH), which decreases with T_e. R also increases with S(Hβ) and τ_c(H I). Statistically, these correlations are the same as those given above for τ_d(λ10830). Unfortunately, most of the few objects common to our lists have nearly the same value

of R, so the direct correlation of R with $\tau_d(\lambda 10830)$ is not striking. The suggestion is, therefore, that dust grains are reducing R either by absorption of the He II Lyα and O III resonance lines or by sufficiently altering the ionization structure around the filaments. Due to the large optical depths in the He II and O III transitions, typically 2×10^5 and 2×10^4 respectively, the mean-free-path between resonance scatterings is too small for a uniform dust density of grains ($\tau_d \sim 0.5$) to markedly reduce the energy density of O III $\lambda 303$ before it is lost by branching decay. This emphasizes the need for a calculation which takes into account filamentary or toroidal structure and dust. It is interesting to note that NGC 2392 has a very large expansion parameter V(R)/V(TH), marked structural features, the lowest value of R, [O I] emission, IR excess emission at short wavelengths and the largest required value of $\tau_d(\lambda 10830)$, assuming again that the idealized models used herein give some indication of the required dust content.

(d) Further Work

In this section some of the results of this work are combined with the author's personal opinions on the subject of "Further Work." Theses often end with the statement "more observations are needed." In the case of the planetary nebulae, further observations, especially at $\lambda \gtrsim 5\mu$,

will undoubtedly be made. What problems should be attacked, and what viewpoints can be adopted in future studies? On the theoretical side, the following categories emerge:

(1) Stellar Evolution

The fact that planetaries are observable for $\sim 10^4$ years means that a sizable percentage of all main-sequence stars may go through the planetary nebula stage (Osterbrock 1964; Abell and Goldreich 1966). While numerous studies of ejection mechanisms have been made recently, the correlation of $\tau_d(\lambda 10830)$ with V(R)/V(TH) is suggestive of a continuing acceleration of matter through radiation pressure on grains and gas. NGC 2392 and BD+30°3639 fit into this scheme rather well, as they possess large expansion parameters. We might reasonably suppose that the progenitor stellar systems have a lot to do with the eventual appearance of the nebulae (cf. Section VII-[e]).

(2) Dust Formation

What is the composition of the particles? Graphite flake condensation in M-star atmospheres has been suggested by Hoyle and Wickramasinghe (1962). Recent work cited by Neugebauer et al (1971) also suggests the presence of silicates.

(3) Filaments

What is the history of a dense filament in a planetary, or for that matter in an H II region? The problem is a large and difficult one, embracing fluid instability theory, radiation transfer, ionization structure and the energy balance. It could also involve the λλ3889, 10830 transfer problem. If the filament cores are neutral as Williams (1970) and Capriotti et al (1971) suggest, how much mass is involved? Can the ideas be applied to other objects such as novae or even supernovae shells?

On the observational side, there are numerous experiments to be performed, which, in the author's opinion, would greatly extend the preliminary work presented in this thesis, as well as provide input to the theoretical studies suggested above. For example:

(1) Simultaneous multiwavelength spectrophotometry with 2 arc sec resolution is within the reach of the 200-inch plus multichannel spectrometer combination. No more than five drift scans (à la Münch and Persson 1971) across NGC's 7662, 2392 or 7027 could settle the questions of the temperature fluctuations, He I emission, and [O I] emission.

(2) Image tube photography through 50 A interference filters (Capriotti et al 1971) is very useful, and

Capriotti's first results are most interesting in view of the conclusions reached in this work. This type of study is pertinent to the structure/filament problems, and may be useful photometrically also.

(3) A survey of planetaries at $\lambda \geq 20\mu$ is a must. F_ν is increasing with λ beyond 11μ in all objects observed so far.

(4) Higher spatial resolution intensity maps of the nebulae at several IR wavelengths would supplement the optical studies.

(5) NGC 7293, the closest planetary (distance $\sim$ 140 pc) is a truly remarkable object. Carranza et al (1968) and Vorontsov-Velyaminov (1968) have recently discussed the evolution and structure of the nebula and its numerous comet-like condensations. Spectra and motions of these filaments are crucial to our understanding of planetary nebulae.

(e) Summary and Conclusions

(1) Published He I line-transfer models of planetary nebulae are modified to include the effects of solid particles within the ionized regions. These particles are most effective in absorbing the H I Lyα and He I λ10830 photons which are resonantly trapped inside the nebulae.

A reduction of the mean Lyα energy density lowers the average depopulation rate of metastable He I 2^3S slightly. Neglect of λ10830 attenuation by this mechanism leads to empirical determinations of the 2^3S depopulation rate which are too high, sometimes by orders-of-magnitude. A simple, homogeneous model for the grain distribution is used to estimate the dust optical depths.

(2) New observations of the He I lines and values of the ratios $R_1 \equiv I(\lambda 10830)/I(\lambda 5876)$ and $R_2 \equiv I(\lambda 7065)/I(\lambda 5876)$ are presented. They show that the homogeneous models, while very useful, are too simple to describe real nebulae.

(3) Recent IR ($2.2\mu \leq \lambda \leq 12\mu$) flux and color measurements are studied in order to derive order-of-magnitude estimates of the dust optical depths for highly idealized thermally reradiating dust models.

(4) The observations and theory are compiled to show that the discrepancies between the theoretical and observationally inferred 2^3S depopulation rates exist for a larger sample of nebulae than that discussed by Capriotti (1967c). There is agreement to within a factor of two between D_1 (derived from R_1) and D_t (theoretical), and D_2 (from R_2) and D_t for over half the nebulae studied, but generally $D_1 > D_t > D_2$. The depopulation rate comparisons are shown to be as sensitive to other input parameters, especially

T_e, as they are to the line ratio observations, which for some nebulae are quite uncertain. Values of the dust optical depths at λ10830 which force $D_l = D_t$ are derived for idealized model nebulae assuming that the theoretical depopulation rates are the true rates.

(5) Nebular structural features are shown to be involved with the interpretation of the He I line ratio observations and the theory in a complicated way. High spatial resolution observations of NGC 3242 and NGC 7662 emphasize this point. Existing high wavelength-resolution observations of the λ10830 line profile are qualitatively explained using simple, inhomogeneous models.

(6) Correlations between derived depopulation rate discrepancies and nebular parameters are shown to exist, but firm conclusions cannot be based upon them because of the simplicity of the models and the complexity of real nebulae. The present work does suggest, however, that many of the nebular structural features (high S[Hβ] regions) have dusty cores; that the [O I] emission arises around these cores; that the low observed efficiency of the Bowen fluorescence mechanism may be affected by the dust grains; that the dust shells or rings which surround many (progenitor) M-stars are perhaps responsible for the inhomogeneities and toroidal features which are common to most nebulae; and that gradients in the energy densities of

resonance lines due to grain density gradients or inhomogeneities may provide part of the acceleration of the planetary shells.

APPENDIX 1.

THE EFFECT OF THE He I SINGLET LEVELS

We wish to show that there is negligible population of 2^3S or 2^3P by transitions from the singlet states. Let p be the probability that population of 2^1P is followed by population of 2^3P or 2^3S.

$$p = \frac{N_e q(2^1P \rightarrow 2^3S, 2^3P) + A(2^1P \rightarrow 2^3S)}{A(2^1P \rightarrow 1^1S)}$$

$$+ \left[\frac{A(2^1P \rightarrow 2^1S) + N_e q(2^1P \rightarrow 2^1S)}{A(2^1P \rightarrow 1^1S)} \right]$$

$$\times \left[\frac{N_e q(2^1S \rightarrow 2^3S, 2^3P)}{N_e q(2^1S \rightarrow 2^1P) + A(2^1S \rightarrow 1^1S) + N_e q(2^1S \rightarrow 2^3S, 2^3P)} \right]$$

The first term in this equation is the relative probability of direct collisional or radiative transition to 2^3S and 2^3P, where the notation $q(2^1P \rightarrow 2^3S, 2^3P)$ denotes the sum of the rates to the states 2^3S, 2^3P. The second term is the product of the relative probability of transition to 2^1S, and the probability of collisional transitions to 2^3S or 2^3P. The second term enclosed in brackets is the probability of populating 2^3S or 2^3P following population of 2^1S. The A-values are $A(2^1P \rightarrow 1^1S) = 18 \times 10^8 sec^{-1}$, $A(2^1P \rightarrow 2^1S) = 0.01976 \times 10^8 sec^{-1}$. Dalgarno and Drake (1968) have recently reported $A(2^1S \rightarrow 1^1S) = 51.3\ sec^{-1}$ (two-photon

decay) and $A(2^1P \rightarrow 2^3S) = 1.72\ sec^{-1}$. Seaton (1968) used the results of Burke et al (1967) to evaluate the q's for different values of T_e, assuming a Maxwell-Boltzmann distribution of electron velocities, obtaining at $T_4 = 1$, $q(2^3S \rightarrow 2^1S) = 3.1\times10^{-8} cm^3\ sec^{-1}$, $q(2^3S \rightarrow 2^1P) = 1.4\times10^{-8} cm^3\ sec^{-1}$, $q(2^1S \rightarrow 2^1P) = 79\times10^{-8} cm^3\ sec^{-1}$ and $q(2^1S \rightarrow 2^3P) = 9.9\times10^{-8} cm^3\ sec^{-1}$. Ignoring the energy differences between the four states, the collisional rates are in proportion to the statistical weights of the final states, and substitution of numerical values leads to

$$p \sim \frac{1.72}{18\times10^8} + 10^{-3}\left[\frac{19.2\times10^{-4}}{51.3}\right] \sim 4\times10^{-8},$$

for $N_e = 10^4\ cm^{-3}$ and $T_4 = 1$. The probability of populating 2^3S or 2^3P by populating 2^1S is $s = 4\times10^{-4}$. Let the number of resonance scatterings of a He I $Ly\alpha$ photon before destruction or escape be Q. An upper limit to Q is set by the probability of loss or conversion to the two-photon continuum, so that if η = the probability of destruction per scattering, $Q = 1/\eta$, and

$$\eta = \frac{A(2^1P \rightarrow 2^1S)}{A(2^1P \rightarrow 1^1S)} \times \frac{A(2^1S \rightarrow 1^1S) + N_e q(2^1S \rightarrow 2^3S, 2^3P)}{A(2^1S \rightarrow 1^1S) + N_e q}$$

$$+ \frac{A(2^1P \rightarrow 2^3S)}{A(2^1P \rightarrow 1^1S)}$$

$\sim 10^{-3}\times1 + 10^{-9}$, where q is now the sum of all collisional

rates out of 2^1S. Q is thus $\sim 10^3$, and the destruction of He I Lyα does not depend upon transitions to the triplet states. The total probability per 2^1P recombination that a transition to the triplets will occur is thus the product of p and Q. The recombination rate to 2^3S by conversion of singlet recombinations is thus $\alpha^* \simeq s\alpha(2^1S) + pQ\alpha(2^1P)$. Substitution of numerical values for the α's gives $\alpha^* \sim 10^{-4}\alpha(2^3S)$, so the singlet recombinations may be neglected in comparison to the triplet recombinations. The $2^3S \rightarrow 2^1S$, 2^1P collisional transitions thus represent a mode for the conversion of 2^3S excitation into the $2^1S \rightarrow 1^1S$ two-photon continuum, without any reverse process population rates of importance.

APPENDIX 2.

VALUES OF $f(\lambda 10830)$

Problems concerning the transfer of resonance radiation (usually Lyα) in optically very thick media have been considered by many authors. The function which specifies the redistribution of photon frequencies and directions upon scattering has been studied in various degrees of approximation by Henyey (1940), Unno (1952), Hummer (1962; and references cited therein) and applied to general equations of transfer by Unno (1952), Field (1959) and others. Osterbrock (1962), O'Dell (1965) and Hummer (1964) have estimated mean escape probabilities for resonance photons in various geometries, and Capriotti (1965; 1967b) has reconsidered this work with a view to applying the derived values of Q_α and f_α to the He I 2^3S depopulation rate problem. Auer (1968) has employed Monte Carlo techniques to the static, plane-parallel problem. It would appear promising to extend these methods to more realistic geometries.

Capriotti (1967b) tried to obtain upper limits to f_α to see if it would be at all possible to meet the depopulation rate requirements with Lyα ionization of He I 2^3S. As stated in Chapter II, the linear dependence of D_α upon f_α is lost when a small dust optical depth is introduced,

so the calculation of f_α becomes much less important than finding values of $f_1 \equiv f(\lambda 10830)$. It is emphasized that realistic nebulae containing impurities, condensations, toroidal structure, differential expansion, temperature gradients and fluctuations present insurmountable problems.

We follow Capriotti (1965) in his calculation of the mean escape probability $\varepsilon \equiv 1/Q$ for homogeneous expanding spheres. The damping parameter a for $\lambda 10830$ is less than that for Lyα so that for the optical depths considered, $\tau_0 < 2000$, a pure Doppler profile is adequate; i.e., the nebula becomes optically thin at a frequency displacement x from line center (in units of $\Delta\nu_d$) where the emission profile $(1/\sqrt{\pi})\phi(x) = (1/\sqrt{\pi})\exp(-x^2)$ is a good approximation. The calculation will be developed for a one-component $\lambda 10830$ line, but computations are also performed for a "real" three-component line, since $\lambda 10830$ consists of the components (Vaughan 1968): $\lambda\lambda$10829.087, 10830.250, and 10830.341, with statistical weights 1, 3 and 5 respectively. At $T_4 = 1$, $\Delta\lambda_d = 0.233$ A, and the separations are $5\Delta\lambda_d$ and $0.4\Delta\lambda_d$. We denote f_1 for three components by f_3.

Consider a spherically symmetric, homogeneous, isothermal nebula expanding with a velocity gradient k so that at a distance r from the center the outward velocity is $V(r) = kr$. The relative radial velocity between any two points whose separation is y is then ky. In a frame

at rest with respect to the emitting volume at r, where emission is around the central frequency ν_0, the absorption profiles of atoms a distance y away appear centered at

$$\nu(y) = \nu_0 \left[1 + \frac{ky}{c}\right]. \qquad (A1)$$

For pure Doppler broadening, the optical depth seen by a photon leaving r in a direction μ so that the distance to the surface is s, is

$$\tau_\nu(r,s) = \int_0^s Ne^{-\left(\frac{\nu-\nu(y)}{\Delta\nu_d}\right)^2} \kappa_0 dy. \qquad (A2)$$

Letting $w = \left(\frac{\nu - \nu(y)}{\Delta\nu_d}\right)$, $x = \left(\frac{\nu - \nu_0}{\Delta\nu_d}\right)$ we have

$$\tau_x(r,s) = \tau_0 \frac{V(TH)}{V(R)} \int_{x-\frac{ks}{V(TH)}}^{x} \exp(-w^2)\,dw \qquad (A3)$$

where V(TH) is the He thermal velocity, V(R) is the expansion velocity at the surface, and $\tau_0 = N\kappa_0 R$ is the radial line center optical depth. Solving equation (A3) for x when $\tau_x(r,s) = 1$ gives the frequency shifts x_1 and x_2 at which the optical depth to the surface (in direction μ at r) is unity. Following Osterbrock (1962) we identify the escape probability with the probability per scattering that a photon will be emitted beyond x_1 or x_2, so that if

$x_1 < 0 < x_2$

$$\frac{1}{Q} \equiv \varepsilon \equiv \frac{1}{\sqrt{\pi}} \left[\int_{\infty}^{x_1} \exp(-x^2)dx + \int_{x_2}^{\infty} \exp(-x^2)dx \right] . \qquad (A4)$$

The mean-free-path for a photon at displacement x, traveling in direction μ from r is

$$\ell(x,r,s) = \frac{s}{\tau_x(r,s)} , \qquad (A5)$$

and the profile-averaged mean-free-path (O'Dell 1965) is

$$\ell(r,s) = \int_{x_1}^{x_2} \ell(x,r,s) \frac{\exp(-x^2)}{\sqrt{\pi}} dx . \qquad (A6)$$

Dividing the sphere into a number of radial zones, we compute s, $\tau_x(r,s)$, x_1 and x_2, $\ell(x,r,s)$, $\ell(r,s)$ and $\varepsilon(r,s)$ at various angles, form the quantities $f(r,s) = \ell(r,s)/\varepsilon(r,s)R$, and average these quantities over the volume to obtain f. Each value will then depend only on the parameters τ_0 and $\xi \equiv V(R)/V(TH)$. This calculation is independent of photon loss within the nebula, since it finds probabilities and not creation and emission rates.

The proper calculation of ε depends upon choosing the radial points to be very closely spaced near the nebular boundary, since most photons excape from this region. For large optical depths this becomes very time consuming. The

calculation of f, however, is practically independent of the choice of radial points since the resonance scattering process takes place throughout the volume. The average values of Q for expanding spheres are so much smaller than those in static, source-at-center models, that the 2^3P leakage rate becomes entirely unimportant as a λ10830 loss mechanism; e.g.: at $\tau_0 = 10^3$, $\xi = 3$, Q is 220, leading to a loss of $\sim$ 0.4%.

The results are given in Table A1. Usually 10 radial points and 5 angular points (Gaussian division) were used, although the values of f are quite insensitive to these choices. As expected, the derived values of f are smaller than those of Osterbrock (1962), and decrease somewhat with ξ. For larger optical depths, $f_3 > f_1$, as there is a transfer of photons between the three components of the line; but for smaller τ_0 this transfer is lost, and f_3 becomes $< f_1$, since each component tends to act independently.

We use the values of f_3 given in this table to compute the λ10830 dust absorption loss.

TABLE A1

VALUES OF f_1 AND f_3

V(R)/V(TH) →	1		3		5		0†
$\tau_d(\lambda 10830)$	f_1	f_3	f_1	f_3	f_1	f_3	f_0
100	4.44	3.57	3.12	3.39	2.70	2.87	9.2
200	4.98	4.96	3.64	4.17	3.22	3.45	10.6
500	5.75	7.29	4.34	5.22	3.96	4.26	12.4
1000	6.30	9.14	4.86	6.02	4.43	4.89	13.8
2000	6.88	10.57	5.40	6.74	4.94	5.46	15.2

†Osterbrock's (1962) values of f.

REFERENCES

Abell, G., and Goldreich, P. 1966, Pub. A.S.P., 78, 232.

Allen, C. W. 1964, Astrophysical Quantities (London: Athlone Press).

Aller, L. H. 1956, Gaseous Nebulae (London: Chapman-Hall).

Aller, L. H. 1964, in Landholt-Bornstein: Numerical Data and Functional Relatioship in Science and Technology (Berlin: Springer-Verlag), Group VI, Bd I, 556.

Aller, L. H. 1968, I.A.U. Symposium 34 (Dordrecht: Reidel), p. 339.

Aller, L. H., Bowen, I. S., and Minkowski, R. 1955, Ap. J., 122, 62.

Aller, L. H., and Czyzak, S. J. 1968, I.A.U. Symposium 34 (Dordrecht: Reidel), p. 209.

Aller, L. H., and Kaler, J. B. 1964, Ap. J., 140, 621.

Aller, L. H., and Liller, W. 1968, Interstellar Matter ed. B. M. Middlehurst and L. H. Aller (Chicago: University of Chicago Press).

Andrillat, H. 1954, Comptes rendu, 238, 1781.

Auer, L. H. 1968, Ap. J., 153, 783.

Becklin, E. E., Frogel, J. A., Hyland, A. R., Kristian, J., and Neugebauer, G. 1969, Ap. J. (Letters), 158, L133.

Bell, K. L., Dalgarno, A., and Kingston, A. E. 1968, J. Phys. B. ser. 2, I, 18.

Blifford, I. H. 1966, Appl. Opt., 5, 105.

Böhm, K. H. 1968, I.A.U. Symposium 34 (Dordrecht: Reidel), p. 297.

Burgess, A., and Seaton, M. J. 1960, M.N.R.A.S., 121, 76.

Burke, P. G., Cooper, J. W., Ormonde, S., and Taylor, A. J. 1967, Internat. Conf. Phys. Electronic and Atomic Collisions (Leningrad: Nauka), pp. 368, 376.

Campbell, W., and Moore, J. H. 1918, Pub. Lick Obs. Bull., 13, 75.

Campbell, W. A. 1968, Pub. A.S.P., 80, 689.

Capriotti, E. R. 1965, Ap. J., 142, 1101.

Capriotti, E. R. 1967a, Ap. J., 147, 979.
Capriotti, E. R. 1967b, Ap. J., 150, 79.
Capriotti, E. R. 1967c, Ap. J., 150, 95.
Capriotti, E. R. 1971, Ap. J., 166, 563.
Capriotti, E. R., Cromwell, R. H., and Williams, R.E. 1971, Astrophys. Lett., 7, 241.
Carranza, G., Courtes, G., and Louise, R. 1968, I.A.U. Symposium 34 (Dordrecht: Reidel), p. 249.
Cassinelli, J. P. 1971, Ap. J., 165, 265.
Collins, G. W., Daub, C. T., and O'Dell, C. R. 1961, Ap. J., 133, 471.
Curtis, H. D. 1918, Pub. Lick Obs. Bull., 13, 55.
Czyzak, S. J., Krueger, T. K., and Martins, P. de A. P. 1968, I.A.U. Symposium 34 (Dordrecht: Reidel), p. 138.
Dalgarno, A., and Drake, G. W. F. 1968, Mem. Roy. Soc. Sci. Liège. series V, t XVII, 69.
Dalgarno, A., Drake, G. W. F., and Victor, G. A. 1969, Phys. Rev., 176, 194.
Drake, G. W. F., and Dalgarno, A. 1968, Ap. J. (Letters), 152, L121.
Duncan, J. C. 1937, Ap. J., 86, 496.
Feinberg, G., and Sucher, J. 1971, Phys. Rev. Lett., 26, 681.
Ferguson, E. E., and Schluter, H. 1962, Planet. Space Sci., 9, 701.
Field, G. B. 1959, Ap. J., 129, 551.
Field, G. B., and Steigman, G. 1971, Ap. J., 166, 59.
Gehrz, R. D., and Woolf, N. J. 1971, Ap. J., 165, 285.
Geisel, S. L. 1970, Ap. J. (Letters), 161, L105.
Geisel, S. L., Kleinmann, D. E., and Low, F. J. 1970, Ap. J. (Letters), 161, L101.
Gillett, F. C., Knacke, R. F., and Stein, W. A. 1971, Ap. J. (Letters), 163, L57.
Gillett, F. C., Low, F. J., and Stein, W. A. 1967, Ap. J. (Letters), 149, L97.
Gillett, F. C., and Stein, W. A. 1969, Ap. J. (Letters), 155, L97.

Gillett, F. C., and Stein, W. A. 1969, Ap. J. (Letters), 155, L97.

Gillett, F. C., and Stein, W. A. 1970, Ap. J., 159, 817.

Griem, H. R. 1969, Ap. J. (Letters), 156, L103.

Griem, H. R. 1970, Ap. J. (Letters), 161, L155.

Gull, T. R. 1971, Thesis, Cornell University.

Gurzadyan, G. A. 1969, Planetary Nebulae (trans. and ed. by D. G. Hummer) (N. Y.: Gordon and Breach).

Harman, R. J., and Seaton, M. J. 1966, M.N.R.A.S., 132, 15.

Harper, D. A., and Low, F. J. 1971, Ap. J. (Letters), 165, L9.

Harrington, J. P. 1968, Ap. J., 152, 943.

Henyey, L. G. 1940, Ap. J., 26, 50.

Herbig, G. H. 1969, Mem. [8°] Soc. Roy. Sci. Liège, quart. sér. (in press); Contr. Lick Obs. No. 302 (in press).

Herbig, G. H. 1970, Ap. J., 162, 557.

Hjellming, R. M., and Gordon, M. A. 1971, Ap. J., 164, 47.

Holtz, J. Z., Geballe, T. R., and Rank, D. M. 1971, Ap. J. (Letters), 164, L29.

Hoyle, F., and Wickramasinghe, N. C. 1962, M.N.R.A.S., 124, 417.

Huang, S.-S. 1948, Ap. J., 108, 354.

Hummer, D. G. 1962, M.N.R.A.S., 125, 21.

Hummer, D. G. 1964, Ap. J., 140, 276.

Hummer, D. G., and Rybicki, G. B. 1968, Ap. J. (Letters), 153, L107.

Kaler, J. B. 1967, Ap. J., 149, 383.

Kaler, J. B. 1968, Astrophys. Lett. 1, 227.

Kaler, J. B. 1970, Ap. J., 160, 887.

Kinchin, G. H. 1953, Proc. Roy. Soc., 217, 9.

Krishna Swamy, K. S., and O'Dell, C. R. 1968, Ap. J. (Letters), 151, L61.

Lee, P. D. 1968, Astrophys. Lett., 1, 225.

Liller, W. and Aller, L. H. 1963, Proc. N.A.S., 149, 675.

Martin, P. G. 1971, Ap. Lett., 7, 193.
Mathews, W. G. 1967, Ap. J., 147, 965.
Mathews, W. G. 1969, Ap. J., 157, 583.
Mathis, J. S. 1957, Ap. J., 125, 318.
Mathis, J. S. 1968, Ap. J., 153, 65.
Menzel, D. H. 1968, I.A.U. Symposium 34 (Dordrecht: Reidel), p. 279.
Minkowski, R., and Osterbrock, D. E. 1960, Ap. J., 131, 537.
Moore, C. E. 1949, N.B.S. Circ. 467, Vol. I.
Münch, G. 1964, Carnegie Yrb., 63, 25.
Münch, G. 1968, I.A.U. Symposium 34 (Dordrecht: Reidel), p. 259.
Münch, G. 1970, in Spectroscopic Astrophysics, ed. G. H. Herbig (Berkeley: University of California Press), p. 306.
Münch, G., and Persson, S. E. 1971, Ap. J., 165, 241.
Münch, G., and Wilson, O. C. 1962, Zs. f. Ap., 56, 127.
Neugebauer, G., and Garmire, G. 1970, Ap. J. (Letters), 161, L91.
Neugebauer, G., Becklin, E., and Hyland, A. R. 1971, preprint. To appear in Ann. Rev. Astron. Astrophys., 9.
Nordsieck, K. H. 1971, Ap. J., 163, 287.
O'Dell, C. R. 1962, Ap. J., 135, 371.
O'Dell, C. R. 1963a, Ap. J., 138, 293.
O'Dell, C. R. 1963b, Ap. J., 138, 1018.
O'Dell, C. R. 1965, Ap. J., 142, 1093.
O'Dell, C. R., and Terzian, Y. 1970, Ap. J., 160, 915.
Oke, J. B. 1969, Pub. A.S.P., 81, 11.
Oke, J. B., and Schild, R. E. 1970, Ap. J., 161, 1015.
Osterbrock, D. E. 1962, Ap. J., 135, 195.
Osterbrock, D. E. 1964, Ann. Rev. Astron. Astrophys., 2, 95.
Osterbrock, D. E. 1970, Ap. J., 159, 823.

Osterbrock, D. E., Capriotti, E. R., and Bautz, L. P. 1963, Ap. J., 138, 62.

Osterbrock, D. E., Miller, J. S., and Weedman, D. W. 1966, Ap. J., 145, 697.

Peimbert, M. 1967, Ap. J., 150, 825.

Perek, L., and Kohoutek, L. 1967, Catalogue of Galactic Planetary Nebulae (Prague: Academy of Sciences).

Persson, S. E. 1970, Ap. J. (Letters), 161, L51.

Petrosian, V. 1970, Ap. J., 159, 833.

Pottasch, S. R. 1961, Ap. J., 135, 385.

Rank, D. M., Holtz, J. Z., Geballe, T. R., and Townes, C. H. 1970, Ap. J. (Letters), 161, L185.

Rees, M. J., Sciama, D. W., and Stobbs, S. H. 1968, Astrophys. Lett. 2, 243.

Robbins, R. R. 1968a, Ap. J., 151, 497.

Robbins, R. R. 1968b, Ap. J., 151, 511.

Robbins, R. R. 1968c, Ap. J. (Letters), 151, L35.

Robbins, R. R. 1970a, Ap. J., 160, 519.

Robbins, R. R. 1970b, Ap. J., 162, 507.

Seaton, M. J. 1958, Rev. Mod. Phys., 30, 979.

Seaton, M. J. 1960, Rept. Prog. Phys., 23, 313.

Seaton, M. J. 1966, M.N.R.A.S., 132, 113.

Seaton, M. J. 1968, I.A.U. Symposium 34 (Dordrecht: Reidel), p. 129.

Seaton, M. J., and Osterbrock, D. E. 1957, Ap. J., 125, 66.

Sobolev, V. V. 1960, Moving Envelopes of Stars (trans. S. Gaposhkin) (Cambridge: Harvard University Press).

Spitzer, L. 1968, Diffuse Matter in Space (New York: Wiley) p. 142 et seq.

Stoy, R. H. 1939, Pub. A.S.P., 51, 233.

Terzian, Y. 1968, I.A.U. Symposium 34 (Dordrecht: Reidel) p. 87.

Thompson, A. R. 1967, Astrophys. Lett., 1, 25.

Thompson, A. R. 1968a, I.A.U. Symposium 34 (Dordrecht: Reidel) p. 112.

Thompson, A. R. 1968b, Astrophys. Lett., 2, 201.

Unno, W. 1952, Pub. Astr. Soc. Japan, 3, 158.

Unno, W. 1955, Pub. Astr. Soc. Japan, 7, 81.

Vaughan, A. H. 1968, Ap. J., 154, 87.

Vorontsov-Velyaminov, B. A. 1968, I.A.U. Symposium 34 (Dordrecht: Reidel), p. 256.

Weedman, D. W. 1968, Ap. J., 153, 49.

Weymann, R. J., and Williams, R. E. 1969, Ap. J., 157, 1201.

Wickramasinghe, N. C. 1967, Interstellar Grains (London: Chapman and Hall), p. 10.

Wickramasinghe, N. C., Donn, B. D., and Stecher, T. P. 1966, Ap. J., 146, 590.

Williams, R. E. 1970, Ap. J., 159, 829.

Willner, S., Becklin, E., and Visvanathan, N. 1972, (in preparation).

Wilson, O. C. 1948, Ap. J., 108, 201.

Wilson, O. C. 1950, Ap. J., 111, 279.

Wilson, O. C., and O'Dell, C. R. 1962, Pub. A.S.P., 74, 511.

Woolf, N. J. 1969, Ap. J. (Letters), 157, L37.